REPORT NO.
UCD/CGM-97/01

CENTER FOR GEOTECHNICAL MODELING

DYNAMIC PROPERTIES OF SHERMAN ISLAND PEAT

BY

ROSS W. BOULANGER
RAJENDRAM ARULNATHAN
LESLIE F. HARDER, JR.
RAPHAEL A. TORRES
MICHAEL W. DRILLER

Research supported by the U. S. Geological Survey (USGS), Department of the Interior, under USGS award number 1434-95-G-2531, and the Department of Water Resources, State of California. The views and conclusions contained in this document are those of the authors and should not be interpreted as necessarily representing the official policies, either expressed or implied, of the U.S. Government or the State of California.

DEPARTMENT OF CIVIL & ENVIRONMENTAL ENGINEERING
COLLEGE OF ENGINEERING
UNIVERSITY OF CALIFORNIA AT DAVIS

APRIL 1997

DYNAMIC PROPERTIES OF SHERMAN ISLAND PEAT

by

Ross W. Boulanger and Rajendram Arulnathan
Department of Civil & Environmental Engineering, University of California, Davis, CA

Leslie F. Harder, Jr., Raphael A. Torres, and Michael W. Driller
Department of Water Resources, State of California, Sacramento, CA

Research supported by the U. S. Geological Survey (USGS), Department of the Interior, under USGS award number 1434-95-G-2531, and the Department of Water Resources, State of California. The views and conclusions contained in this document are those of the authors and should not be interpreted as necessarily representing the official policies, either expressed or implied, of the U. S. Government or the State of California.

Report No. UCD/CGM-97/01

Center for Geotechnical Modeling
Department of Civil & Environmental Engineering
University of California
Davis, California

April 1997

ABSTRACT

The dynamic properties of peat and organic soils have been identified as major source of uncertainty in the evaluations of seismic hazards throughout the Sacramento-San Joaquin Delta in California. This report summarizes the results of a laboratory study of the dynamic properties of a layer of peaty organic soil (or "peat") underlying the south levee on Sherman Island near the western side of the Delta. Conventional Shelby tube sampling procedures were able to obtain high quality samples because of the compactness of this peat layer, located between depths of 9 and 16 m. The specimens tested were very fibrous and had ash contents of 35-56%. Staged cyclic triaxial loading was used to measure the stress-strain behavior of several specimens under cyclic shear strains ranging from about $5x10^{-4}$% to 10%. Other tests included piezo-ceramic bender element tests to measure the shear wave velocity of specimens within the triaxial device, and undrained monotonic triaxial compression and extension tests. The effects of loading frequency, cyclic degradation, consolidation stress history, and structural anisotropy are evaluated. The resulting modulus reduction and damping relationships for this Sherman Island peat are compared with published results for other peats, solid waste materials, and various mineral soils. The experimental procedures and results are presented in detail because of the limited experimental data currently available for peats and organic soils.

ACKNOWLEDGEMENTS

Support for this research was provided by the U. S. Geological Survey (USGS), Department of the Interior, under USGS award number 1434-95-G-2531, and the California Department of Water Resources (CDWR), State of California. The views and conclusions contained in this document are those of the authors and should not be interpreted as necessarily representing the official policies, either expressed or implied, of the U. S. Government or the State of California.

The National Science Foundation funded development of the triaxial testing equipment under NSF award number BCS-9310669, and acquisition of the digital oscilloscope, function generator, and other components used to perform the bender element tests under award number CMS-9502530.

The samples used for this research were provided by the CDWR, and tested by the University of California at Davis. Brent Lampkin of the CDWR assisted with the drilling and sampling work. William Gookin at U.C. Berkeley assisted with the laboratory testing, and developed the software for transferring data from the digital oscilloscope.

All of the above support and assistance is greatly appreciated.

TABLE OF CONTENTS

1. INTRODUCTION

The Sacramento-San Joaquin Delta in California contains over 60 low-lying "islands" with ground levels below sea level. These islands are protected against inundation from adjoining rivers and sloughs by over 1700 kilometers of levees. These levees have been generally constructed of uncompacted sands, silts, clays and peat, and are underlain by thick deposits of peat and highly organic soils across much of the Delta. The expected seismic response of these levees, which affects the potential for liquefaction of the cohesionless materials within the levees, is dependent on factors that include the subsurface stratigraphy (layering sequence and layer thickness), dynamic properties of each stratum, frequency content of the earthquake, level of shaking, and duration of shaking. Reasonable guidance regarding most of these factors can be found in the technical literature. There is, however, only limited experimental data regarding the dynamic properties of peat and highly organic soils. Consequently, an improved understanding of the dynamic properties of organic soils was identified as a primary need for future evaluations of seismic hazards throughout the Sacramento-San Joaquin Delta (California 1992).

Previous research on the dynamic properties of "peat" include efforts by Seed and Idriss (1970), Kramer (1993, 1996), and Stokoe et al. (1994). Note that the term "peat" will hereafter be used to refer to both peat and peaty organic soils. Seed and Idriss (1970) analyzed the motions recorded at an 18-m deep deposit of unconsolidated[1] peat at Union Bay during a magnitude 4.5 earthquake. Seed and Idriss concluded that peat exhibited stronger nonlinearity and higher damping ratios than clays (Fig. 1-1). While their modulus reduction and damping curves for peat have been widely used, Idriss (personal communication) has long since conveyed to his colleagues that these studies needed to be revisited and the resulting curves likely revised.

Stokoe et al. (1994) presented results for two peat specimens from a bridge site in New York tested in a resonant column and torsional shear device. These two specimens had water contents of 210 and 285%, ash contents of 37 and 65%, and came from depths of about 9 m where the in situ vertical effective stress was about 114 kPa. Each specimen was subjected to a series of resonant column and torsional loadings at six different consolidation stresses, varying duration of confinement, and varying loading frequencies. The test results showed very linear behavior, with negligible modulus reduction (e.g., $G/G_{max} > 0.98$) and low damping ratios (<3% for <1 Hz loading) at shear strains ranging up to 0.1%. Shear moduli increased by 5-8% per log cycle increase in loading frequency (using 1 Hz as the reference frequency) based on tests with cyclic shear strains of 0.001%, 0.01% and 0.1% and loading frequencies of 0.1-30 Hz. Damping ratios also increased with loading frequency, with variable differences of 0.0-0.9% damping per log cycle of loading frequency.

Kramer (1996) presented results of resonant column tests in a follow-up to an earlier study involving cyclic triaxial and piezo-ceramic bender element tests (Kramer 1993). Both studies used tube samples of peat from Mercer Slough in Washington, which is a fibrous peat

[1]"Unconsolidated" is used to describe peat which has only been consolidated under its own, largely submerged, weight. This results in a relatively small consolidation stress. For example, 18 m of submerged peat having a total unit weight of 10.2 kN/m^3 will generate an effective overburden pressure of only 7 kPa.

having in situ water contents of 500 to 1,200%. Specimens were consolidated to effective confining pressures ranging from 1.5 to 12 kPa for the resonant column tests, and about 19 kPa for the cyclic triaxial tests. The modulus reduction and damping ratio versus shear strain results for the tests at effective confining pressures of 1.5 to 12 kPa are shown in Fig. 1-2. These results are compared in Fig. 1-3 (Kramer 1996) with the results at confining pressures of about 19 kPa, and with the previously described results by Stokoe et al. (1994). Note that Stokoe et al.'s results in Fig. 1-3 are for an isotropic confining pressure of about 75 kPa, which represents the in situ mean effective consolidation stress for the two samples tested. Based on the trends in these results, Kramer (1996) concluded that the variation of modulus reduction (i.e., G/G_{max}) and damping with shear strain for Mercer Slough peat was dependent on the effective confining pressure, with the peat showing more linearity (i.e., higher G/G_{max} ratios and lower damping) with increasing effective confining pressure.

This report presents the results of a laboratory study of the dynamic properties of a layer of consolidated peat underlying the south levee of Sherman Island near the western side of the Delta. Details of the site conditions, in situ test data, sampling procedures, laboratory testing equipment, and laboratory testing procedures are described. Experimental results are presented in detail because of the limited experimental data currently available for peat. The effects of loading frequency, cyclic degradation, consolidation stress history, and structural anisotropy are evaluated. The resulting modulus reduction and damping relationships for the Sherman Island peat are compared with published results for other peats, mineral soils, and solid waste materials.

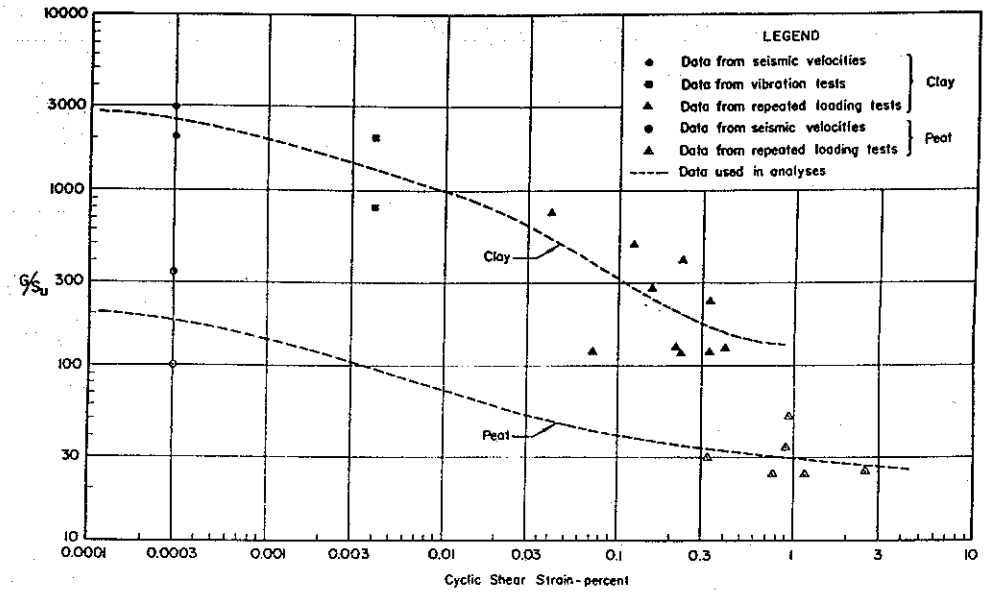

FIG. 2. Moduli for saturated clay and peat.

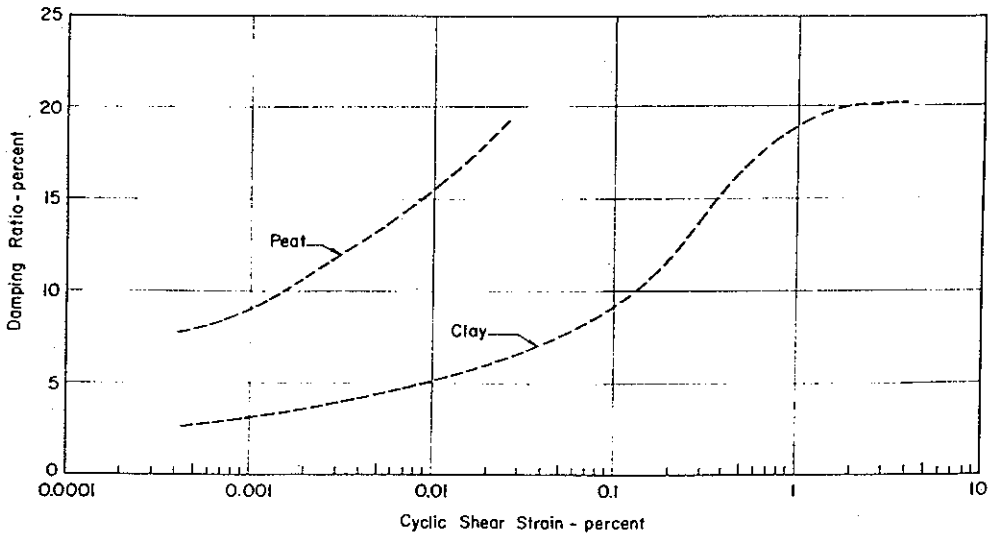

FIG. 1-1. Moduli and Damping Ratios for Saturated Clay and Union Bay Peat (Seed and Idriss 1970)

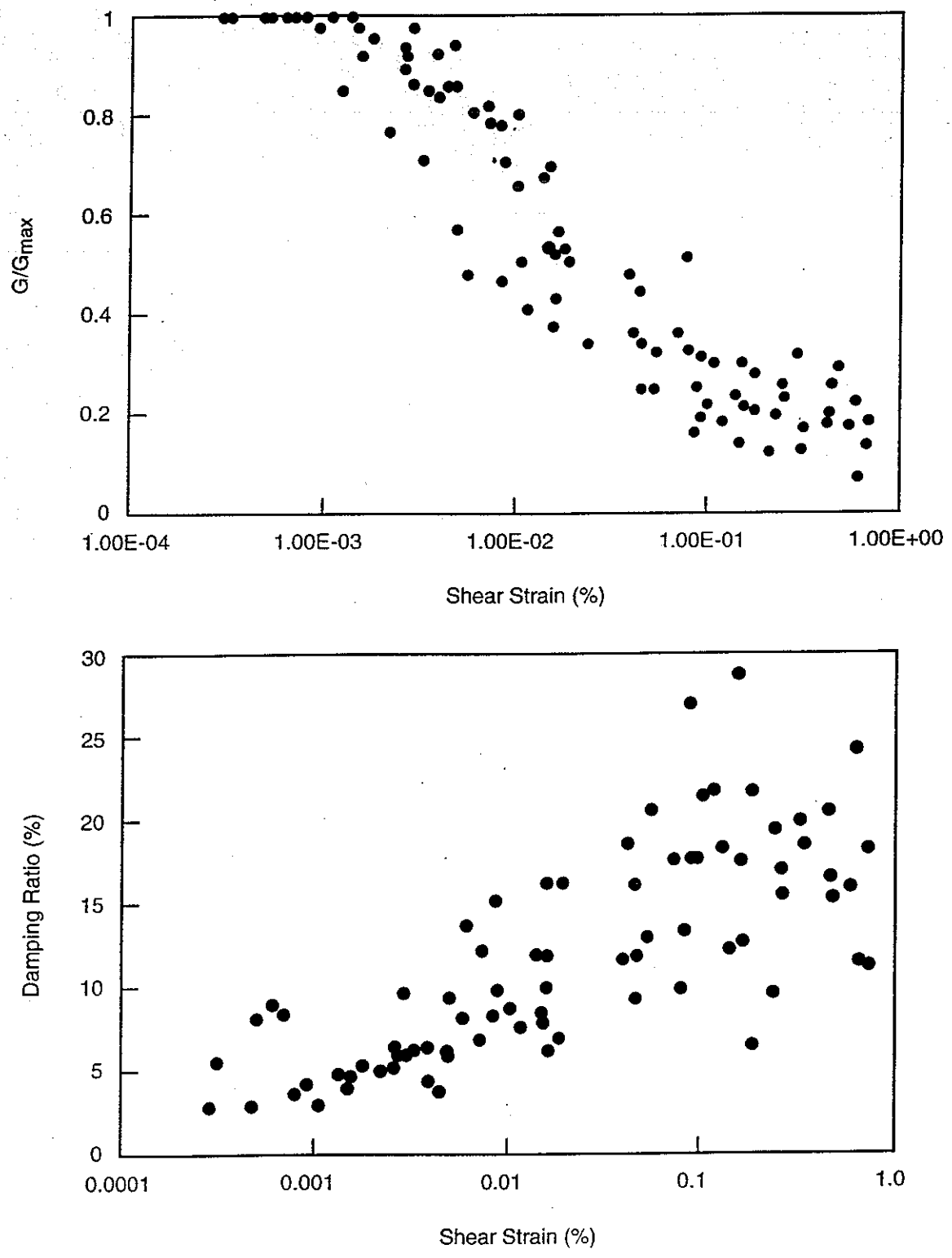

FIG. 1-2. Modulus Reduction and Damping Behavior for Normally Consolidated Mercer Slough Peat Specimens at Effective Confining Pressures of 1.5 to 12.5 kPa (Kramer 1996)

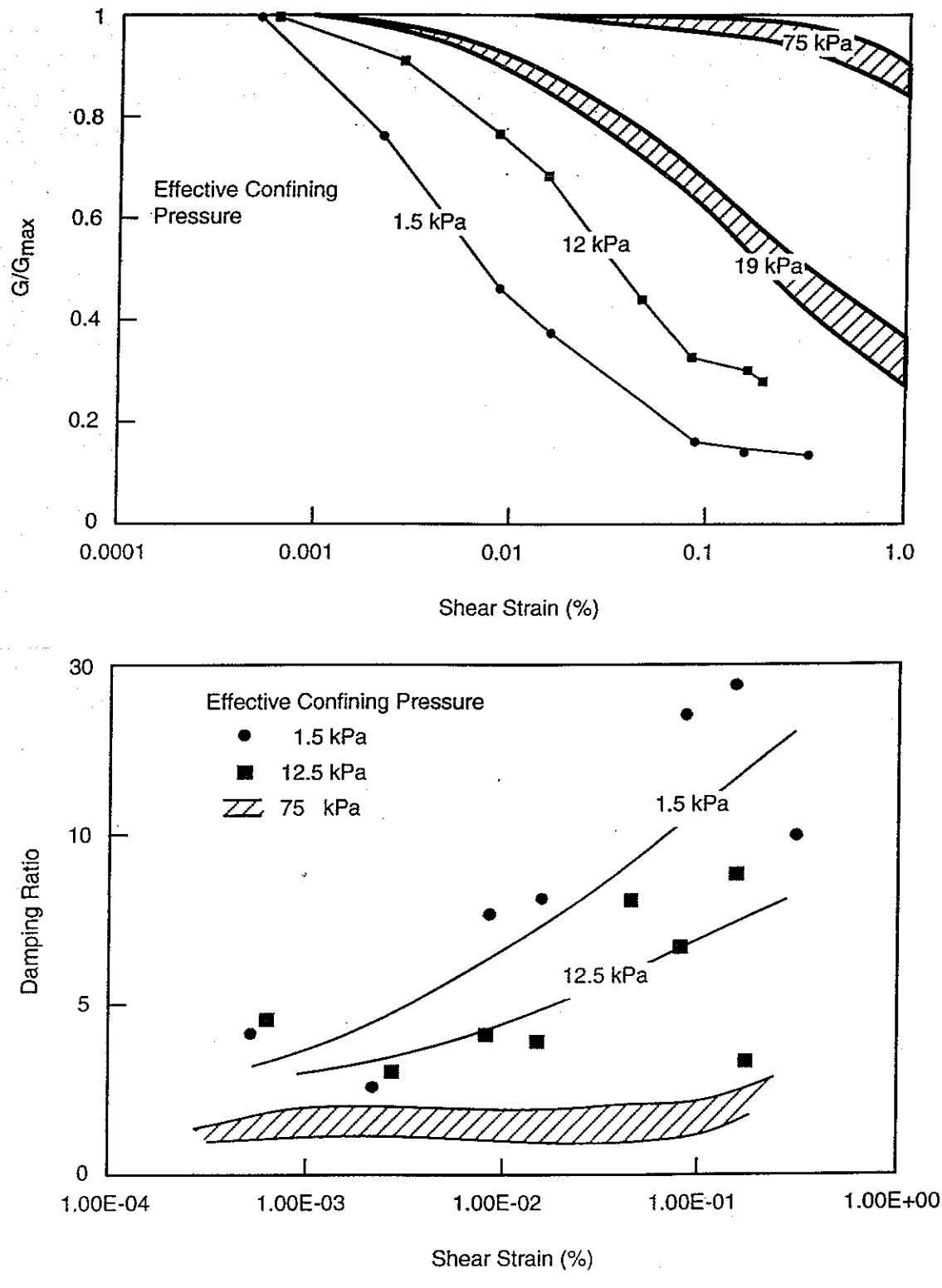

FIG. 1-3. Variation of Modulus Reduction and Damping Behavior With Effective Confining Pressure (Kramer 1996)

2. SAMPLING LOCATION AND PROCEDURES

2.1. South Levee on Sherman Island

Samples of peat were obtained by the Department of Water Resources, State of California (CDWR) from borings along the south levee on Sherman Island, just east of the Highway 160 bridge that connects the island to Antioch across the San Joaquin River (Fig. 2-1). These borings were located adjacent to a down-hole array of accelerometers installed through the levee crest by the CDWR in 1995. A schematic cross-section of the subsurface conditions at the sampling location is shown in Fig. 2-2.

Results from a CPT sounding and a boring with downhole shear wave velocity (V_s) measurements using the OYO Suspension P-S logging system are shown in Fig. 2-3. These explorations were also carried out by the CDWR approximately 5 to 10 m from the sampling locations. Note that CPT-derived B_q parameter in Fig. 2-3 is given by $B_q=(u_{bt}-u_o)/(q_c-\sigma_v)$, where u_{bt} is the pore pressure measured behind the cone tip, u_o is the hydrostatic pore pressure, q_c is the tip resistance (corrected for area effects), and σ_v is the total vertical stress. While Figs. 2-2 and 2-3 focus on the upper 25 m of stratigraphy, it should be noted that the soil deposits in this area are hundreds of meters thick and that their characteristics are also important for assessing the seismic response of the levees.

The levee materials generally consist of peat and dredged sand, silt and clay, with compacted sandy fill along the crown (Figs. 2-2 and 2-3). Beneath the levee is a thick layer of peat with sandy micaceous silt inter-layers. This peat layer is typically about 12 m thick in the fields away from the levee but has been highly compressed under the weight of the levee. Underlying the peat is an approximately 8 m thick layer of silty clay, followed by an underlying sand stratum.

2.2. General Characteristics of the Peat Layer

The peat layer between depths of 9-16 m beneath the levee (Figs. 2-2 and 2-3) was the subject of this study. Characteristics of the samples used for triaxial testing, all from depths of 12-14 m in this layer, are summarized in Table 2-1. The peat at these depths has a highly fibrous fabric from which individual fibers of 1 to 3 cm length can readily be unraveled. A primarily horizontal orientation of the fibers is visually apparent, and is demonstrated by a relatively easy separation of samples along horizontal planes while a sharp knife is needed to split samples along vertical planes.

Samples used for triaxial testing had water contents of 152-240%. These water contents correspond to a drying oven temperature of 90°C. Water contents for a couple of samples were also determined at oven temperatures ranging from 60°C to 110°C. The water content determined at 110°C was greater than the water content determined at 60°C by as much as 8% water content (i.e., w=201% versus 209%).

Samples used for triaxial testing had ash contents of 35-56%. Ash contents correspond to the ASTM (1991) D2794 standard (oven temperature of 550 °C until completely ashed). Ash contents for a couple of samples were also determined using the guidelines suggested by Landva et al. (1983) (440 °C for 5 hours), the ASTM (1991) standard, and the Muskeg Engineering Handbook (NRC 1969) (800-900 °C for 3 hours or until completely ashed). The ash content determined by the NRC (1969) guidelines was greater than the ash content determined by the Landva et al. (1983) guidelines by about 3% ash content (i.e., ash content of 55.8% versus 58.5%). As expected, the ASTM guidelines resulted in ash contents intermediate to those obtained by the NRC and Landva et al. guidelines.

The "peat" samples tested in this study may best be described as a highly organic soil based on the applicable ASTM standards. ASTM standard D4427-92, "Classification of Peat Samples by Laboratory Testing," defines peat as:

> "A naturally-occurring highly organic substance derived primarily from plant materials. Peat is distinguished from other organic soil materials by its lower ash content (less than 25% by dry weight), and from other phytogenic material of higher rank (that is, lignite coal) by its lower calorific value on a water saturated basis."

Since the samples tested had ash contents greater than 25%, they would be described as organic soil rather than as peat. Note, however, that ASTM D4427-92 relates to agricultural/horticultural and energy uses of peats, as well as to geotechnical uses. ASTM standard D2487-92, "Classification of Soils for Engineering Purposes," which is most commonly used for geotechnical purposes, states that:

> "A sample composed primarily of vegetable tissue in various stages of decomposition and has a fibrous to amorphous texture, a dark-brown to black color, and an organic odor should be designated as a highly organic soil and shall be classified as peat, PT..."

Thus, the samples tested may be described as highly organic soils and classified as peat (PT) by some geotechnical engineers. For the purposes of this report, the highly organic soil samples from Sherman Island will be referred to as "peat" because of their highly fibrous nature and because "peat" is a generic term often used locally to describe these types of organic soil deposits.

Consolidation tests on peat samples (Roger Foott Associates 1991) from a nearby section of levee indicate that the peat layer is nearly normally consolidated beneath the adjacent fields landward of the levee, but is overconsolidated beneath the levee. Preconsolidation pressures beneath the levee were about 120-220 kPa compared to the estimated effective overburden stresses of 95-115 kPa over the corresponding depths. Overconsolidation of the peat beneath the levee may have been the result of desiccation during the progressive build-up of natural levee deposits along the river channel. Another possible factor contributing to overconsolidation of

these materials may be the effects of long-term secondary compression under the weight of the levee.

2.3. Shelby Tube Sampling and Handling

Shelby tube samples of the peat between depths of 12 to 14 m were obtained in hollow stem auger borings. The sample tubes were galvanized steel tubes, with a length of 0.76 m and an outer diameter of 76 mm. A high water level was maintained in the hollow auger at all times to maintain outward seepage at the bottom of the boring. The sample quality appeared very high, with 100 percent recovery in most cases, because of the relatively compact nature of the peat beneath the levee. The high quality of the samples was in sharp contrast with the problems usually encountered with sampling the unconsolidated peat in the fields away from the levees. Samples were immediately sealed, placed upright in a padded box, and transported to the laboratory where they were stored in a chamber at 13 °C and greater than 96% humidity. X-ray photographs of the sample tubes were taken to aid in selecting intervals for testing. The first specimen was tested about 1 week after drilling, and subsequent tests averaged about 1 week each to complete. The date of testing for each specimen is listed on its summary sheet in Appendix C.

TABLE 2-1. Summary of Triaxial Testing Program and Sample Characteristics

Test No.	Sample No.	Depth (m)	Water Content (%)[a]	Ash Content (%)[b]	Total γ (kN/m^3)	In situ σ_{vo}' (kPa)	Triaxial σ_{3c}' (kPa)	Bender V_s (m/s)	Type of triaxial test
1	5D-P4(1)	13.6	200	56	11.5	134	200	81.1	cyclic
2	5E-S2(1)	13.5	180	54	11.3	132	132	-[d]	cyclic
3	5E-S2(2)	13.4	202	41	11.2	132	132	80.9	cyclic
4	5E-S2(3)	13.2	185	42	11.3	131	131	86.4	cyclic
5	5G-S4(1)	13.7	196	54	11.3	136	136	84.0	cyclic
6	5G-S4(2)	13.5	186	37	11.3	132	132	83.2	cyclic
7	5G-S4(3)	13.3	240	42	11.1	131	200	87.9	cyclic
8	5F-S4(1)	13.7	164	37	11.4	136	136	-[e]	compression
9	5F-S4(2)	13.5	169	37	11.6	132	66[c]	86.6	cyclic
10	5F-S4(3)	13.3	194	35	11.4	131	66[c]	82.6	cyclic
11	5G-S3(1)	12.9	152	36	11.8	130	130	-[e]	extension
12	5G-S3(2)	12.8	205	44	11.2	128	128	87.0	cyclic

[a] Oven drying temperature of 90°C.

[b] ASTM (1991) D2794 standard.

[c] Specimen was first consolidated to a σ_{3c}' of 132 kPa, and then rebounded to a σ_{3c}' of 66 kPa.

[d] Bender element did not function.

[e] Bender elements were not installed in the triaxial device that was used for monotonic loading tests.

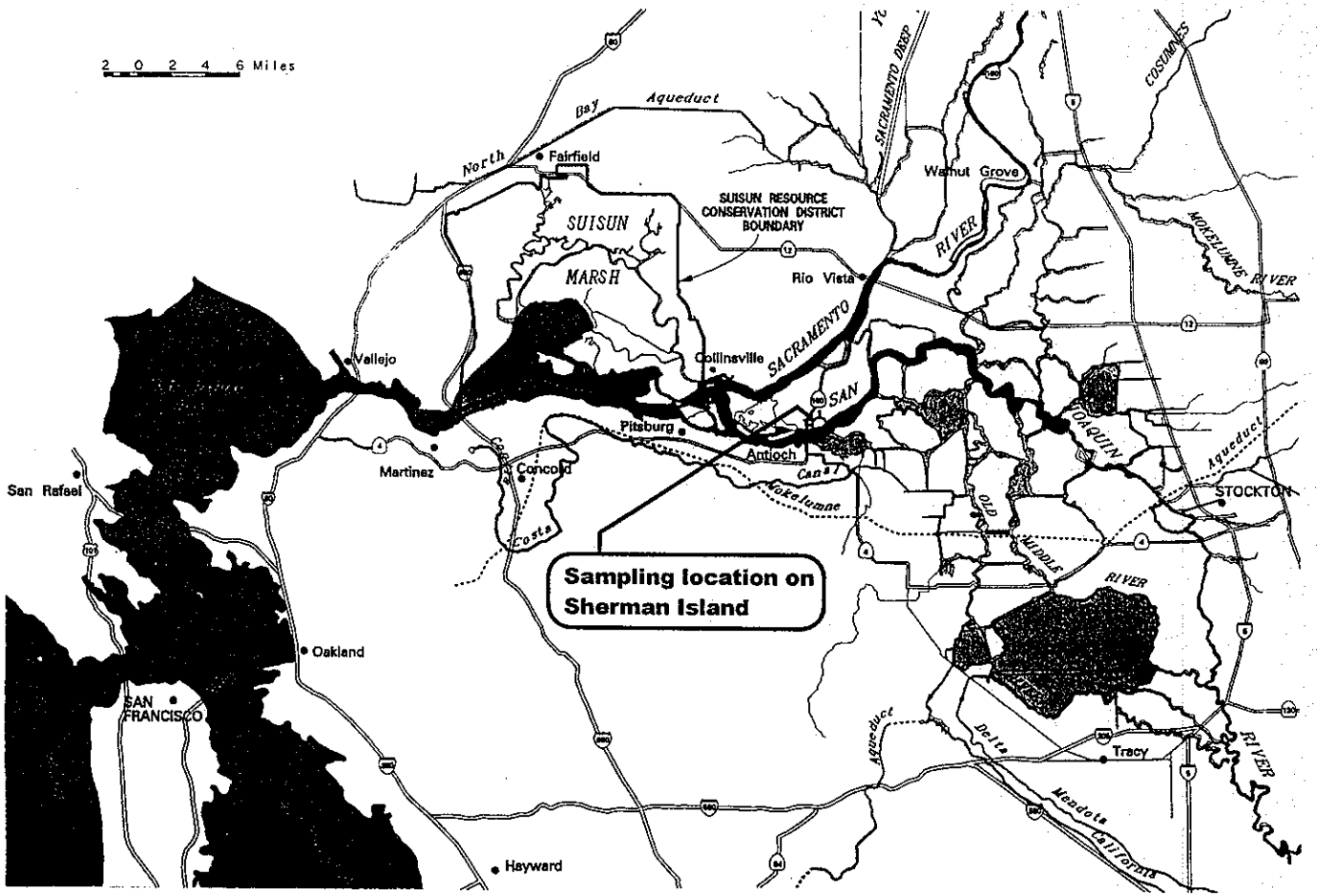

FIG. 2-1. Location of Sherman Island

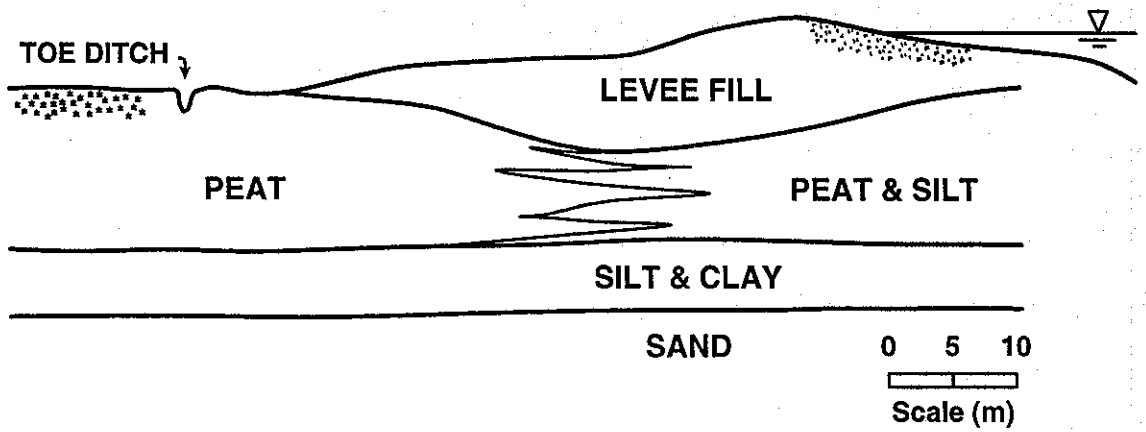

FIG. 2-2. Schematic of a Typical Sherman Island Levee

Profile1.grf

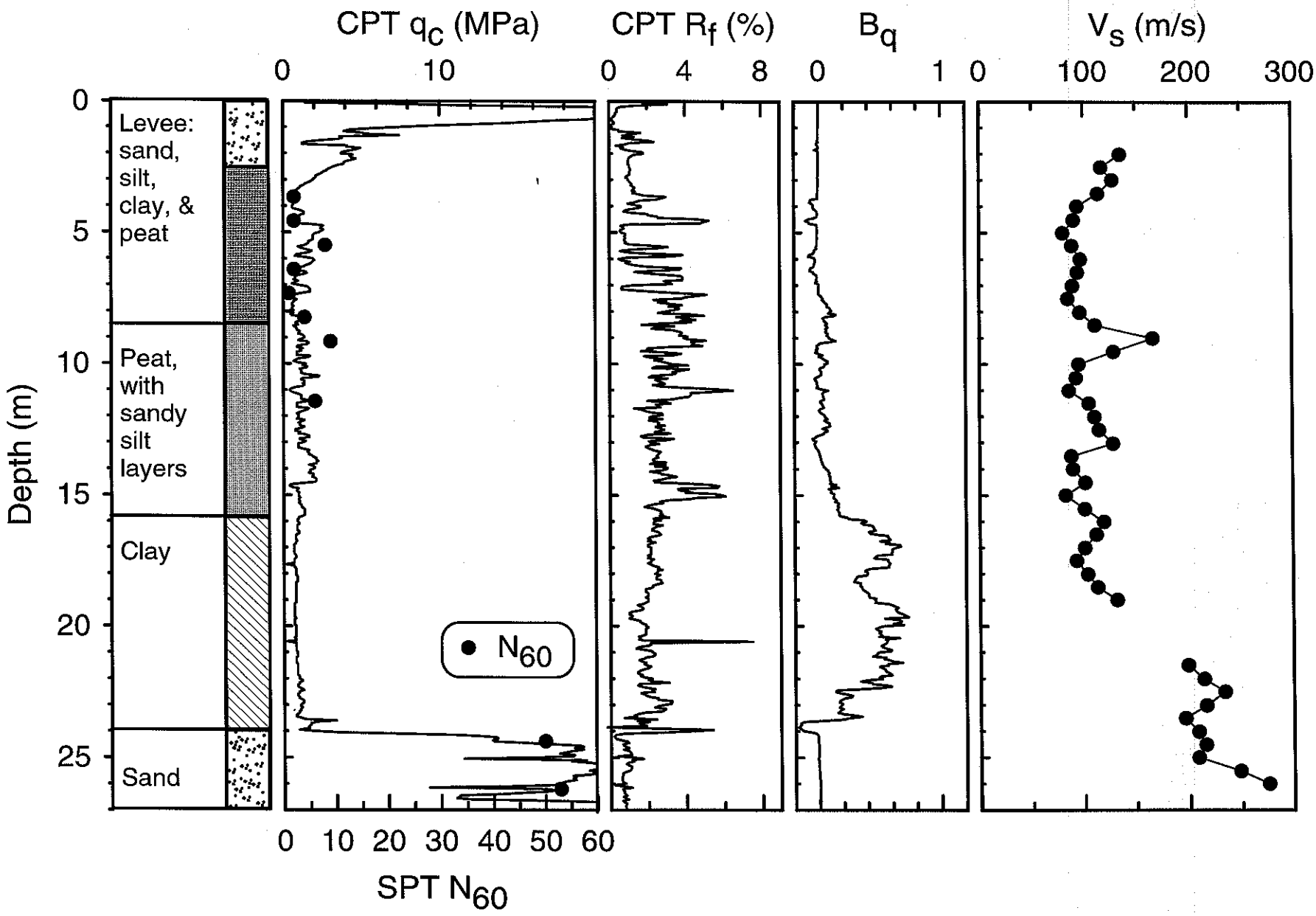

FIG. 2-3. CPT and Shear Wave Velocity Data at Sherman Island

InSitu-1.GRF

3. TRIAXIAL TESTING EQUIPMENT AND PROCEDURES

3.1. Cyclic Triaxial Equipment

All tests were performed in a cyclic triaxial device designed to measure stress-strain behavior over a wide range of strains (Gookin et al. 1996). Axial strains are measured three ways to provide overlapping data: high-resolution proximity transducers and a LVDT located inside the cell measure displacements of the top cap for calculating small strains, and another LVDT located outside the cell for calculating large strains. Loads for very small strains are measured using a low-capacity, protected load cell inside the cell, while loads at larger strains are measured using a larger capacity load cell outside the cell. A schematic of the testing device is shown in Fig. 3-1.

In addition, piezo-ceramic bender elements are mounted in the top and bottom caps to measure shear wave velocities (V_s) prior to cyclic loading, and hence obtain the maximum shear modulus (G_{max}). As illustrated in Fig. 3-2, a function generator is used to excite a transmitting bender element in the bottom cap, while a digital oscilloscope is used to simultaneously record the excitation signal at the transmitting bender element and the output signal from the receiving bender element in the top cap.

Tatsuoka et al. (1994) reported that axial strains measured from the top cap in triaxial tests on granular soils tend to be larger than those measured locally on the specimen, with the difference attributed to bedding errors between the specimen and the end caps. The sources of bedding errors depend on the end boundary conditions, and may include: (1) compliance at lubricated ends, which often consist of alternating layers of membrane and grease at the ends; (2) compliance between full-face porous stones and end caps; and (3) compliance at the bedding contact between the soil and the end caps or full-face porous stones. Another potential error can arise from nonuniform strains along the length of the specimen due to the constraining effects of nonlubricated end caps. This error may be expected to cause axial strains measured from the top cap to be smaller than those measured locally on the middle portion of the specimen. Tatsuoka et al. (1994) concluded that bedding errors were important except for tests on soft clays. Since the Sherman Island peat specimens are softer (in terms of stiffness) than most soft clays, Tatsuoka's conclusion suggests that axial strain measurements from the end caps would be as accurate as local strain measurements in the current study.

In addition, our experience with local versus end cap measurements of small strains on sand specimens have shown good agreement, with the local strain measurements actually being slightly greater in some cases (Gookin et al. 1996). The good agreement between local strain measurements and end cap measurements observed in our tests are attributed to the nonlubricated end conditions, the porous stones being small inserts in the end caps, and the use of internal proximeter transducers having a much greater resolution than those used by Tatsuoka (1994). Regarding this last item, the full range of the proximeter transducers used in this study cover an axial strain of only 0.02%, whereas Tatsuoka used proximeter transducers that covered axial strains as great as 5%. Consequently, local strain measurements were not considered necessary

in the current study because of our good past experience with high resolution proximeter transducers and the soft nature of the peat being tested.

3.2. Sample Preparation and Consolidation

In preparation for sample extrusion, a 22 cm length of the tube containing the desired sample interval was cut from the Shelby tube using a pipe cutter. The tube was supported by 2.5-cm-thick aluminum ring clamps immediately above and below the pipe cutter, and held in a vertical position during the cutting process. These very stiff ring clamps minimized any potential distortion of the tubes or enclosed soil during the cutting process. After the pipe cutter had broken through the tube, a wire saw was used to cut across the enclosed soil prior to separating the two halves of the tube. A deburring tool was used to remove the recessed edge of the top cut, the sample was extruded about 1 cm, and the sample cut smooth across the top of the tube. A 15 to 17 cm length of sample was extruded, cut across it's bottom, and carefully transferred upright onto the bottom triaxial cap. A membrane was then placed around the specimen, a full vacuum applied for typically one hour, and then the specimen transferred to the triaxial cell for testing.

Specimens were first back-pressure saturated with a back-pressure of typically 100 kPa, while the effective confining stress was maintained constant at about 100 kPa. Specimens were then isotropically consolidated to the desired confining stress. End-of-primary consolidation typically took about 12 hours, after which about 6 hours of secondary compression was allowed to occur. Drainage lines were then closed, and the specimen left for another hour prior to cyclic testing.

The testing sequence began with a bender element test, and was then followed by a series of staged cyclic loading tests as described in a following section. B-values were measured prior to cyclic loading and just after cyclic testing, with all but one specimen having B values greater than 0.96 at both times. Test No. 10 had a B value of only 0.82, but, interestingly, its behavior during cyclic loading was indistinguishable from that of the other specimens.

Diffusion of air into the cell water and across the specimen membrane was a concern because of the long duration of the tests. Normally, air diffusion can be avoided in 1 or 2 day tests by completely filling the cell with water, but this was not possible because the internal LVDT and load cell were not submersible. This potential problem was circumvented by filling the cell with water to the middle of the top cap (submerging the specimen), and then replacing the cell water with freshly de-aired water after 12 hours. The success of this approach was confirmed by the good B values obtained before and after cyclic testing.

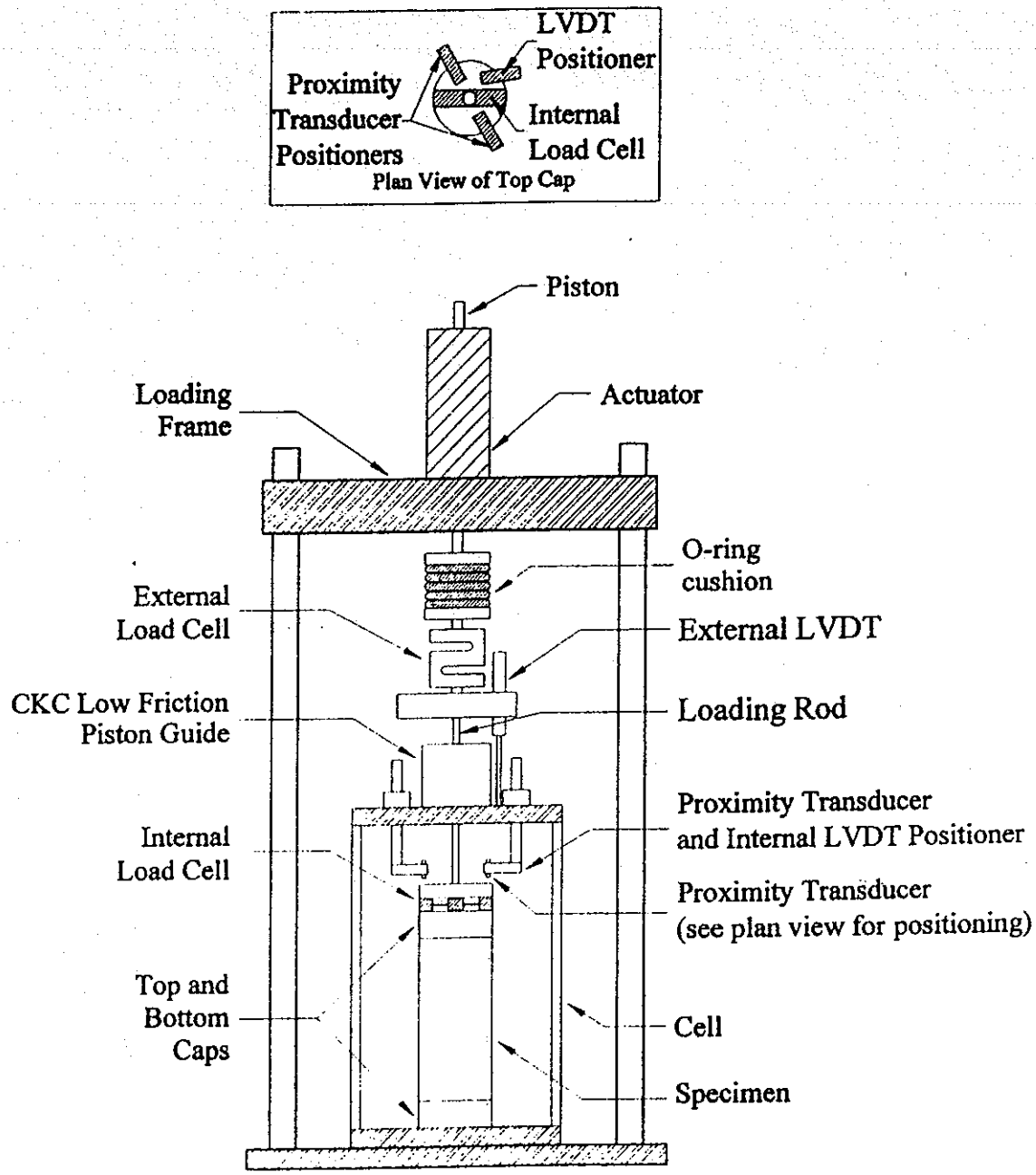

FIG. 3-1. Schematic Diagram of Cyclic Triaxial Device (Gookin et al. 1996)

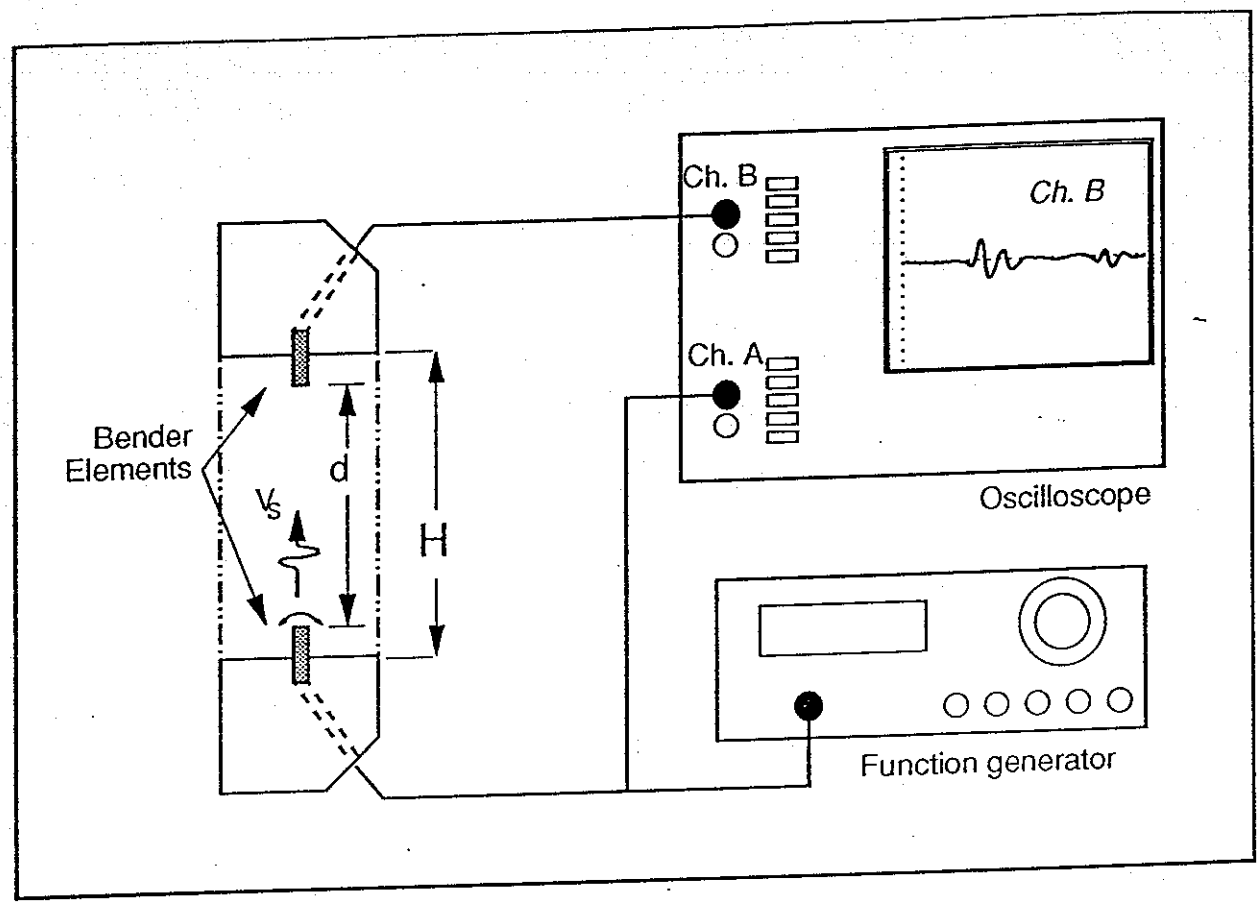

FIG. 3-2. Schematic Diagram of Bender Element Arrangement

4. BENDER ELEMENT TESTS

4.1. Interpretation of Bender Element Signals

Bender element tests were performed prior to cyclic loading, and the measured shear wave velocity (V_s) used to calculate G_{max} as:

$$G_{max} = \rho \times V_S^2 \tag{4.1}$$

where ρ is the density of the specimen. Time histories of the transmitted signal and the received signal for a typical test are shown in Fig. 4-1(a). There are several methods for interpreting the travel time (and hence V_s) of the shear waves in the soil based on the transmitted and received signals. One approach is the use of characteristic points (usually the peaks), in which the travel time would be taken as the time between point A on the transmitted signal and point A′ on the received signal (or B to B′). A second approach is the use of cross-correlation techniques, where the transmitted and received signals are cross-correlated as:

$$CC(\tau) = \int_{-\infty}^{\infty} S_1(t+\tau) \times S_2(t)\, dt \tag{4.2}$$

where S_1 is the transmitted signal, S_2 is the received signal, τ is a time shift applied to S_1, and $CC(\tau)$ is the cross-correlation. Travel time is then the time shift τ producing the peak cross-correlation [point D in Fig. 4-1(b)]. However, the use of either of these methods is only appropriate when the same wave is measured at two spaced points. This necessary condition is not satisfied in the triaxial device for two main reasons (Arulnathan et al. 1996). First, the signals are affected by waves reflected from the relatively rigid end caps, and thus represent a complex interaction of incident and reflected waves. Second, there are phase (or time) lags between the electrical signals and the physical waves in the soil, particularly at the transmitting bender element.

An alternative approach to interpretation of bender element tests is to use the second arrival in the received signal: the second arrival refers to that part of the signal that is produced when the originally transmitted wave arrives at the receiver cap for the second time (Arulnathan et al. 1996). In this case, the first and second arrivals of the shear wave at the receiver cap are equally affected by the above two sources of error (wave reflection, and phase lags between electrical and physical waves). Thus, it is theoretically acceptable to estimate travel time using the time between the characteristic peaks A′ and A″ (or 'B and B″, C′ and C″) in Fig. 4-1(a). Similarly, the received signal can be cross-correlated with itself to obtain the travel time between the first and second arrivals. For clarity, this is done by breaking the received signal into two dummy signals prior to cross-correlating them: one dummy signal containing the first arrival and zero signal elsewhere, and the second dummy signal containing the second arrival and zero signal elsewhere. This approach was used to produce the cross-correlation in Fig. 4-1(c), with the travel time being at point E. Note that very nearly the same answer can be obtained as the

difference between points D and D′ on the cross-correlation of the input and output signals [Fig. 4-1(b)].

A comparison of V_s values calculated by the above procedures for the test shown in Fig. 4-1 is presented in Table 4-1. The methods that use the transmitted and received signal gave V_s values of 87-89 m/s for this specimen, while the second arrival methods gave V_s values of about 81-82 m/s. Thus, the methods that use the transmitted and received signals gave V_s values that were about 9% greater than by the second arrival methods, which corresponds to a 18% difference in G_{max} values.

4.2. Comparison of In Situ and Laboratory Shear Wave Velocities

The results of the bender element tests, as summarized in Table 2-1, showed V_s values ranging from 81 to 87 m/s (average of 84 m/s) for the specimens that were reconsolidated to their in situ vertical effective stress. These samples were obtained between depths of 12.8 and 13.7 m, and were specifically selected for their high organic contents. The corresponding OYO V_s measurements at these depths (Fig. 2-3) show V_s values ranging from approximately 83 to 90 m/s. Slightly higher V_s values were recorded at other depths within the peat layer (9.5 to 15.5 m depth), but a comparison of the borehole logs and the V_s profile indicates that these higher V_s values tend to occur where there are sandy silt interlayers. Thus, there is very good agreement between the in situ and laboratory V_s data, which suggests that the low strain shear moduli of the laboratory specimens were not significantly affected by sampling disturbance.

TABLE 4-1. Comparison of V_s Interpretation Methods for Test No. 1

	Using Transmitted & Received Signals	*Using First & Second Arrivals in Received Signal*
Characteristic peaks	87.3 m/s [a]	80.5 m/s [b]
Cross-correlation	88.7 m/s	81.7 m/s [c]

Notes. Input signal frequency was 1.1 kHz. The resulting ratio of wave length (λ) to bender element length (l_b) was $\lambda/l_b = 15$, and the ratio of wave travel distance for first arrival ("d" in Fig. 3-2) to λ was $R_d=d/\lambda=2.3$.

[a] Using the average of the travel times indicated by the two strongest peaks in the signals.

[b] Using the average of the travel times indicated by the three strongest peaks in the signals.

[c] Received signal split into two dummy signals containing first and second arrivals, respectively.

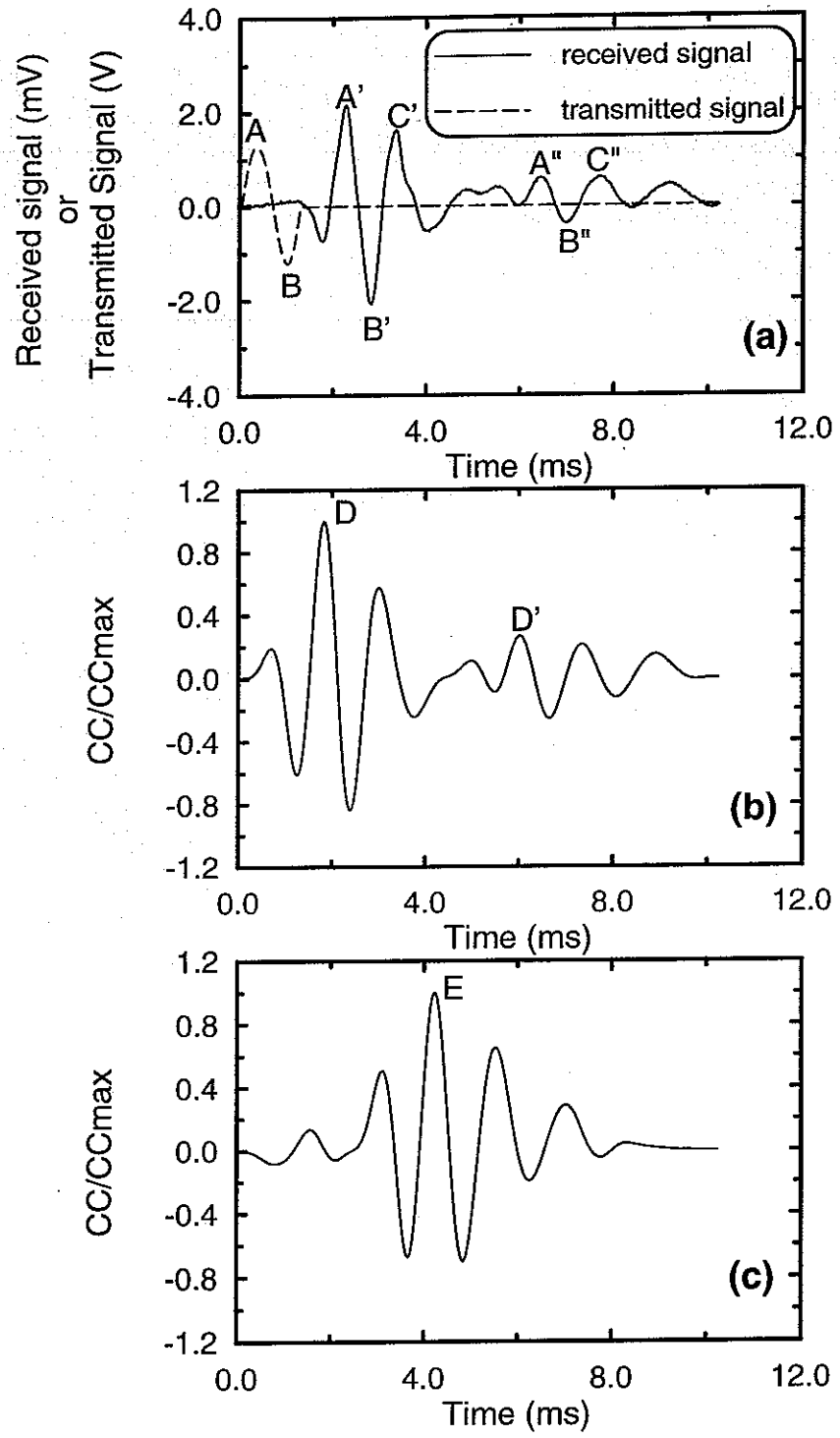

FIG. 4-1. Bender Element Results for Test No. 1: (a) Transmitted and Received Signals; (b) Cross- Correlation of Transmitted and Received Signals; (c) Cross-Correlation of First and Second Arrivals in Received Signal.

5. CYCLIC TRIAXIAL TESTING

A summary of the cyclic testing program is given in Table 2-1. Six specimens were isotropically consolidated to an effective stress (σ_{3c}') equal to their in situ vertical effective stress (σ_{vo}') of about 132 kPa. Two specimens were consolidated to about 200 kPa, or about 1.5 times their σ_{vo}'. Another two specimens were consolidated to their σ_{vo}' of about 132 kPa, and then rebounded to a σ_{3c}' of 66 kPa to evaluate the effects of stress history. Measurements of axial strain (ε_a) and axial Young's modulus (E_a) from undrained loading of these saturated specimens were converted to equivalent shear strain (γ) and shear modulus (G) as $\gamma=1.5\varepsilon_a$ and $G=E_a/3$.

Undrained, strain-controlled cyclic testing was performed in stages on each specimen as follows. Each stage consisted of five uniform cycles at a strain level greater than used in the previous stage. For shear strains (single amplitude) less than about $1x10^{-3}$%, some stages were repeated a second time to obtain less noisy measurements, or the strain level was increased by a factor of 1.5 to 2.0 for the next stage of cycles. For shear strains above $1x10^{-3}$%, the strain levels for each stage were generally increased by about one-half a log-cycle (i.e., a factor of about 3). Specimens were kept undrained throughout all stages of loading. Using these staged testing procedures, it was believed that the effect of prior stages of cyclic loading on the secant shear modulus measured in the fifth cycle of a subsequent stage of loading would be small (e.g., Tatsuoka et al. 1991). The reasonableness of this approach for these peats was later verified by the test data (in the following section) which showed that the rate of cyclic degradation was relatively small.

The loading frequency for all cyclic tests except No. 12 (see Table 2-1) was 1.0 Hz for cyclic shear strains of up to 5%, after which it was reduced to 0.25 Hz due to the limitations of the hydraulic loading system. For test No. 12, loading frequencies of 0.01 Hz and 1.0 Hz were used for different stages to evaluate frequency effects.

Typical cyclic test results are shown by the stress-strain curves for test No. 1 in Fig. 5-1, and the corresponding plots of secant modulus and equivalent damping ratio versus shear strain (single amplitude) in Fig. 5-2. The stress-strain curves in Fig. 5-1 show almost linear behavior for shear strains of up to 0.1%, and very little degradation with increasing number of loading cycles even for shear strains of 3%. Stress and strain data for all cyclic loading stages on test No. 1 are presented in Appendix B. Noise in the stress and strain measurements at shear strains less than about $1x10^{-2}$% was filtered using the procedures described in Appendix A. These filtering procedures had no significant effect on the calculation of secant shear modulus, but did improve the reliability of equivalent damping ratio calculations.

The effects of loading frequency and cyclic degradation on shear modulus are illustrated in Fig. 5-3 showing the variation in secant shear modulus with number of loading cycles for test No. 12. Thirty cycles of loading were applied at shear strains of 0.003% [Fig. 5-3(a)], 0.01% [Fig. 5-3(b)], and 1.0% [Fig. 5-3(c)]. At each stage, the thirty cycles of loading were applied as alternating sets of five cycles at 1.0 Hz and 0.01 Hz. The effect of loading frequency was similar for all three shear strain levels, with the secant modulus being about 15-20% lower at the lower

loading frequency. This difference corresponds to about an 8-10% change in secant modulus per log cycle of loading frequency (using 1 Hz as the reference frequency).

The data in Fig. 5.3 also show that cyclic degradation of the secant modulus was very minor even at cyclic shear strains of 1%. The effect of cyclic degradation can be expressed by the degradation index (δ), which is the ratio of the secant modulus in cycle N (G_N) to the secant modulus in the first cycle (G_1). The value of δ decreases with increasing cycles, and can be approximately represented as (Idriss et al. 1978)

$$\delta = N^{-t} \tag{5.1}$$

where t is the degradation parameter. Referring to the data in Fig. 5-3, the value of t was only about 0.017 at cyclic shear strains of 1%. For comparison, Vucetic and Dobry (1991) used t=0.06 as being representative of high plasticity (PI≈50) clays.

The variation of equivalent damping ratio during the same test as shown in Fig. 5.3 (test No. 12) is shown in Fig. 5-4. Equivalent damping ratios are smaller at the higher loading frequency (1.0 Hz) than at the lower loading frequency (0.01 Hz). The difference between the equivalent damping ratios at 1 Hz and 0.01 Hz increased as the cyclic shear strain was increased. The observed decrease in damping ratio with increasing loading frequency for this specimen is opposite to the effect reported for peat by Stokoe et al. (1994), which was an increase in damping ratio with increasing loading frequency.

Results for all specimens are summarized in Fig. 5-5 showing the secant moduli and equivalent damping ratios versus shear strain for the fifth cycle of loading at a frequency of 1 Hz (0.25 Hz for strains greater than 5%). Summary plots of secant modulus and damping ratio versus shear strain for individual cyclic tests are presented in Appendix C. The six specimens that were reconsolidated to their in situ σ_{vo}' (open symbols in Fig. 5-5) are surprisingly consistent for field samples. Nearly linear behavior, in terms of negligible modulus reduction and low damping ratios, was exhibited for shear strains of up to about 0.1%. The two specimens that were consolidated to σ_{3c}' of 200 kPa (closed circles in Fig. 5-5) showed behavior very similar to the specimens consolidated to their in situ σ_{vo}'. The two specimens that were first consolidated to σ_{3c}' of 132 kPa and then rebounded to σ_{3c}' of 66 kPa (closed diamonds in Fig. 5-5) also showed behavior very similar to that of the other specimens. The fact that G_{max} was relatively unaffected as σ_{3c}' ranged from 66 to 200 kPa would be consistent with the peat having a preconsolidation stress that was close to, or greater than, 200 kPa. Preconsolidation stresses of close to 200 kPa are reasonably consistent with the range of consolidation test results by Roger Foott Associates (1991), as previously described.

The variation in normalized modulus reduction versus shear strain (G/G_{max} versus γ), and equivalent damping ratios versus shear strain, for the fifth cycle of loading on all specimens are shown in Fig. 5-6. A reasonable representation of the G/G_{max} and equivalent damping ratio data are given on Fig. 5-6 as upper range, lower range, and median curves. A set of data points describing the median curves are summarized in Table 5-1. The median G/G_{max} ratio remains

greater than 0.90 for shear strains of up to about 0.05%, and reduces to about 0.50 at shear strains of about 1%. The median damping ratio is less than about 5% for shear strains of up to about 0.05%, and increases to about 10% at shear strains of about 1%.

TABLE 5-1. Median Curves of Modulus Reduction and Equivalent Damping Ratio Versus Shear Strain for Sherman Island Peat

Cyclic Shear Strain (%)	Modulus Reduction Ratio G/G_{max}	Equivalent Damping Ratio (%)
0.0001	1.00	2.0
0.0003	1.00	2.0
0.001	1.00	2.0
0.003	0.99	2.3
0.01	0.96	3.0
0.03	0.92	3.9
0.1	0.85	5.5
0.3	0.76	7.3
1.0	0.54	10.1
3.0	0.30	14.1
10.0	0.08	18.5

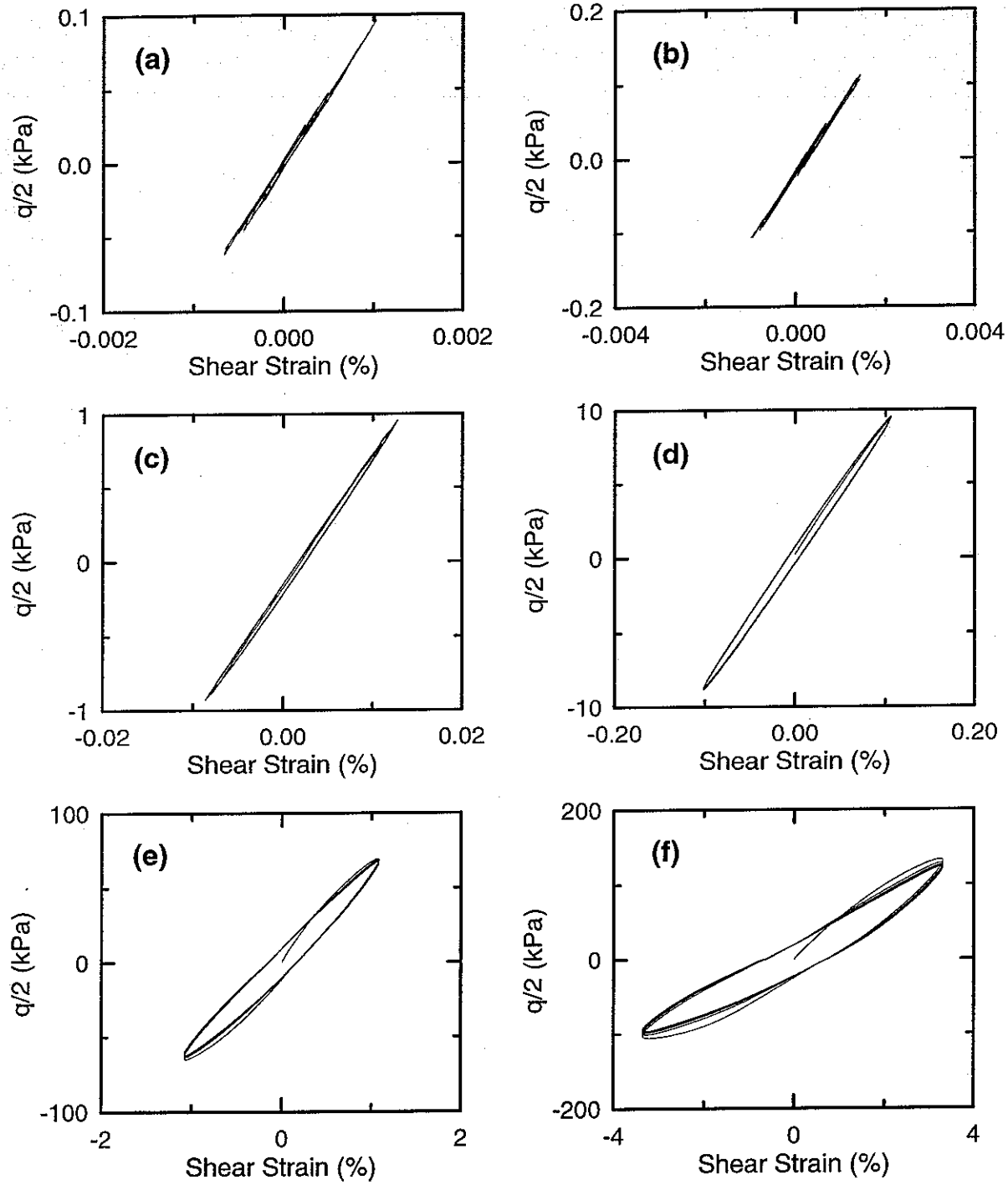

Fig. 5-1. Stress-Strain Curves for Test No.1

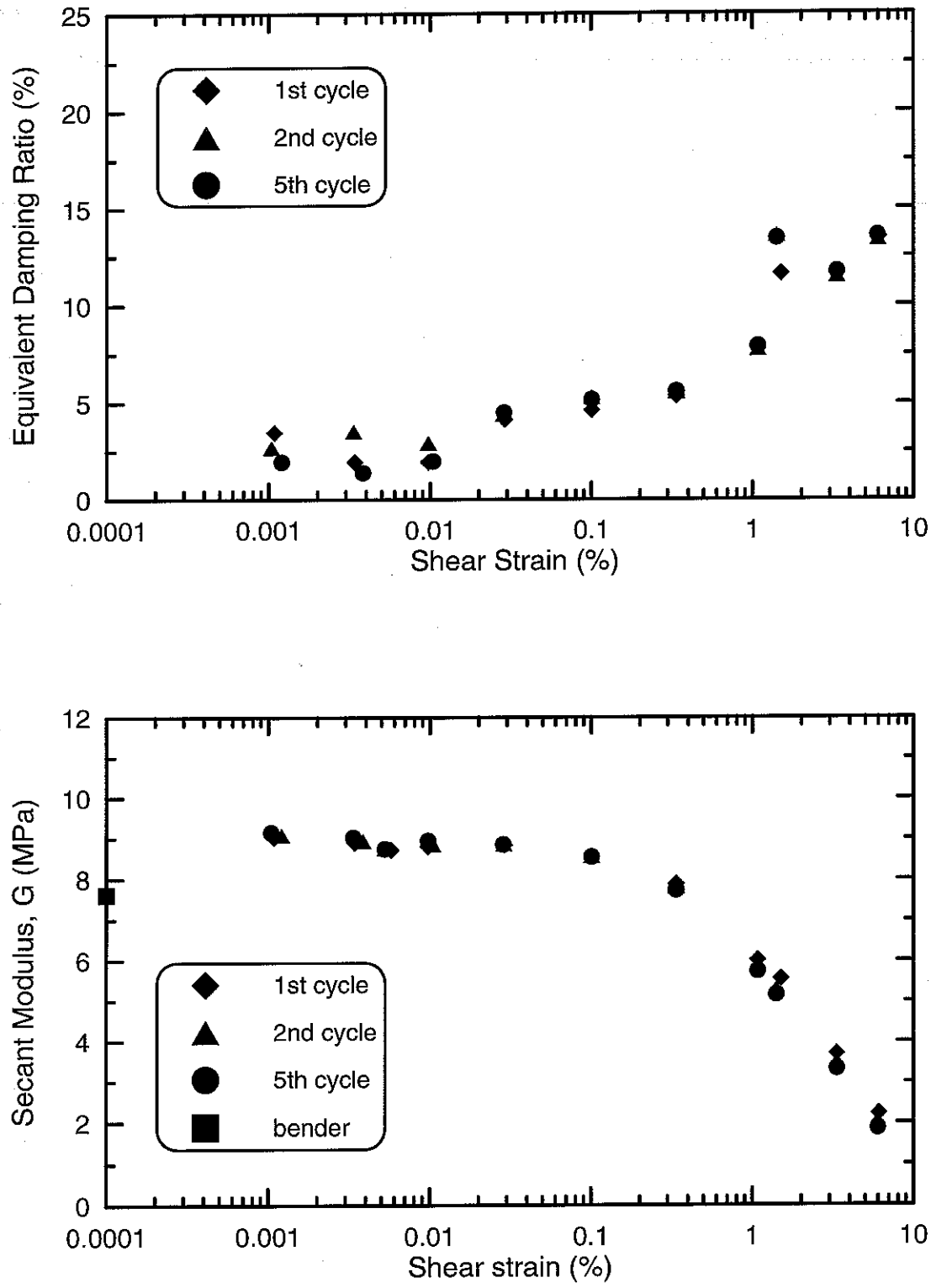

FIG. 5-2. Secant Modulus and Equivalent Damping Ratio Versus Shear Strain for Test No.1

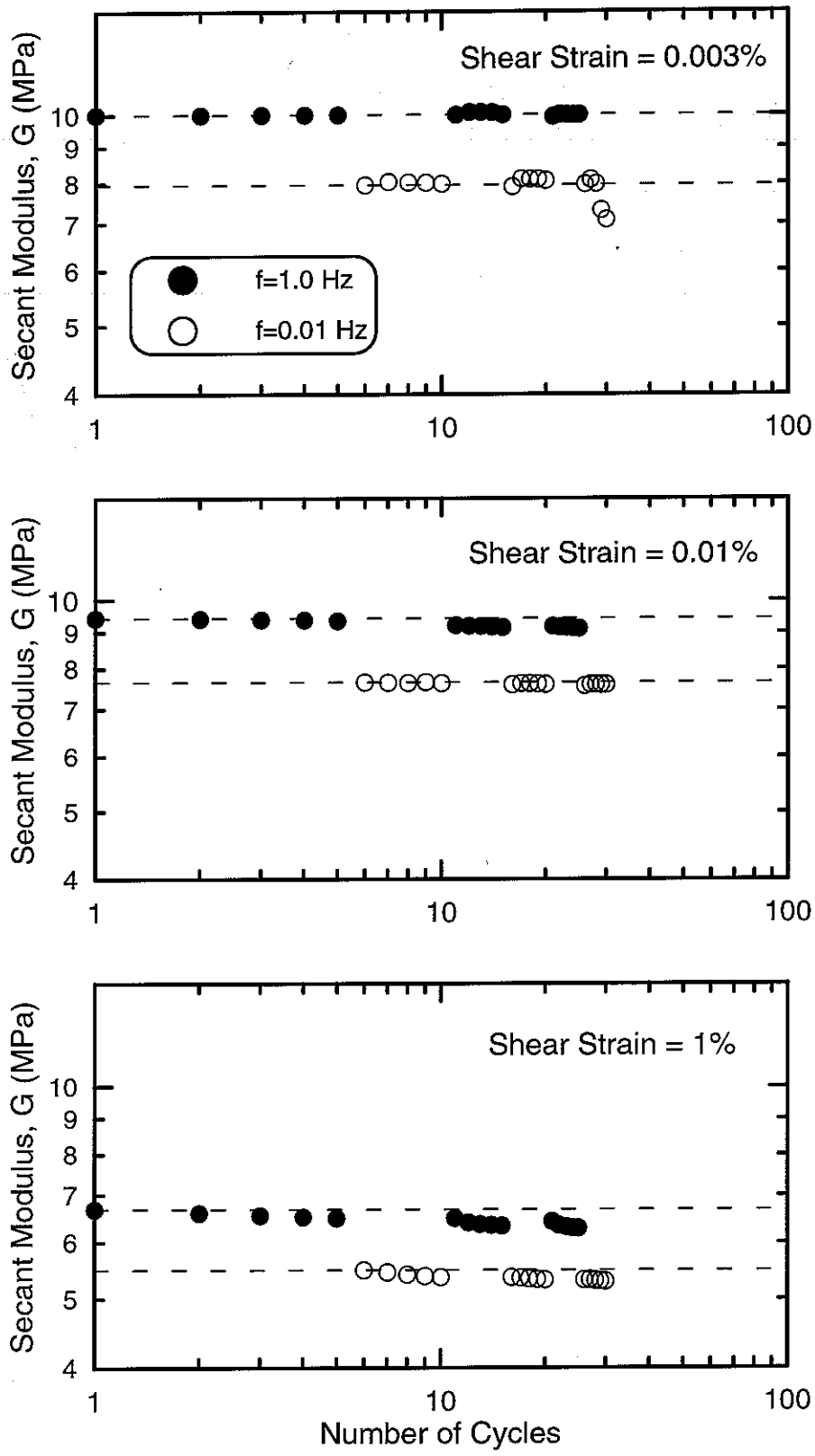

FIG. 5-3. Effect of Loading Frequency and Cyclic Degradation on Secant Modulus for Test No. 12

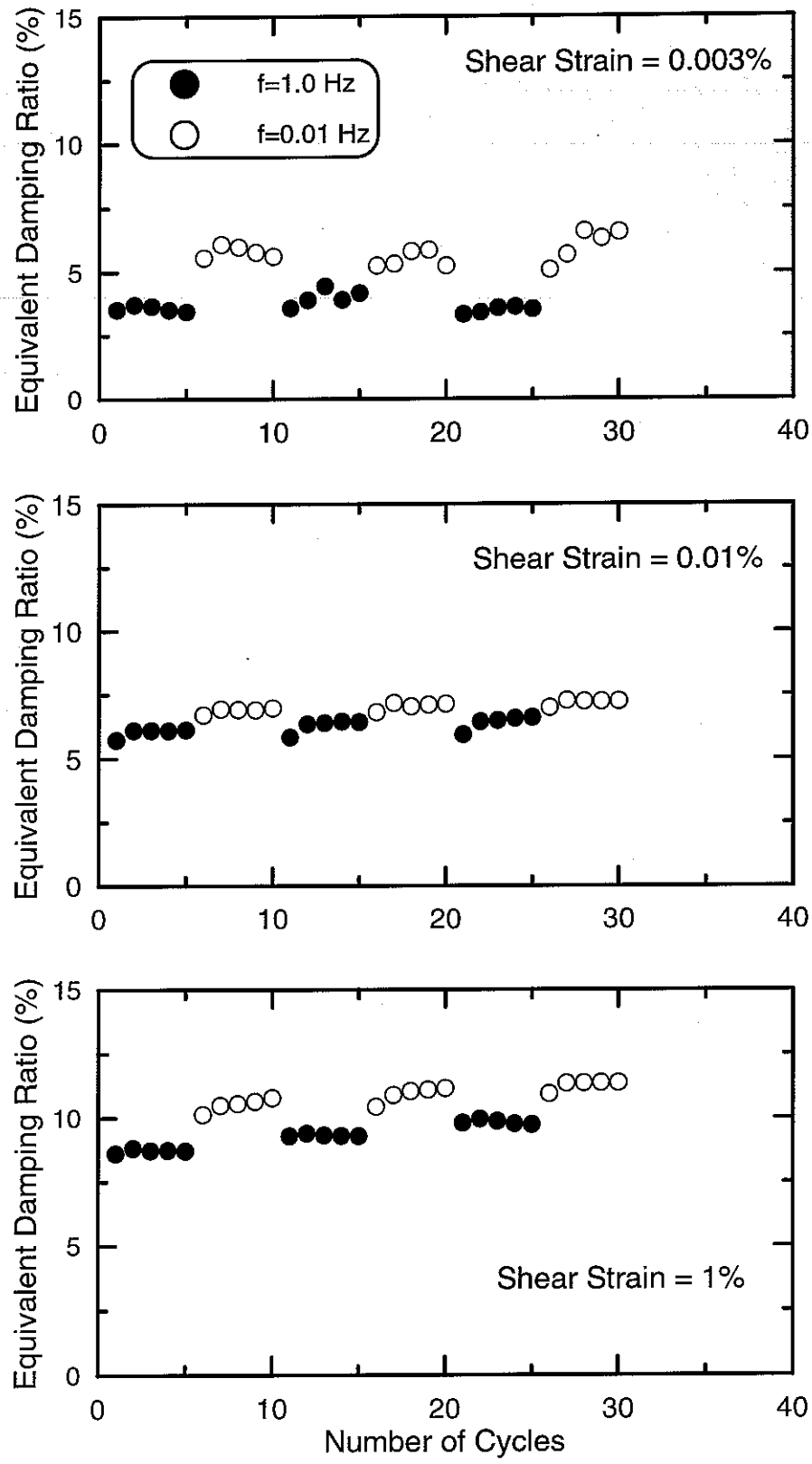

FIG. 5-4. Effect of Loading Frequency and Number of Cycles on Equivalent Damping Ratio for Test No. 12

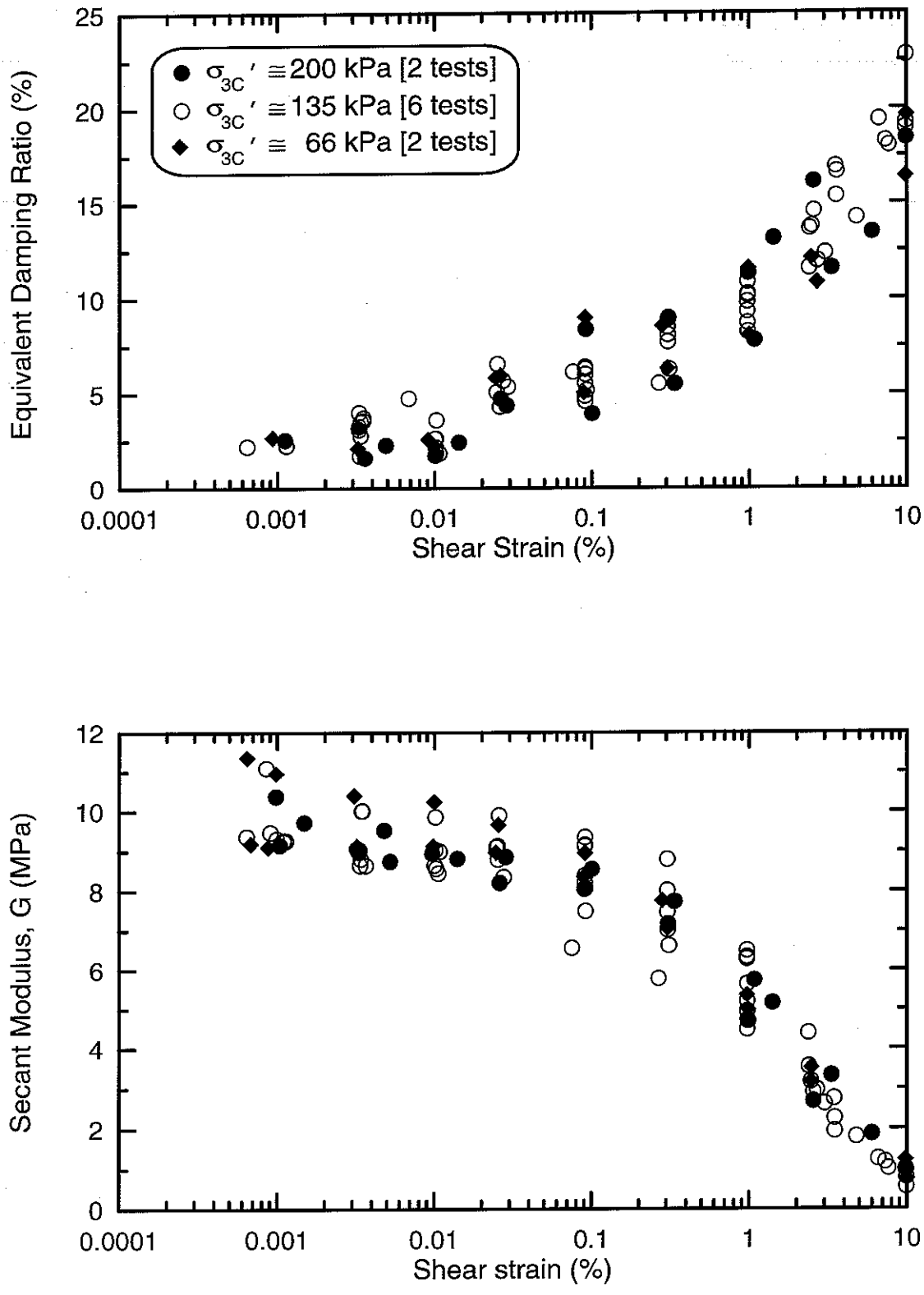

FIG. 5-5. Summary of Secant Modulus and Equivalent Damping Ratios Versus Shear Strain

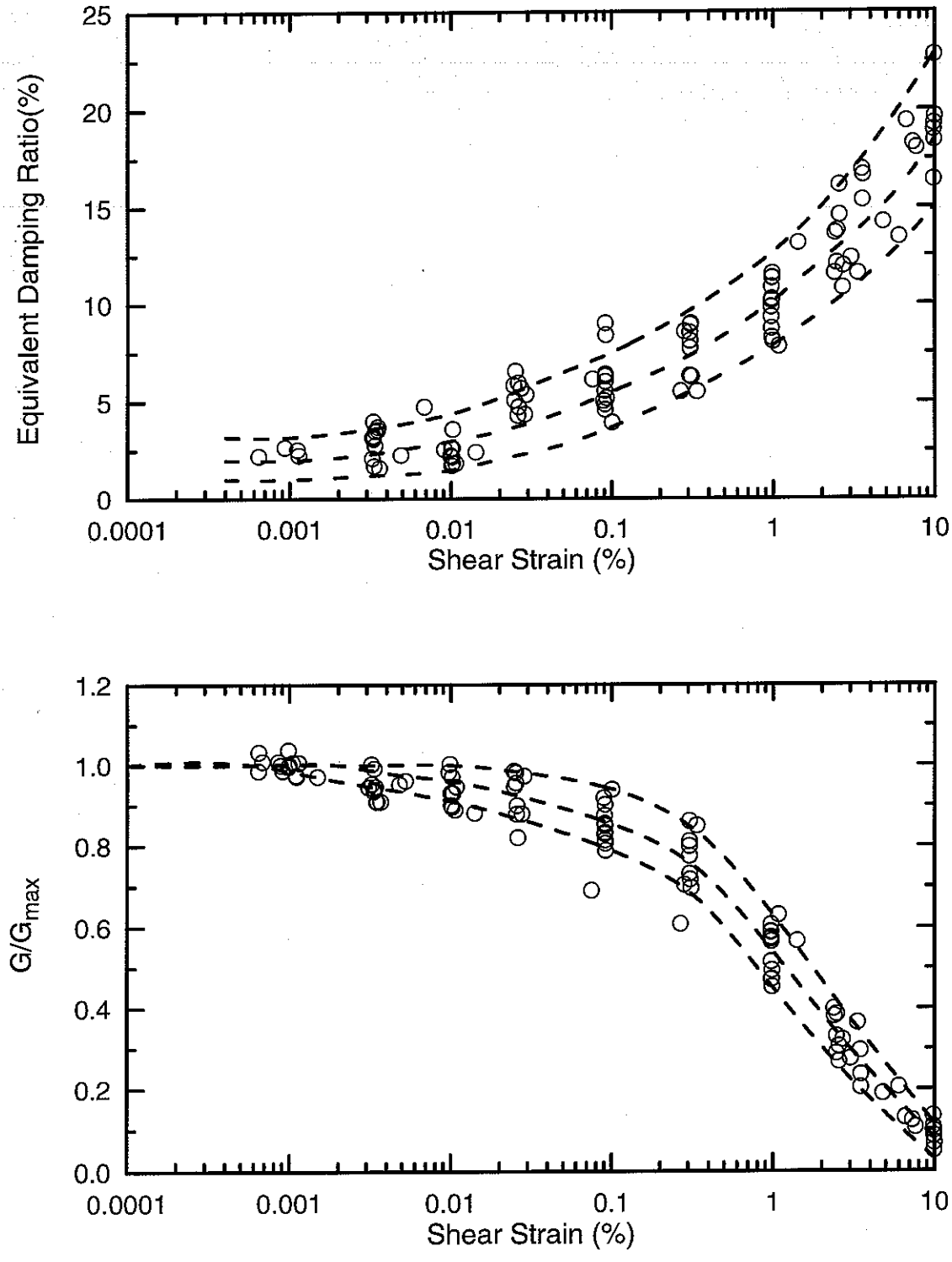

FIG. 5-6. Upper-Range, Median, and Lower-Range Curves of G/Gmax and Damping Ratio Versus Shear Strain for all Specimens

6. MONOTONIC TESTS

The results of the monotonic, strain-controlled triaxial compression and extension tests are presented in Fig. 6-1 as plots of normalized deviator stress (q/p_c') versus axial strain (ε_a) and normalized deviator stress versus normalized mean effective stress (p'/p_c'). These two specimens were isotropically consolidated to a mean effective consolidation stress (p_c') of about 130 kPa, following the same procedures previously described for the cyclic testing program. These tests were run with the drainage lines closed, but the response under compression produces effectively "drained" behavior past point A on Fig. 6-1, as will be discussed below. The loading rate was about 0.33% axial strain per hour, which was sufficiently slow to allow for pore pressure equalization throughout the specimens. These tests will be called "slow" tests herein.

The compression test showed a progressive increase in excess pore pressure (i.e., decreasing p') and deviator stress (q) as axial strain increased up to point A in Fig. 6-1. At point A, the pore pressure equaled the radial confining pressure and thus the radial effective stress (i.e., σ_3') was equal to zero. Past point A, the deviator stress continued to increase with no further change in pore pressure; hence σ_3' remained equal to zero, and p' was equal to $q/3$. Also, there is a notable decrease in the stiffness of the specimen at point A, as shown by the plot of q versus ε_a in Fig. 6-1. The specimen's continued resistance to shear while $\sigma_3'=0$ demonstrates that the reinforcing effects of the organic fibers are extremely important under compressive loading. Note that loading beyond point A resulted in incrementally drained conditions because the confining membrane could easily expand (since $\sigma_3'=0$) to accommodate movement of pore water towards the lateral boundaries.

The extension test showed a progressive decrease in pore pressure and increase in deviator load (extension) as the extension axial strain was increased. Data are only shown for axial strains of up to -6% because the specimen "necked" at that point and any additional data became meaningless.

The stress paths (q versus p') for compression (up to point A in Fig. 6-1) and extension show that the peat specimen has strong cross-anisotropy, with the specimen being stiffer in the horizontal plane than in the vertical direction. Recall that triaxial compression or extension loading of a saturated isotropic elastic material would result in a vertical stress path on the q versus p' diagram. For soils without strong cross-anisotropy, the stress path is nearly vertical at small loading levels and then curves as the soil yields. The stress path for the compression test in Fig. 6-1 is almost linear from the start of compressive loading up to point A, and the stress paths for both the compression and extension tests are clearly inclined to the left for small levels of loading. These stress paths would be expected for cross-anisotropic elastic materials that are stiffer in the horizontal direction than in the vertical direction (Graham and Houlsby 1983).

"Fast" monotonic loading tests using more conventional rates of loading (e.g., 15% axial strain per hour) on these peat specimens resulted in unreliable measurements of pore pressures. In these "fast" tests, excess pore pressures increased to values that exceeded the confining pressure and thus indicated negative values of σ_3'. Negative values of σ_3' cannot occur at the

membranes along the lateral boundaries, and thus it was clear that the pore pressures measurements only represented the conditions near the middle of the end caps. Note that the pore pressure measurement lines connect to small porous stones near the middle of the top and bottom caps, and hence the pore pressure measurements only reflect conditions at these locations. It is also possible that the reinforcing effects of the organic fibers and friction along the end caps resulted in a local increase in total stress in the regions near the porous stones, and thus the calculated value of σ_3' is misleading both for the end zones as well as for the remainder of the specimen. It is clear, however, that significant pore pressure gradients and nonuniform effective stress conditions must have existed within the specimens and thus the effective stress paths are unreliable for these "fast" tests. The choice between "slow" and "fast" testing conditions, however, depends on the type of information that is desired.

The need for "slow" monotonic loading to obtain reliable measurements of pore pressures, and hence effective stresses, has previously been emphasized for clay specimens by Zergoun and Vaid (1994). The effect of loading rate on pore pressure measurements is, however, much greater for peat than for clay. This may be because of the peat's highly fibrous fabric, strong cross-anisotropy, high compressibility, scale effects (i.e., specimen size versus characteristic particle or fiber size), or other factors not yet understood.

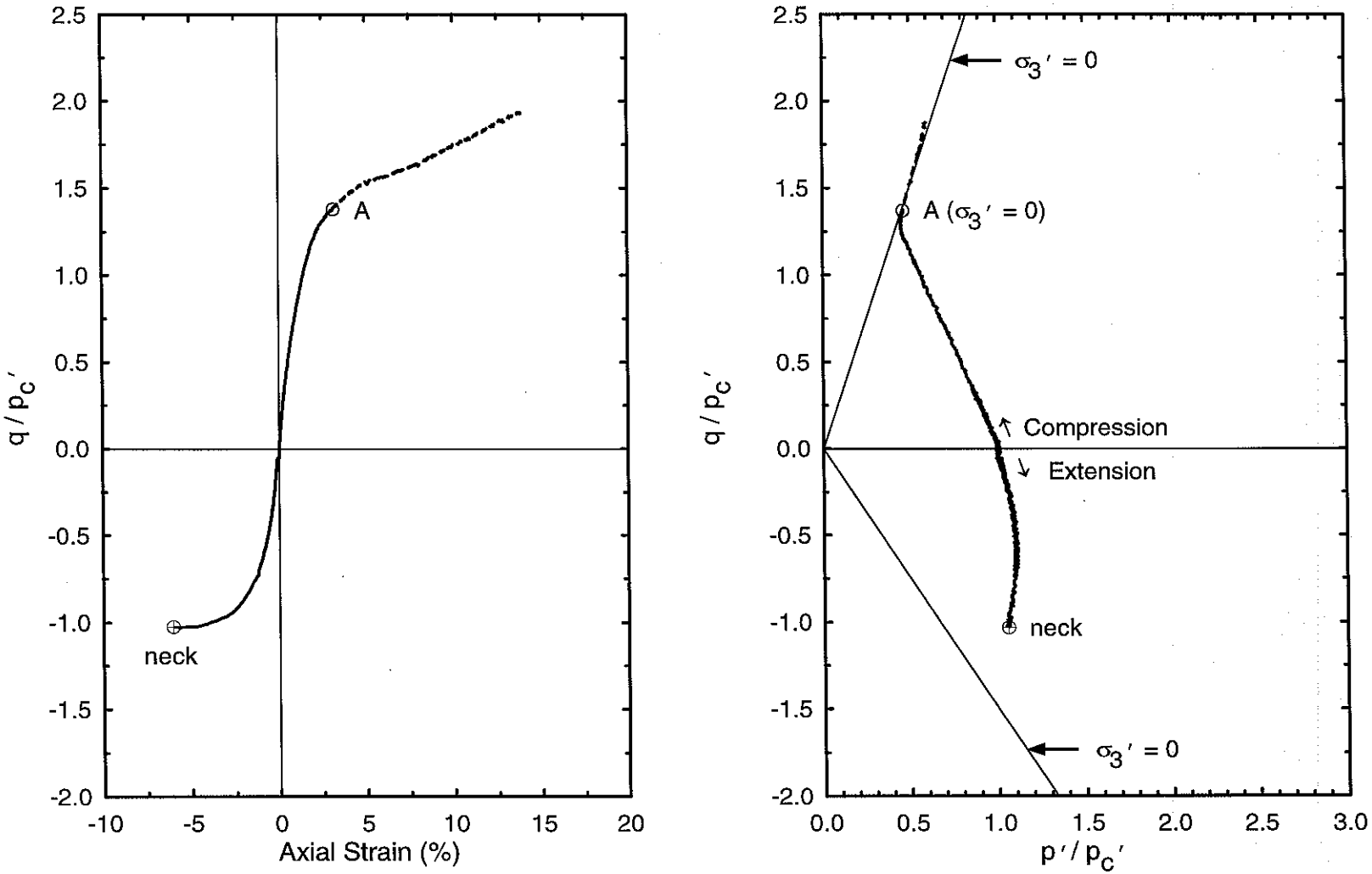

Fig. 6-1. Monotonic Compression and Extension Test Results

7. DISCUSSION

The median modulus reduction and damping relationships for the peat specimens (Fig. 5-6) are compared to the curves recommended by Vucetic and Dobry (1991) for normally and overconsolidated clays of varying plasticity in Fig. 7-1. The peat specimens showed a response that is roughly comparable to that of high plasticity clays with PI's of 100 to 200. This relatively linear behavior is in agreement with the data by Stokoe et al. (1996) for peat from a similar range of consolidation stresses. The behavior is much more linear than obtained by Kramer (1996) for unconsolidated peat, but he also observed that the behavior became more linear with increasing consolidation stress, and thus the difference may be due to the effect of consolidation stress.

The median modulus reduction and damping relationships for the peat specimens are compared, in Fig. 7-2, to the curves derived for Union Bay peat by Seed and Idriss (1970) and the curves derived for solid waste materials based primarily on the recorded earthquake motions at the OII landfill by Idriss et al. (1995), GeoSyntec (1996), and Augello et al. (1997). This comparison is of interest because it has often been suggested that solid waste materials and peat may have similar modulus reduction and damping relationships. As shown in Fig. 7-2, the curves for Sherman Island peat generally show the least modulus reduction, with the closest similarity to the curves by Idriss et al. (1995) and GeoSyntec (1996). The damping ratio curves for Sherman Island peat are generally lower (i.e., more linear behavior) than for any of the other curves.

The relatively linear G/G_{max} behavior of peat does not imply that its shear modulus (G) is greater than that of most clays. For example, the peat can be compared to the underlying clay layer at Sherman Island. As shown in Fig. 2-3, the high plasticity clay between depths of 15.5 and 19 m has an average V_s value of about 109 m/s (range is 93 to 132 m/s), a total unit density of about 1.7 Mg/m^3, and thus a typical G_{max} value of about 20.2 MPa. The peat layers between depths of 9.5 and 15.5 m have an average V_s value of about 87 m/s, a typical total unit density of about 1.15 Mg/m^3, and thus a typical G_{max} of about 8.7 MPa. Thus, the typical G_{max} value for the underlying clay is about 2.3 times the typical G_{max} value for the Sherman Island peat, with about one-half the difference represented by their differences in V_s values and the remainder represented by their differences in density. The shear modulus (G) of the clay would remain greater than that of the peat during earthquake loading as long as the G/G_{max} ratio for the clay was greater than about 0.43 times the G/G_{max} ratio for the peat. It is possible, however, that the modulus of the clay could be reduced below that of the peat by strong enough earthquake shaking, depending on the shear modulus reduction characteristics of the clay (e.g., refer to Fig. 7-1).

The G_{max} values obtained from the bender element tests on the peat specimens were about 20% smaller than those obtained from the direct stress-strain measurements, as shown on Fig. 5-2 for Test No. 1 and in Appendix C for all other tests. This difference in G_{max} could easily be attributable to structural anisotropy, with the peat being softer under the horizontal shearing produced by the bender element tests than under the axial loading condition used to obtain stress-strain measurements. Strong cross-anisotropy of the peat was clearly indicated by the effective stress paths during monotonic compression and extension loading, and is consistent with the

visible layering of fibers within the specimens. Additional research is needed to investigate how structural anisotropy, and other factors such as specimen size, may affect the modulus reduction and damping relationships for peat.

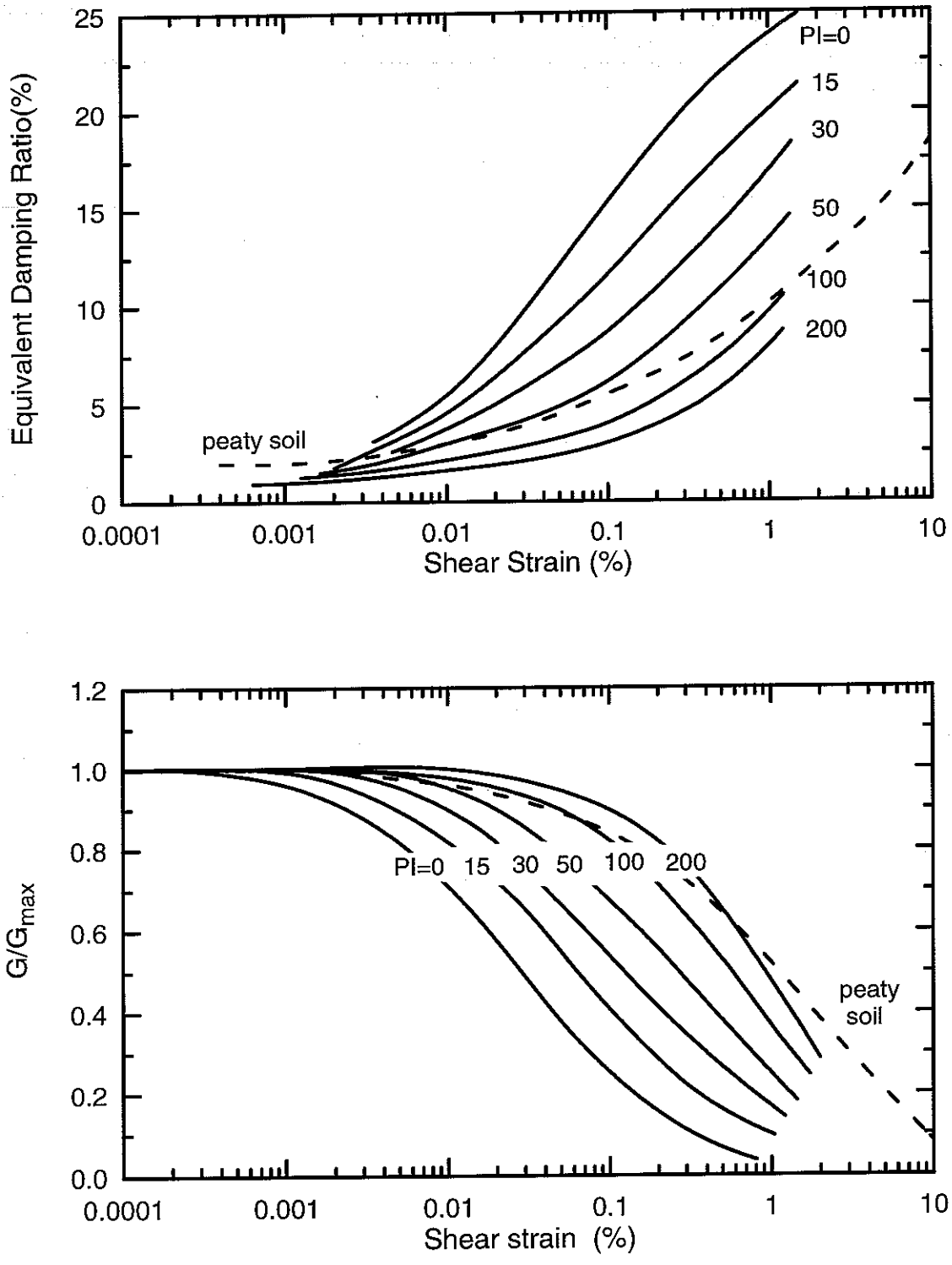

FIG. 7-1. Median G/G_{max} and Damping Ratio Curves for Sherman Island Peat Versus Curves Recommended for Normally Consolidated and Overconsolidated Clays of Varying Plasticity by Vucetic and Dobry (1991)

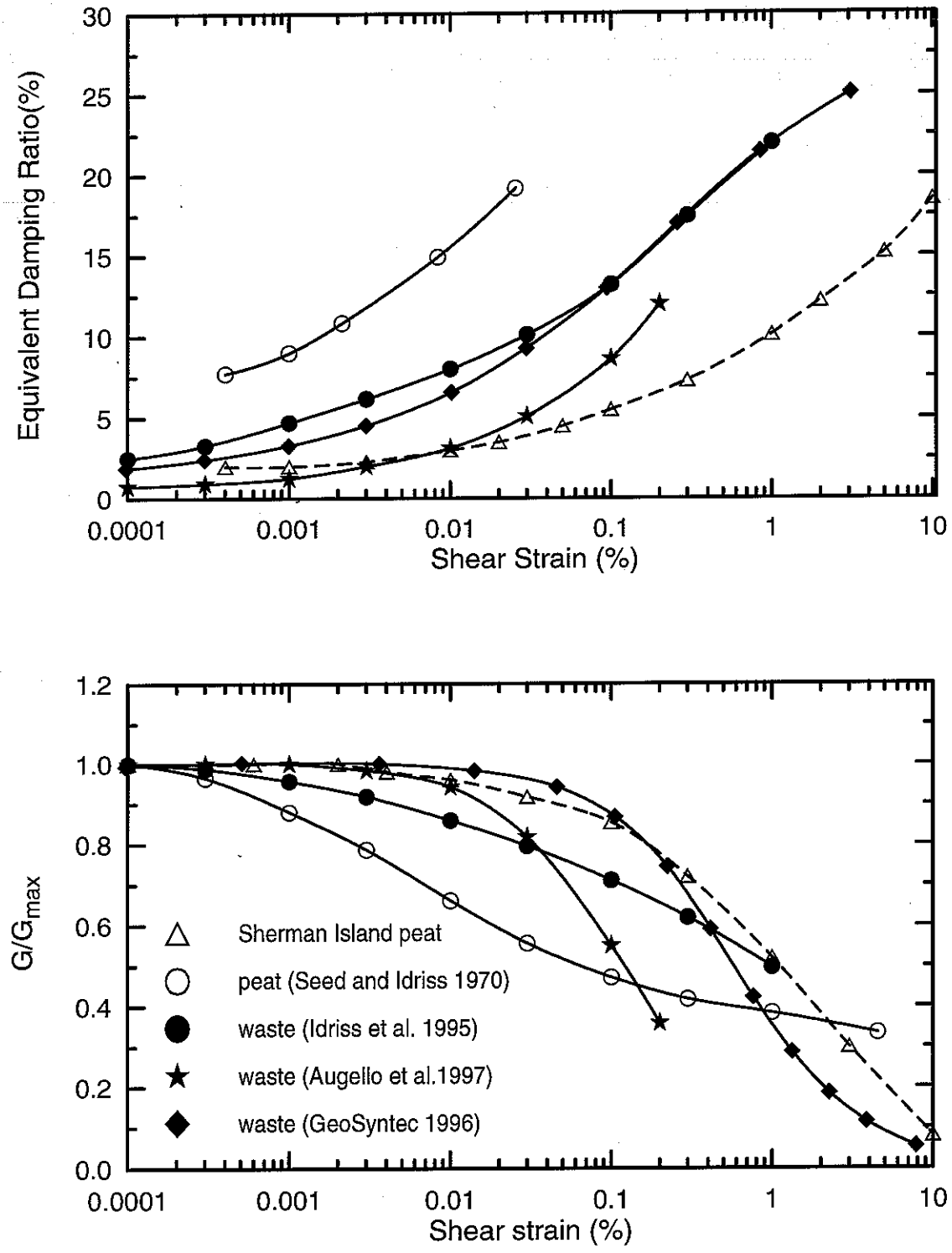

FIG. 7-2. Median G/G_{max} and Damping Ratio Curves for Sherman Island Peat Versus Curves for Union Bay Peat and Solid Waste Materials

8. SUMMARY

This report summarizes the results of a laboratory study of the dynamic properties of a layer of peat underlying the south levee on Sherman Island near the western side of the Sacramento-San Joaquin Delta. Conventional Shelby tube sampling procedures were able to obtain high quality samples because of the compactness of this peat layer, which has been highly compressed under the weight of the levee. The samples tested came from depths of about 13 m where the vertical consolidation stresses (σ_{vc}') were about 132 kPa. The samples tested were very fibrous with ash contents of 35-56%, and would classify as peaty organic soil according to ASTM standards. Staged cyclic loading was used to measure the stress-strain behavior of several specimens under cyclic shear strains ranging from about $5x10^{-4}$% to 10%. The experimental procedures and results were presented in detail because of the limited experimental data currently available for peat and peaty organic soils.

The modulus reduction and damping relationships for the Sherman Island peat were roughly comparable to those recommended for high plasticity clays (PI of 100-200) by Vucetic and Dobry (1991). Secant shear moduli and damping were found to be somewhat dependent on the loading frequency, and relatively unaffected by cyclic degradation. The relatively linear behavior of Sherman Island peat is in agreement with the data by Stokoe et al. (1996) for two peat samples with similar ash contents (37 and 65%) and similar consolidation stresses (σ_{vc}' of about 114 kPa).

Modulus reduction and damping relationships for "peat" may depend on numerous factors that have not yet been explored, including loading path and specimen size effects. Additional laboratory testing is needed on samples from other sites, covering a range of material characteristics (e.g., ash content, fabric) and consolidation stress conditions. Extrapolation of the results presented in this report to other conditions must take these uncertainties into consideration.

REFERENCES

Arulnathan, R., Boulanger, R. W., and Riemer, M. F. (1997). "Analysis of bender element tests." MS report, Department of Civil & Environmental Engineering, University of California, Davis, CA; Also submitted September 1996 to the Geotechnical Testing Journal, American Society for Testing and Materials, Philadelphia, PA.

Augello, A. J., Bray, J. D., Abrahamson, N. A., and Seed, R. B. (1997). "Dynamic properties of solid-waste based on back-analysis of the OII landfill." Submitted to the Journal of Geotechnical Engineering, ASCE, New York, N.Y.

ASTM (1994). "D2487-92 - Classification of Soils for Engineering Purposes." Annual Book of ASTM Standards, Part 19, American Society for Testing and Materials, Philadelphia, PA.

ASTM (1994). "D2794 - Test for moisture, ash, and organic matter of peat materials." Annual Book of ASTM Standards, Part 19, American Society for Testing and Materials, Philadelphia, PA.

ASTM (1994). "D4427-92 - Classification of Peat Samples by Laboratory Testing." Annual Book of ASTM Standards, Part 19, American Society for Testing and Materials, Philadelphia, PA.

California (1992). "Seismic stability evaluation of the Sacramento-San Joaquin Delta levees." Phase I Report: Preliminary Evaluations and Review of Previous Studies, Division of Design and Construction, Department of Water Resources, The Resources Agency, August.

GeoSyntec (1996). "Summary report of findings, seismicity, settlement, and slope stability work plan, Operating Industries, Inc., Landfill, Monterey Park, California." Report No. SWP-9, GeoSyntec Consultants, Huntington Beach, California.

Gookin, W. B., Riemer, M. F., Boulanger, R. W., and Bray, J. D. (1996). "Development of cyclic triaxial apparatus with broad frequency and strain ranges." Transportation Research Record 1548, TRB, National Research Council, Washington, D.C., pp. 1-8.

Graham, J., and Houlsby, G. T. (1983). "Anisotropic elasticity of a natural clay," Geotechnique 33(2), pp. 165-180.

Idriss, I. M., Dobry, R., and Singh, R. D. (1978). "Nonlinear behavior of soft clays during cyclic loading." Journal of Geotechnical Engineering Division, ASCE, 104(12), 1427-1447.

Idriss, I. M., Fiegel, G., Hudson, M. B., Mundy, P. K., and Herzog, R. (1995). "Seismic response of the Operating Industries Landfill." Proceedings, Earthquake Design and Performance of Solid Waste Landfills, Geotechnical Special Publication No. 54, ASCE, New York, NY, pp. 83-118.

Kramer, S. L. (1993). "Seismic response - Foundations in soft soils." Final Research Report, Washington State Department of Transportation, 135 pp.

Kramer, S. L. (1996). "Dynamic response of peats." Final Research Report WA-RD 412.1, Washington State Transportation Center, University of Washington, Seattle, Washington, November.

Landva, A., Korpijaakko, E. O., and Pheeney, P. E. (1983). "Geotechnical classification of peats and organic soils." Testing of Peat and Organic Soils, ASTM STP 820, pp. 141-156.

National Research Council (1969). *Muskeg Engineering Handbook*, by the Muskeg Subcommittee of the NRC Associate Committee on Geotechnical Research, I. C. MacFarlane, ed., University of Toronto Press, 297 p.

Roger Foott Associates, Inc. (1991). "Investigation and treatment of threatened levees on Sherman Island." Job No. 085-002, January 15.

Seed, H. B., and Idriss, I. M. (1970). "Analyses of ground motions at Union Bay, Seattle during earthquakes and distant nuclear blasts." Bulletin Seismological Society of America, 60(1), 125-136.

Stokoe, K. H. II, Bay, J. A., Rosenblad, B. L., Hwang, S.-K., and Twede, M. R. (1996). "In situ seismic and dynamic laboratory measurements of geotechnical materials at Queensboro Bridge and Roosevelt Island." Geotechnical Engineering Report GR94-5, Civil Engineering Department, University of Texas at Austin, June.

Tatsuoka, F., Teachavorasinskun, S., Dong, J., Kohata, Y., and Sata, T. (1994). "Importance of measuring local strains in cyclic triaxial tests on granular materials." Dynamic Geotechnical Testing II, ASTM STP 1213, Ebelhar, Drnevich, and Kutter Eds., American Society for Testing and Materials, Philadelphia.

Tatsuoka, F., Shibuya, S., and Teachavorasinskun, S. (1991). Discussion of "Shear modulus and cyclic undrained behavior of sands," by Alarcon-Guzman, A., Chameau, J. L., Leonards, G. A., and Frost, J. D., 31(2), 202-209.

Vucetic, M., and Dobry, R. (1991). "Effect of soil plasticity on cyclic response." Journal of Geotechnical Engineering, ASCE, 117(1), 89-107.

Zergoun, M., and Vaid, Y. P. (1994). "Effective stress response of clay to undrained cyclic loading." Canadian Geotechnical Journal, 31: 714-727.

APPENDIX A:

FILTERING OF NOISE IN LOW-STRAIN DATA

FILTERING OF NOISE IN LOW-STRAIN DATA

The measurement of stress-strain curves at strain levels less than about $1x10^{-2}$% can be complicated by noise in the signals. This appendix uses an example set of low-strain level data to: (i) illustrate the procedure used to filter out noise in low-strain level test data; and (ii) describe the effects that filtering can have on the test results. Filtering was not performed for stress-strain data at shear strains greater than about $1x10^{-2}$%.

Filtering Procedure

Plots of stress and strain versus time, and of stress versus strain, are shown in Figs. A-1 and A-2 for tests at cyclic shear strains of $3.8x10^{-3}$% and $1.0x10^{-2}$%, respectively. Five hundred data points were recorded per cycle of loading. The time histories of stress and strain contain noise at a frequency higher than that of the 1 Hz physical loading. The resulting plots of stress versus strain are even more obscured by the noise than are the individual measurements of stress or strain versus time.

Noise in the stress and strain measurements were filtered out by the following procedure. The stress and strain data were first padded at the start with signals equal to the starting values of the corresponding measurements, and padded on the end with signals equal to the final values of the corresponding measurements. The padded signals were then shifted by their mean values (to produce new mean values of zero), and then a cosine taper was applied at the ends. These signals were then filtered using a low-pass Butterworth filter with a corner frequency of about 6-10 Hz. Selection of the actual corner frequency was based on an inspection of the Fourier spectra of the stress and strain data. The filtered stress and strain data were then compared to the unfiltered data to evaluate the reasonableness of the filtering process.

The filtered stress and strain time histories for these two examples are shown in Figs. A-3 and A-4, respectively. Comparing Figs. A-1 and A-3, and Figs. A-2 and A-4, it appears that the filtering process has effectively removed the noise while retaining the physical loading data. In particular, the filtering process has greatly clarified the stress-strain response.

Effect of Filtering on Test Results

Secant shear moduli and equivalent damping ratios are calculated from the stress and strain data using a computer program written for this study. The robustness of this computer program was confirmed by analyzing a series of artificial stress-strain curves numerically generated for an ideal spring-dashpot system. This series of artificial stress-strain curves included the following variations: (i) translation of the stress-strain curves in all possible directions along the stress or strain axes; (ii) incorporation of high-frequency noise signals superimposed on the stress and/or strain data; and (iii) varying the theoretically correct shear moduli and damping values. It was found, based on this exercise, that: (i) shear moduli could be reasonably calculated with or without filtering of relatively noisy signals; and (ii) damping ratios were susceptible to errors introduced by noise, and thus more reliable damping ratios could be calculated using filtered signals.

The effect of filtering is illustrated by the calculated shear moduli and damping ratios for the second and fifth cycles of the test data in Figs. A-1 to A-4, as summarized in Table A-1. The filtering procedure had essentially no effect on the calculated secant shear moduli. The filtering procedure did, however, have a very strong effect on the calculated equivalent damping ratios. For these data, the unfiltered signals resulted in obviously incorrect negative damping values. Unrealistic damping values for the unfiltered signals are due to the fictitious hysteretic work within the noisy stress-strain curves. This fictitious hysteretic work can be positive or negative, and thus can cause unrealistically high or low (even negative) equivalent damping ratios for the unfiltered signals. Filtering the signals removes, or greatly reduces, the fictitious hysteretic work associated with the noise in the stress and strain measurements. As shown in Table A-1, the filtered signals resulted in calculated damping ratios of about 1.4-2.1%, which are clearly more reasonable.

In all cases, the filtering procedure resulted in more consistent and reasonable estimates of the equivalent damping ratio for cyclic tests at shear strains less than about $1x10^{-2}$%, while having essentially no effect on the calculated secant shear modulus.

TABLE A-1. Example of the Effect of Filtering on Secant Shear Moduli and Equivalent Damping Ratios

Test		*Shear Moduli (MPa)*		*Damping Ratio (%)*	
		2nd cycle	5th cycle	2nd cycle	5th cycle
DHPt-e	Unfiltered signals	8.93	8.94	-2.4	-2.6
	Filtered signals	8.93	8.93	1.4	2.1
DHPt1-f	Unfiltered signals	8.83	8.85	-5.0	-3.5
	Filtered signals	8.83	8.85	1.8	1.8

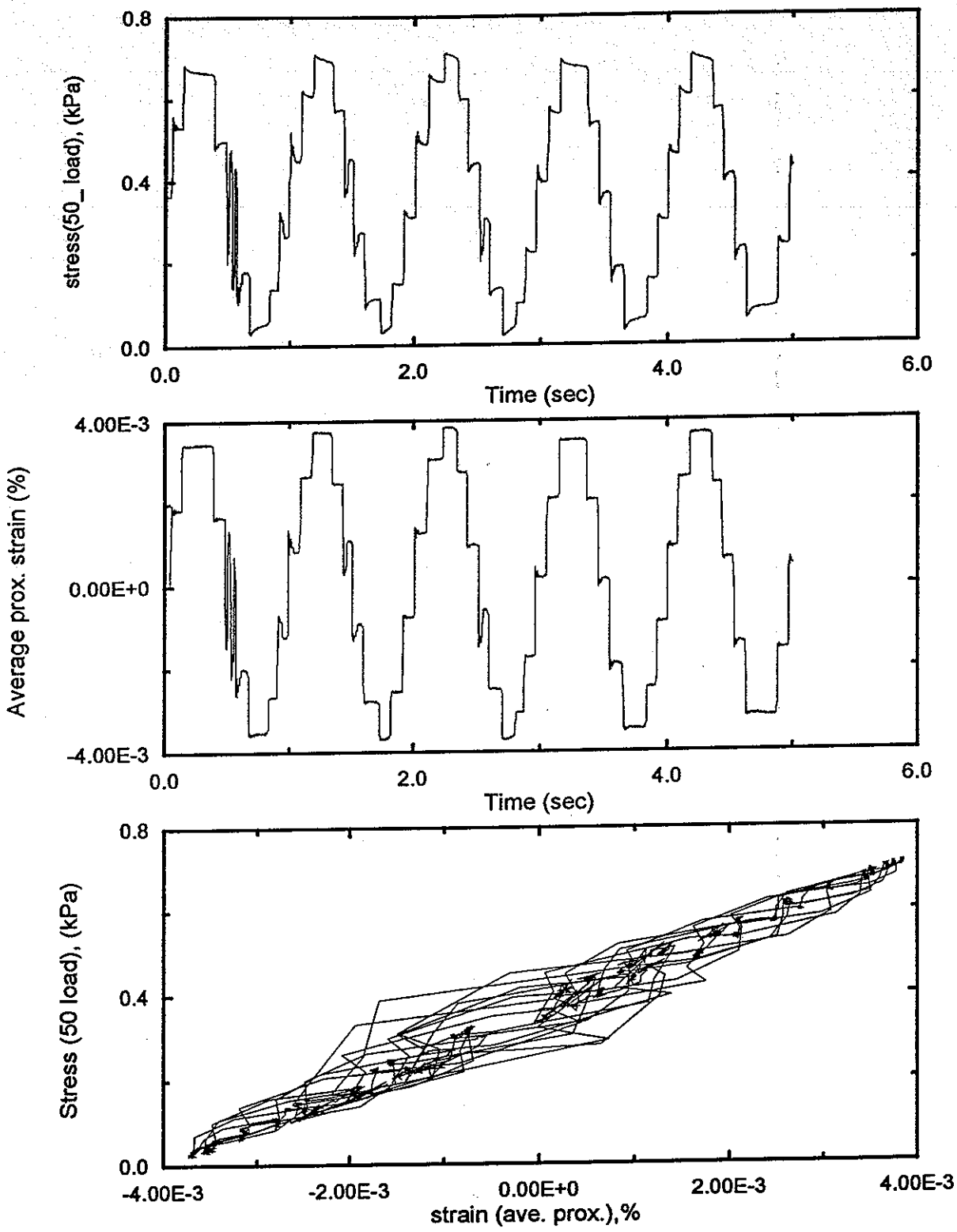

Test : DHPt1-e.ats

depth : 44.6'

DHP-5D-P4

09/18/96

FIG. A-1

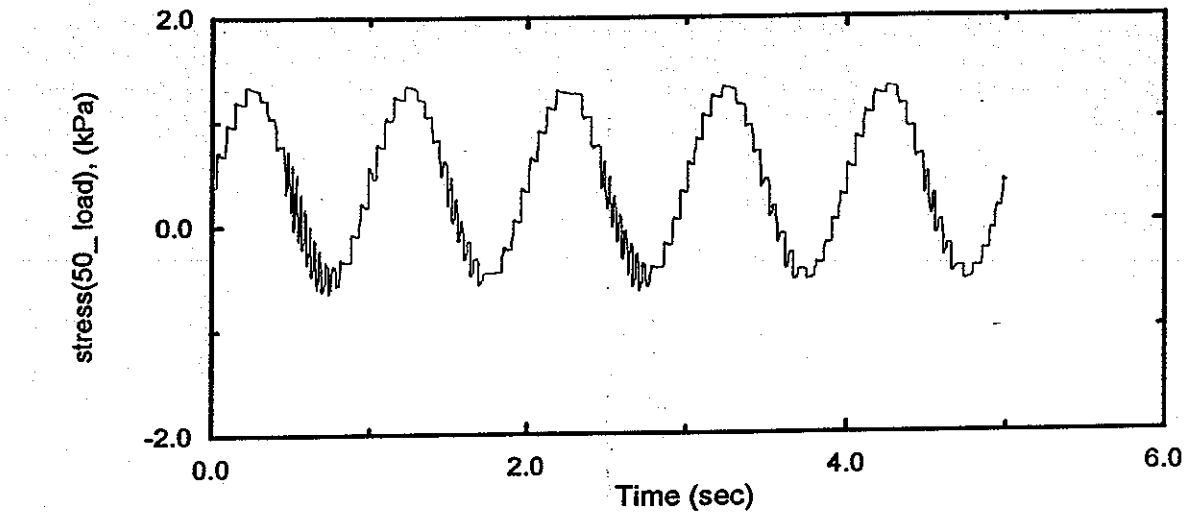

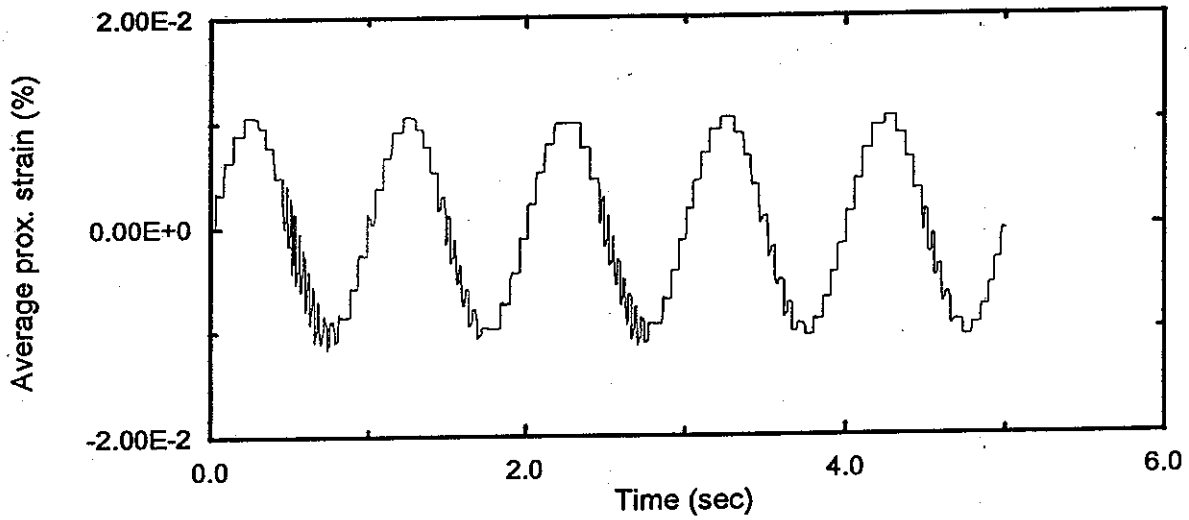

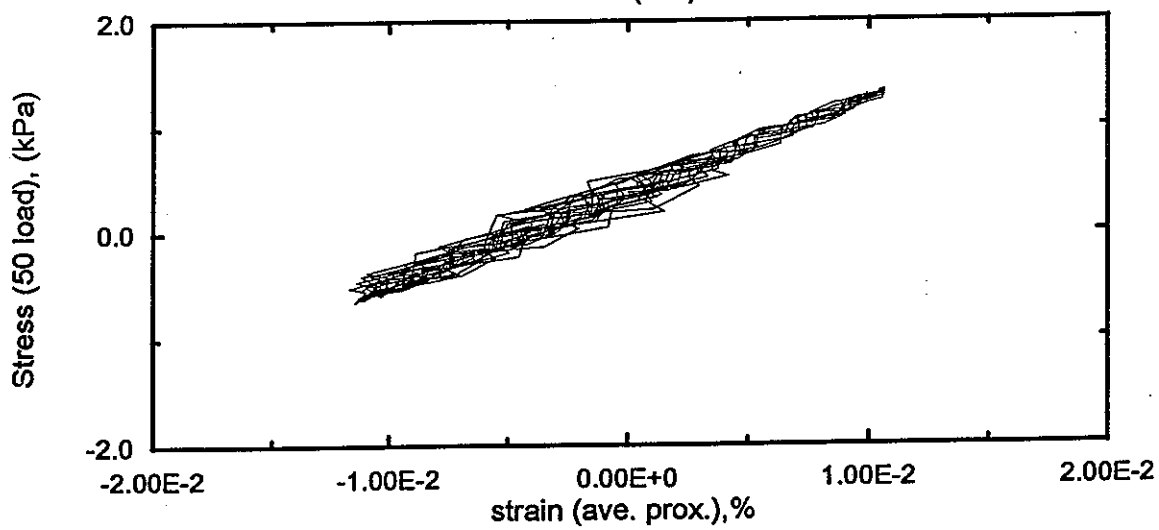

Test : DHPt1-f.ats

depth : 44.6'

DHP-5D-P4

09/18/96

FIG. A-2

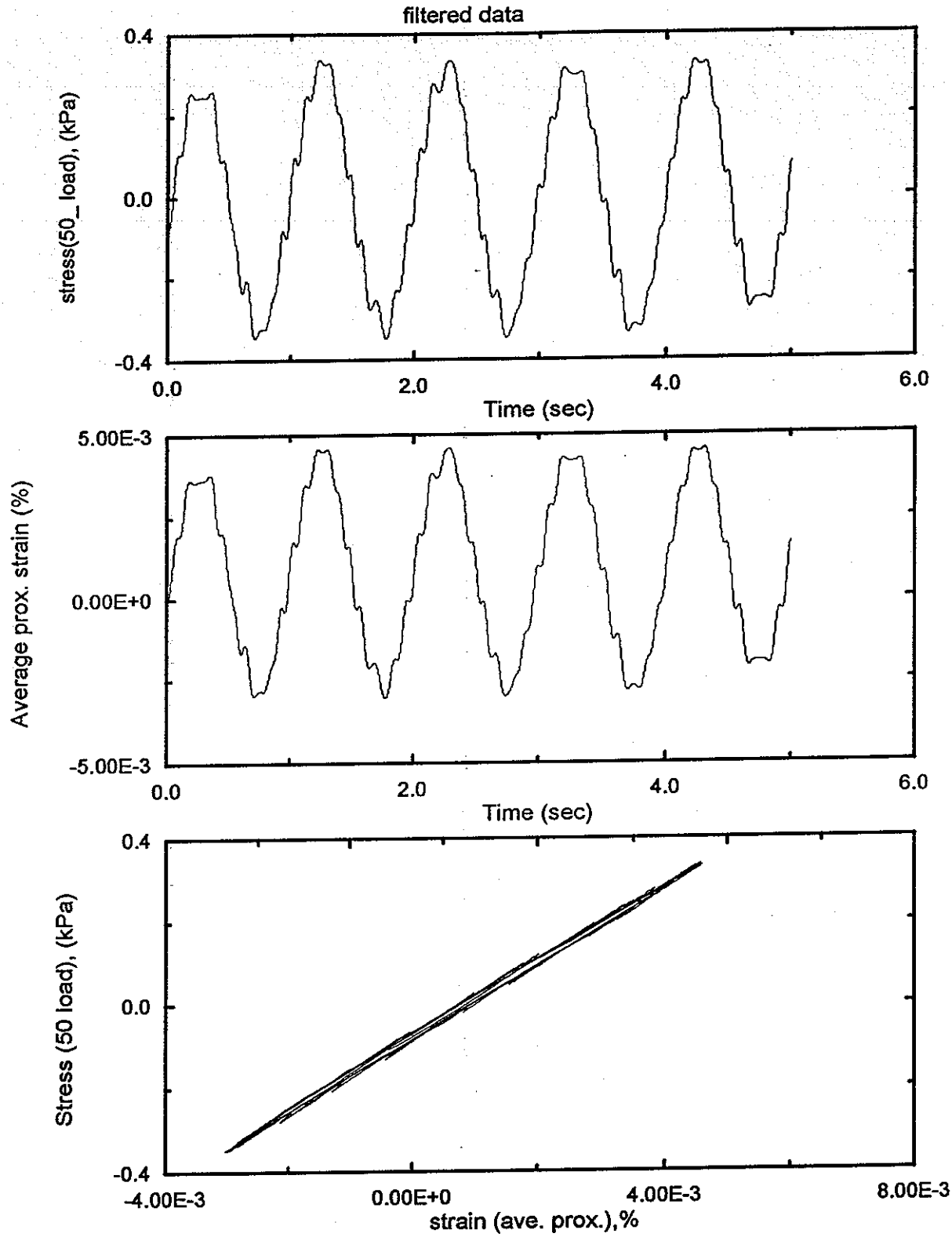

Test : DHPt1-em.ats

depth : 44.6'

DHP-5D-P4

09/18/96

FIG. A-3

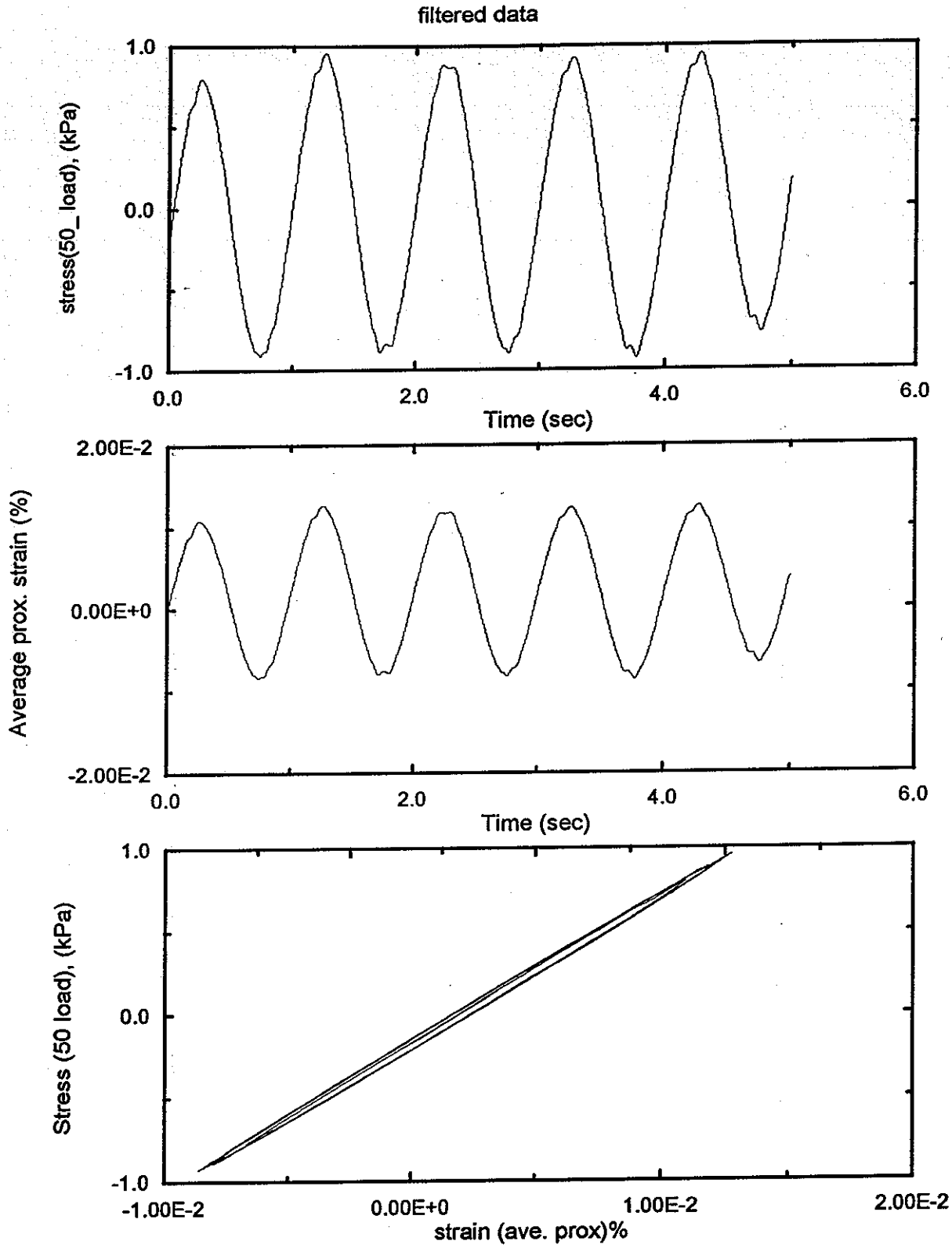

Test : DHPt1-fm.ats

DHP-5D-P4

09/18/96

depth : 44.6'

FIG. A-4

APPENDIX B:

BENDER ELEMENT AND CYCLIC TRIAXIAL TEST DATA FOR TEST NO. 1

MATHCAD WORKSHEET FOR BENDER ELEMENT TEST 1 :

SAMPLE NO ; DHP-5D-P4 DEPTH : 13.6 m (ave)
DATE : 09/18/96 CON. PRESSURE :200kPa

$X := READPRN(peat1\_prn)$ ------ enter the file name (e.g., *.prn). Columns 0,1& 2 are raw data from oscilloscope. Columns 3& 4 are dummy copies of column 1.

$time := X^{<0>}$

$in := X^{<2>}$ $out := X^{<1>}$

$dum1 := X^{<3>}$ $dum2 := X^{<4>}$ ------name the columns of the file

$L := cfft(out)$ ------ fast fourier transforms of the output & dummy2 signals

$Ldum2 := cfft(dum2)$

$a := cfft(in)$ ------ fast fourier transforms of the input & dummy1 signals

$Ldum1 := cfft(dum1)$

$b := \overline{a}$ ------ complex conjugates

$bdum1 := \overline{Ldum1}$

$dt := 0.00002$

$rows(b) = 1.025 \cdot 10^3$

$i := 0 .. 1024$

$rows(L) = 1.025 \cdot 10^3$

$Time_i := i \cdot dt$

$maga := |\overrightarrow{a}|$

$La_i := L_i \cdot b_i$ ------ cross-power spectrum of the signals

$Ldum_i := Ldum2_i \cdot bdum1_i$

$Inverse := icfft(La)$

$Indum := icfft(Ldum)$ ------cross-correlation of the signals

$Jdum := max(Indum)$

$J := max(Inverse)$

$cdum := \frac{Indum}{Jdum}$

$cc := \frac{Inverse}{J}$ $max(Inverse) = 0.0225$

$max(cc) = 1$ $max(cdum) = 1$

$min(cc) = -0.8352$

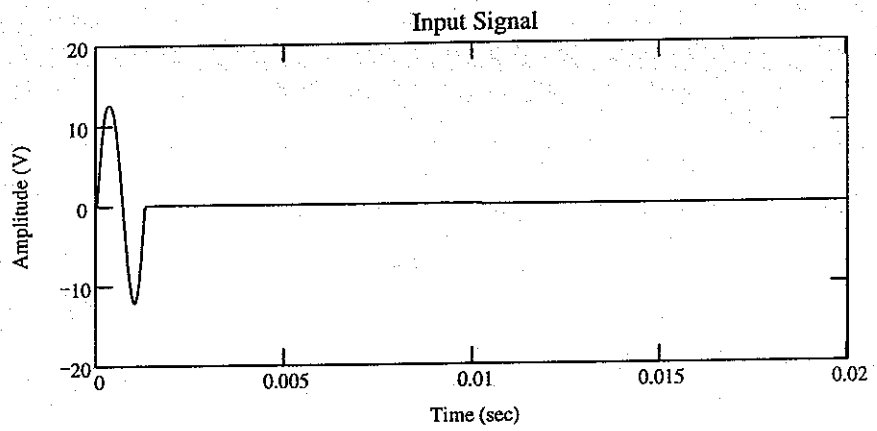
Input Signal
20
10
0
-10
-20
Amplitude (V)
0
0.005
0.01
0.015
0.02
Time (sec)

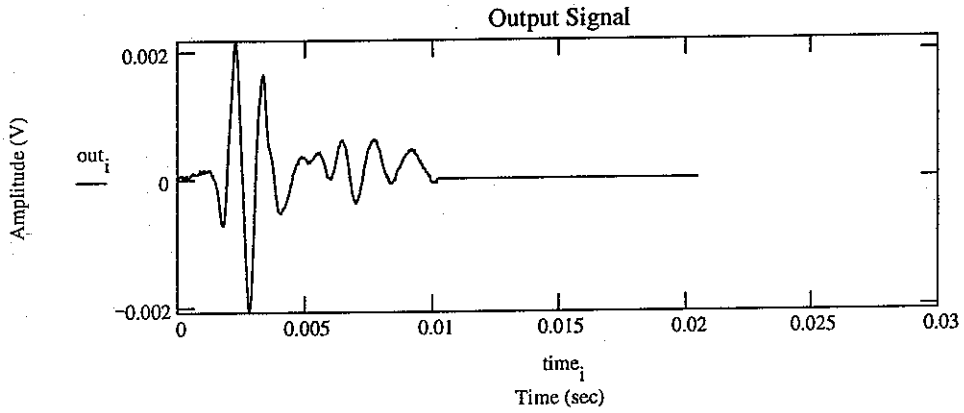
Output Signal
0.002
0
-0.002
Amplitude (V)
out_i
0
0.005
0.01
0.015
0.02
0.025
0.03
time_i
Time (sec)

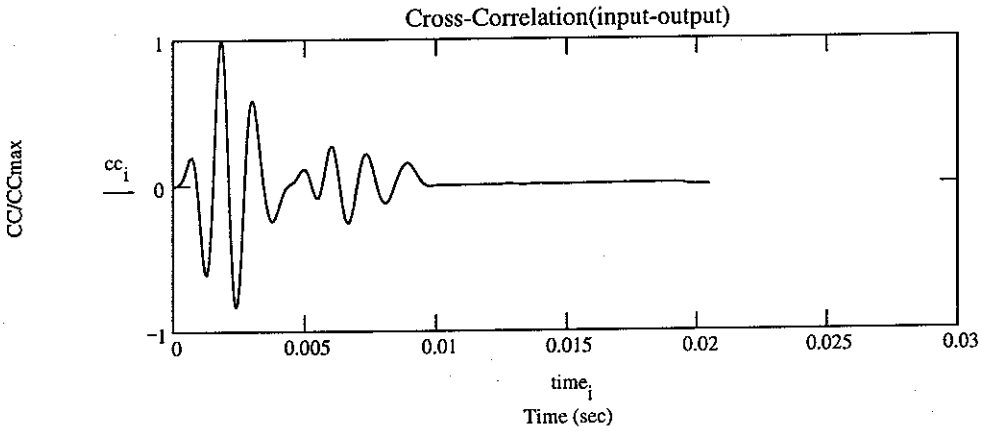
Cross-Correlation(input-output)
1
0
-1
CC/CCmax
cc_i
0
0.005
0.01
0.015
0.02
0.025
0.03
time_i
Time (sec)

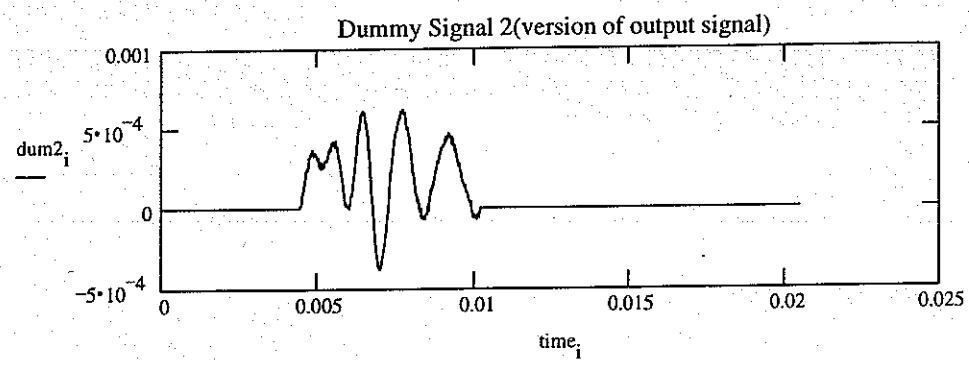
Dummy Signal 2(version of output signal)
0.001
5•10^-4
0
-5•10^-4
dum2_i
0
0.005
0.01
0.015
0.02
0.025
time_i

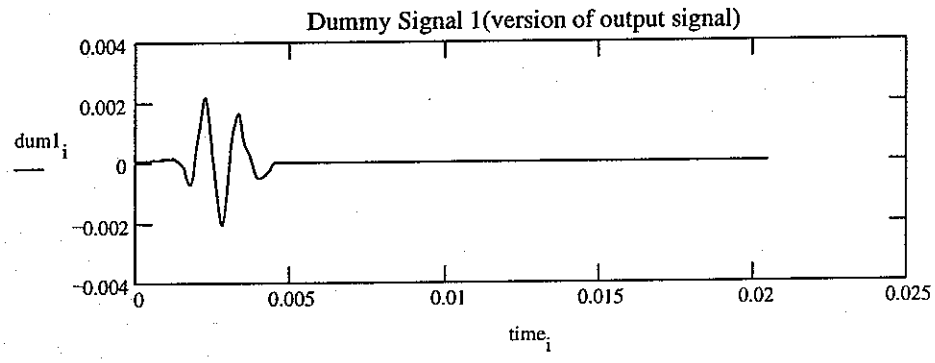
Dummy Signal 1(version of output signal)
0.004
0.002
0
-0.002
-0.004
dum1_i
0
0.005
0.01
0.015
0.02
0.025
time_i

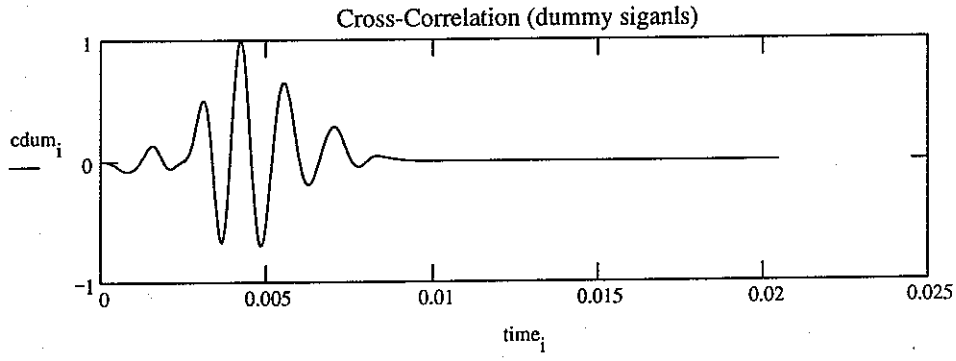
Cross-Correlation (dummy siganls)
1
0
-1
cdum_i
0
0.005
0.01
0.015
0.02
0.025
time_i

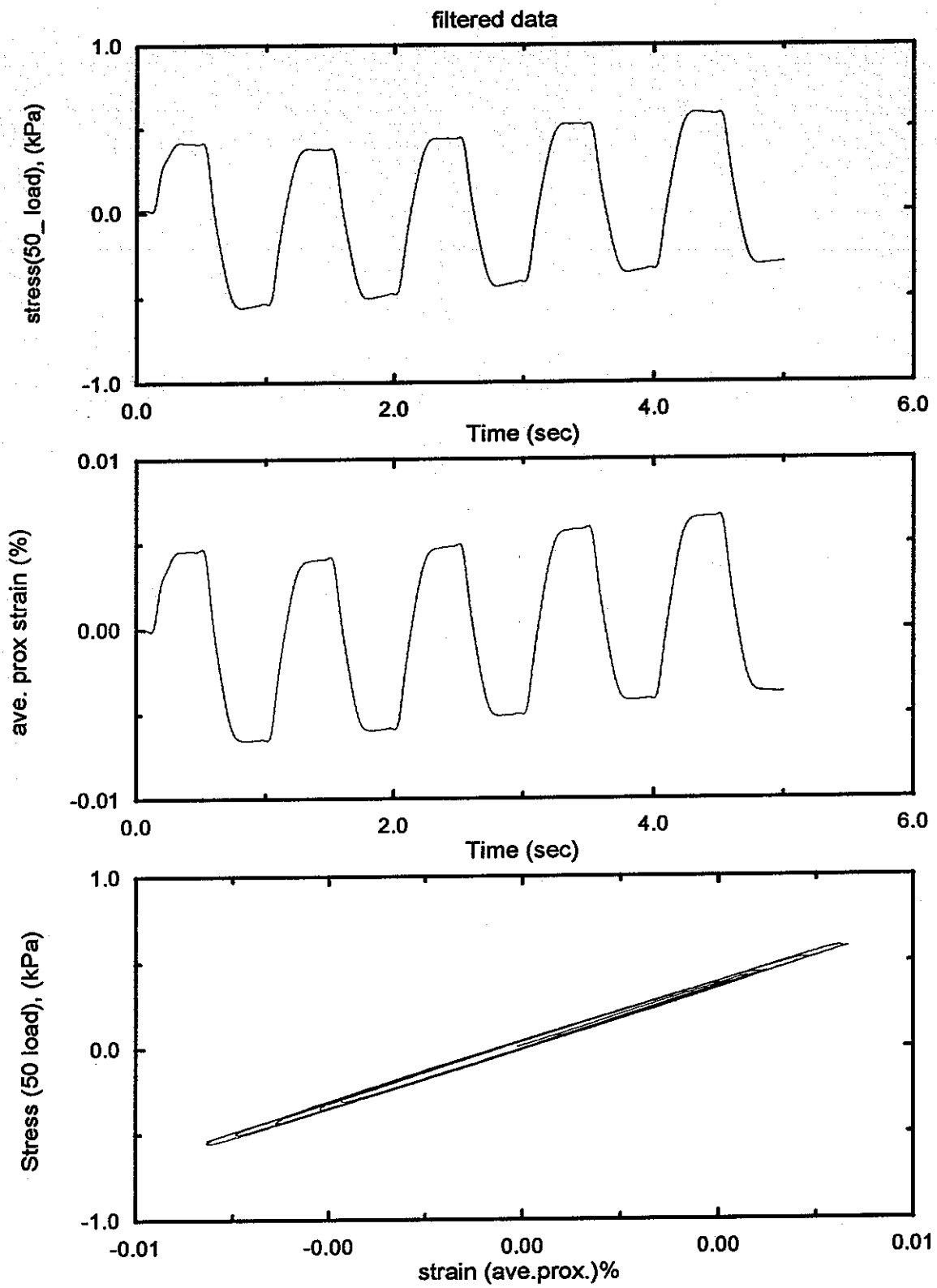

Test : DHPt1-bm.ats

depth : 13.6 m(44.6')

DHP-5D-P4

09/18/96

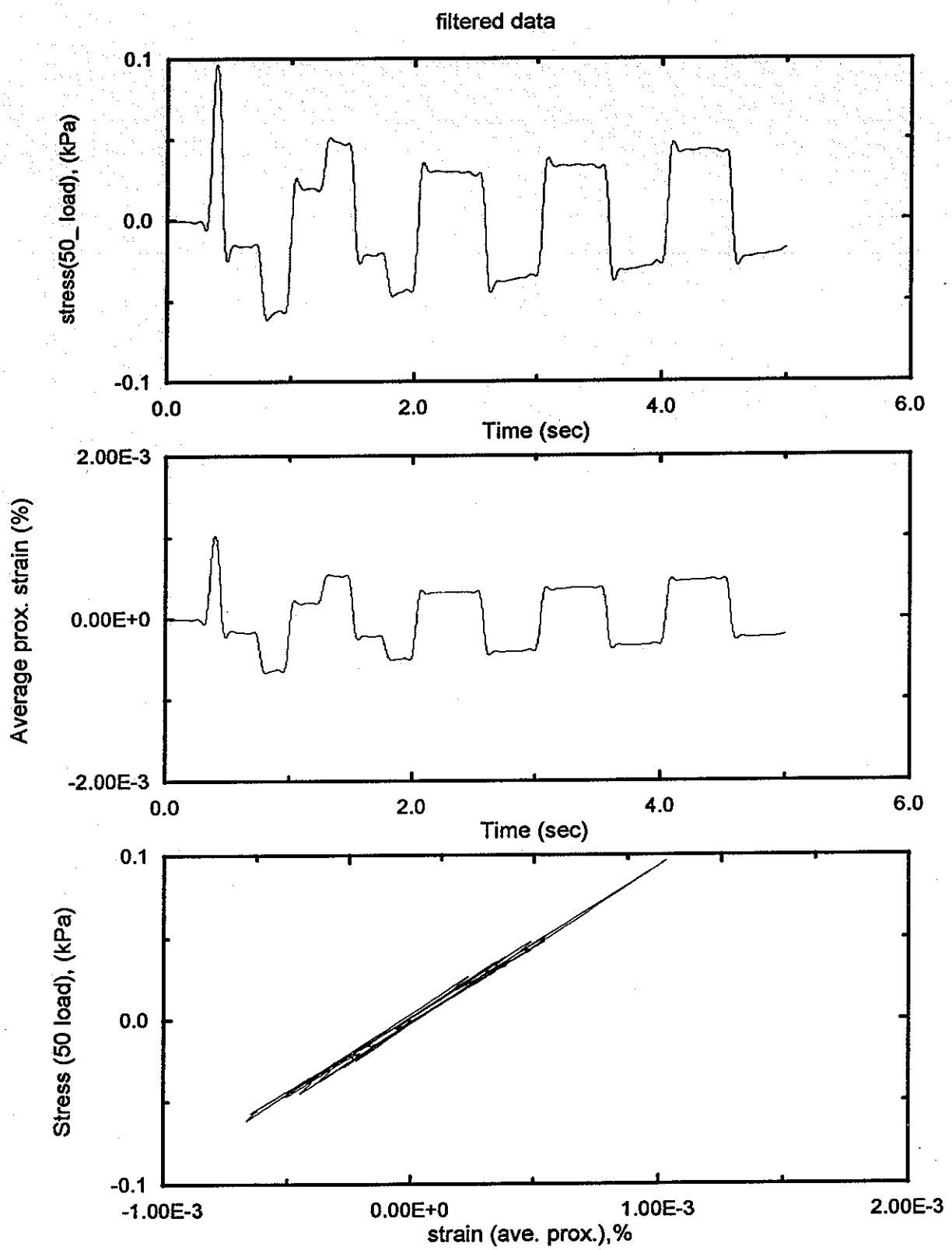

Test : DHPt1-cm.ats

depth : 44.6'

DHP-5D-P4

09/18/96

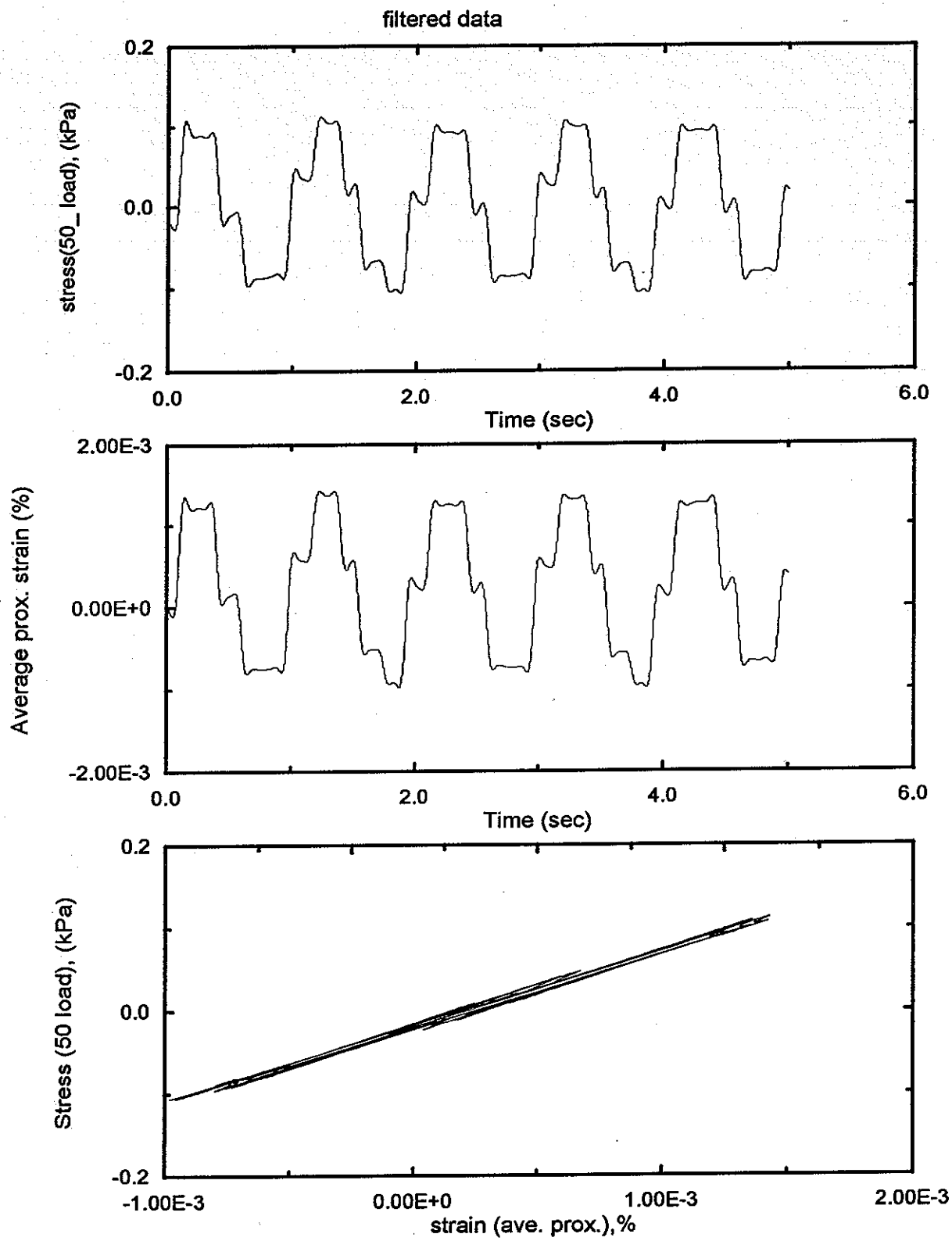

Test : DHPt1-dm.ats

depth : 44.6'

DHP-5D-P4

09/18/96

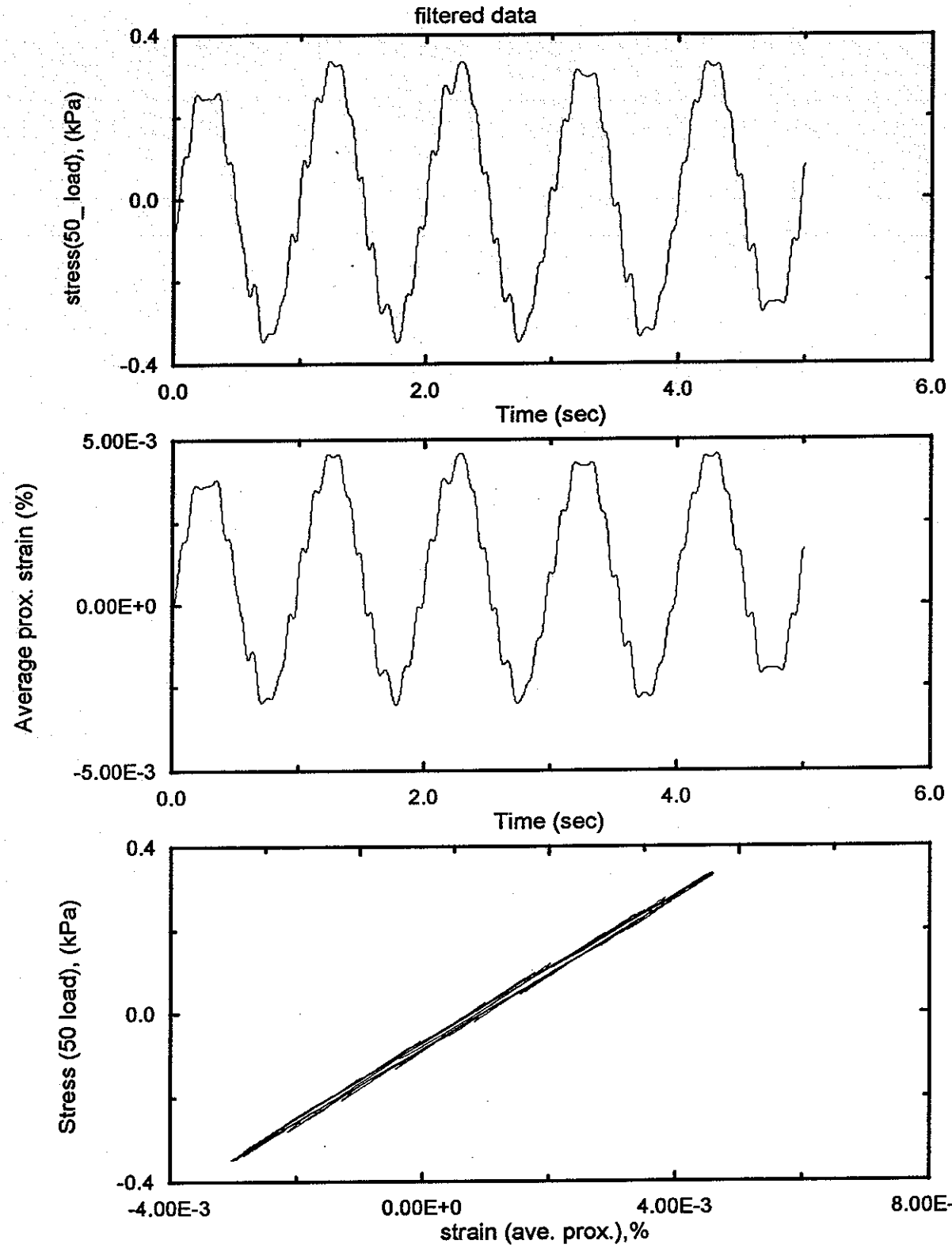

Test : DHPt1-em.ats

depth : 44.6'

DHP-5D-P4

09/18/96

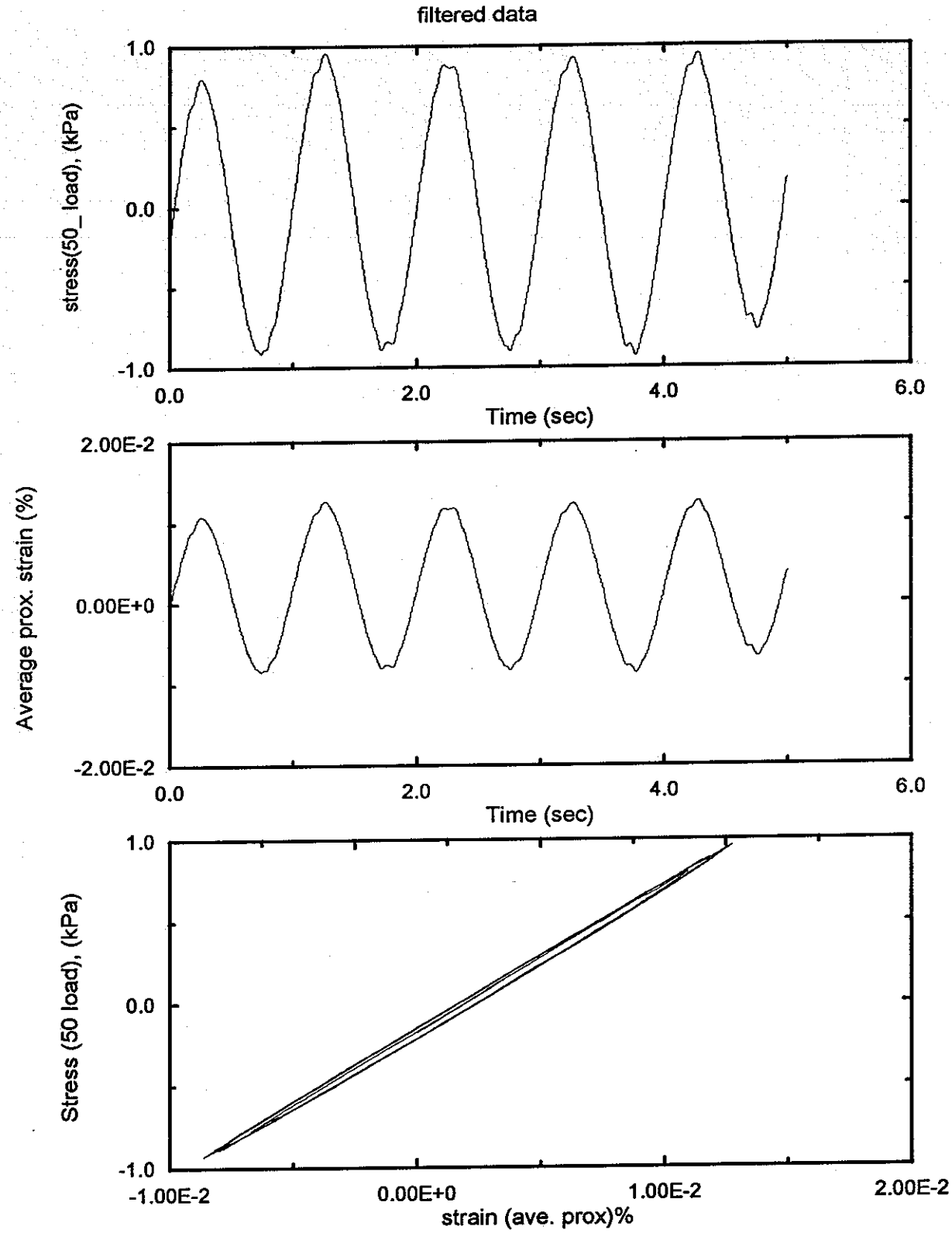

Test : DHPt1-fm.ats

DHP-5D-P4

09/18/96

depth : 44.6'

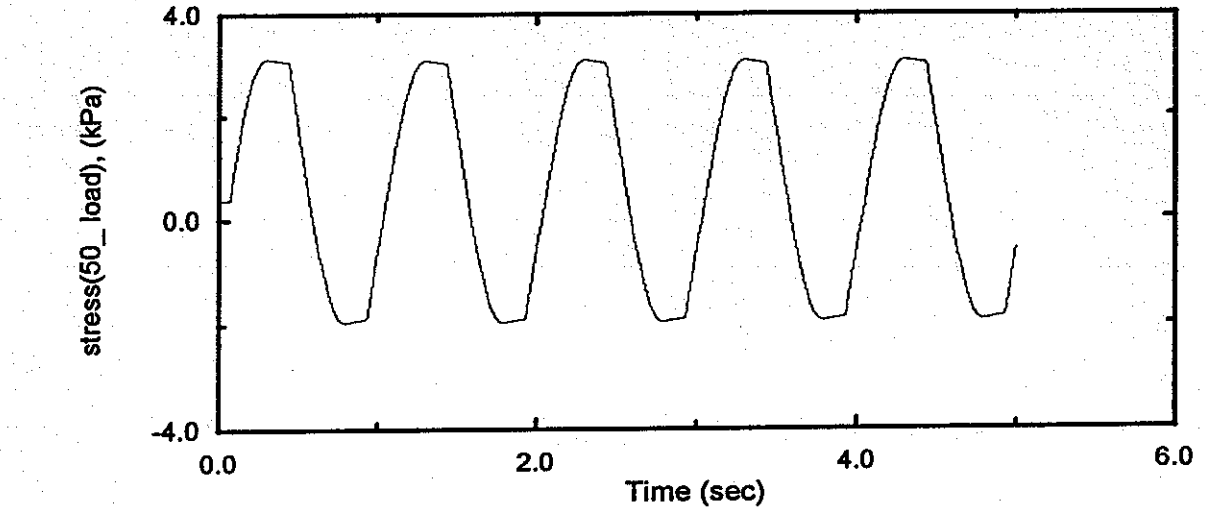

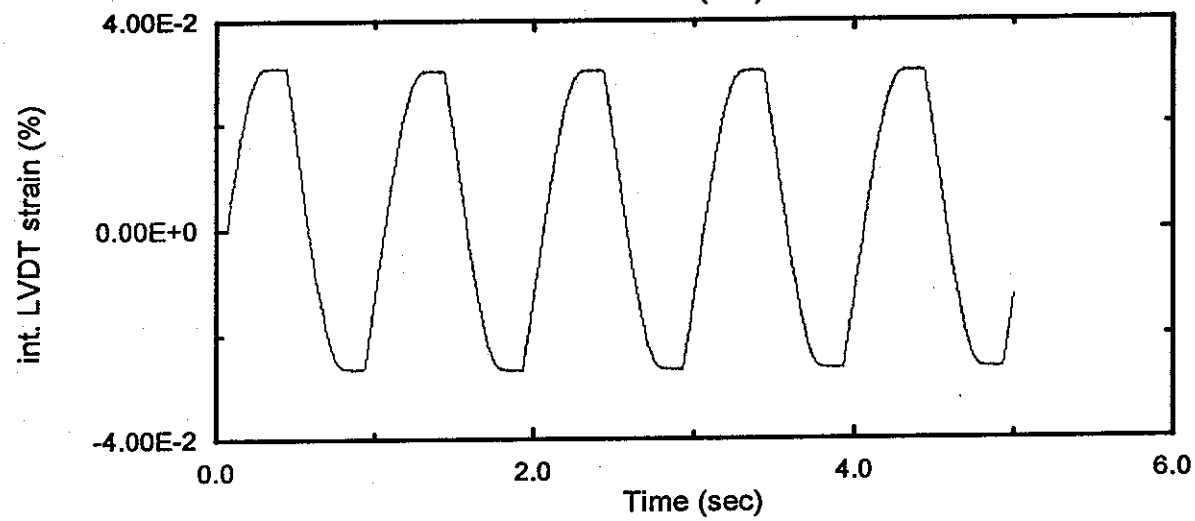

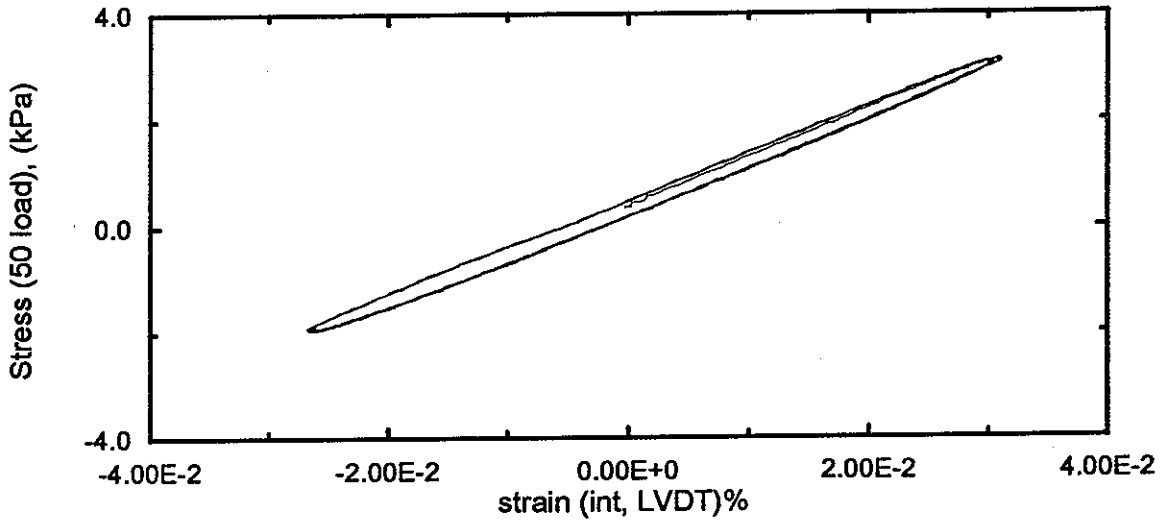

Test : DHPt1-g.ats

depth : 44.6'

DHP-5D-P4

09/18/96

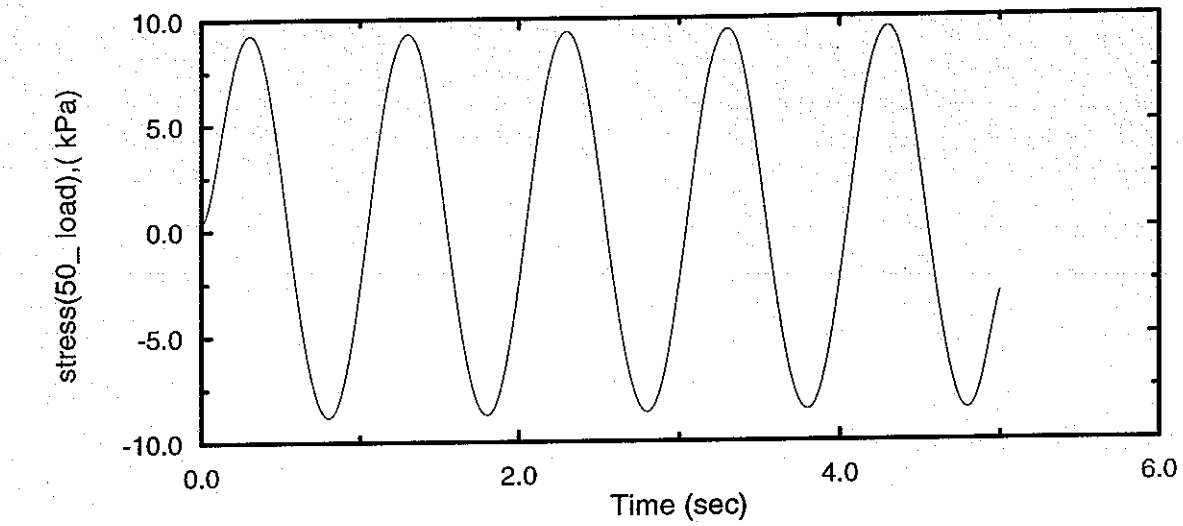

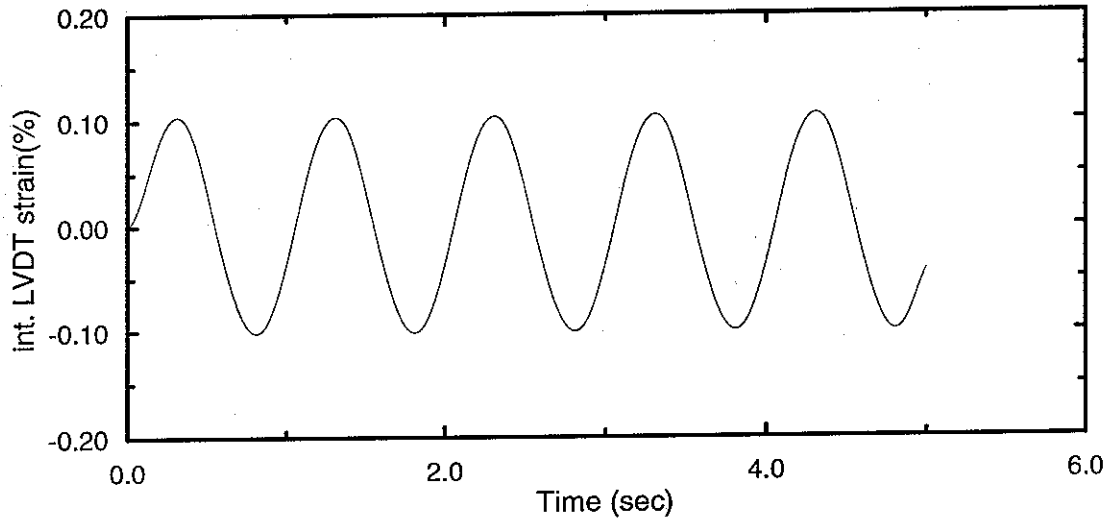

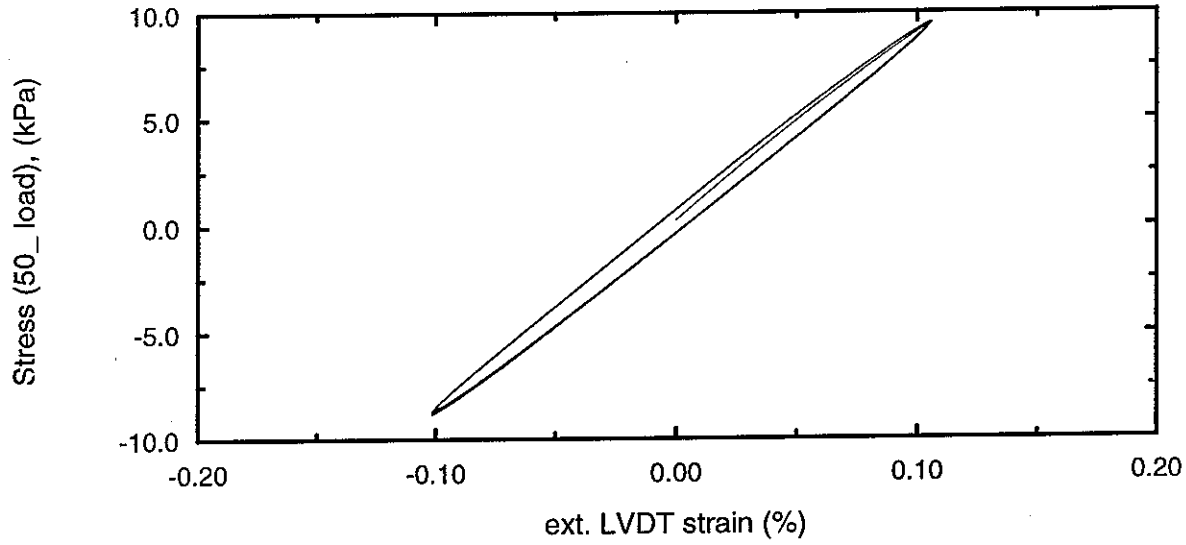

Test : DHPt1-hm.ats

depth : 13.6 m

DHP-5D-P4

09/18/96

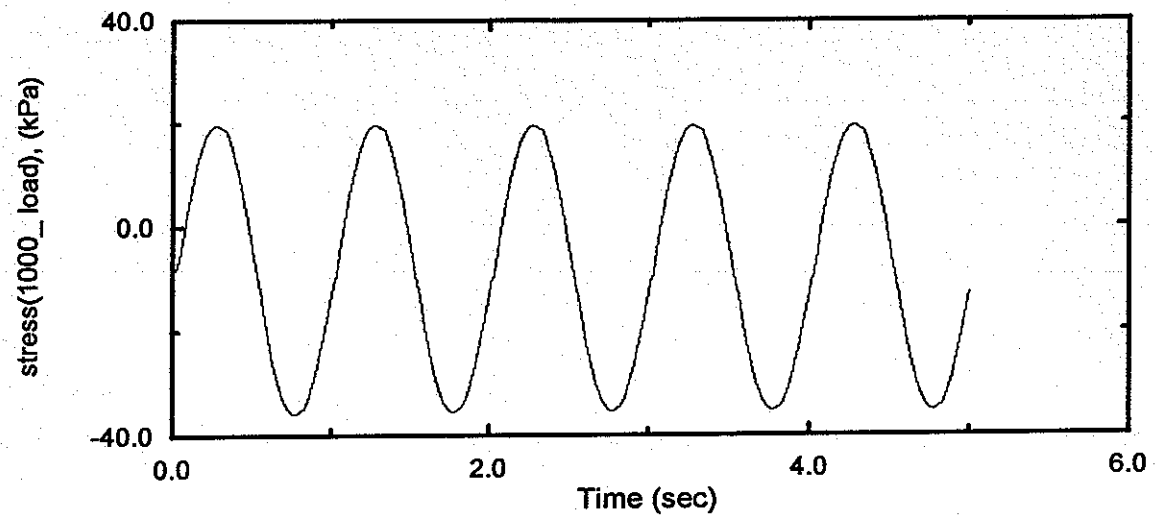

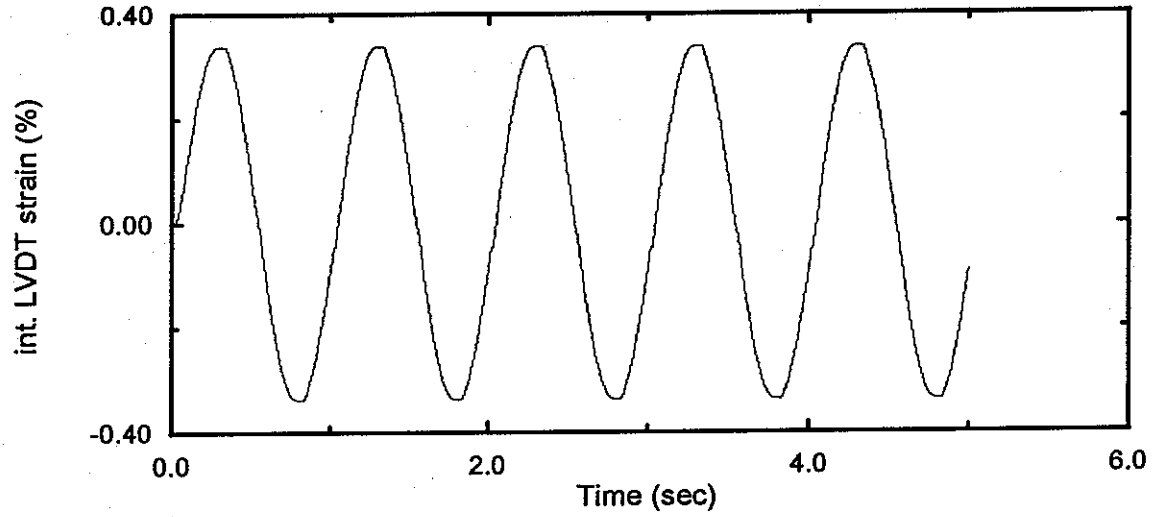

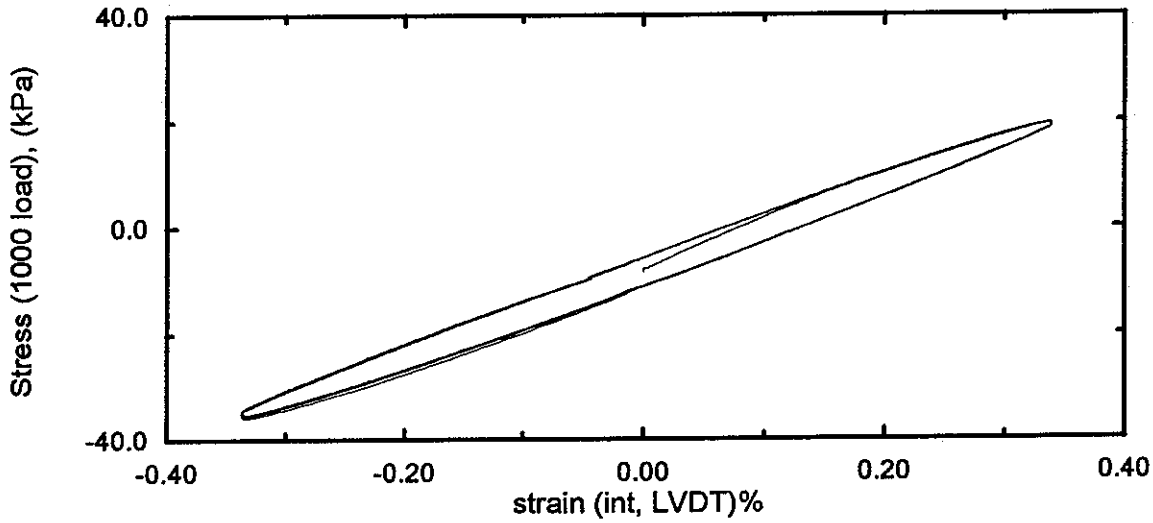

Test : DHPt1-i.ats

depth : 44.6'

DHP-5D-P4

09/18/96

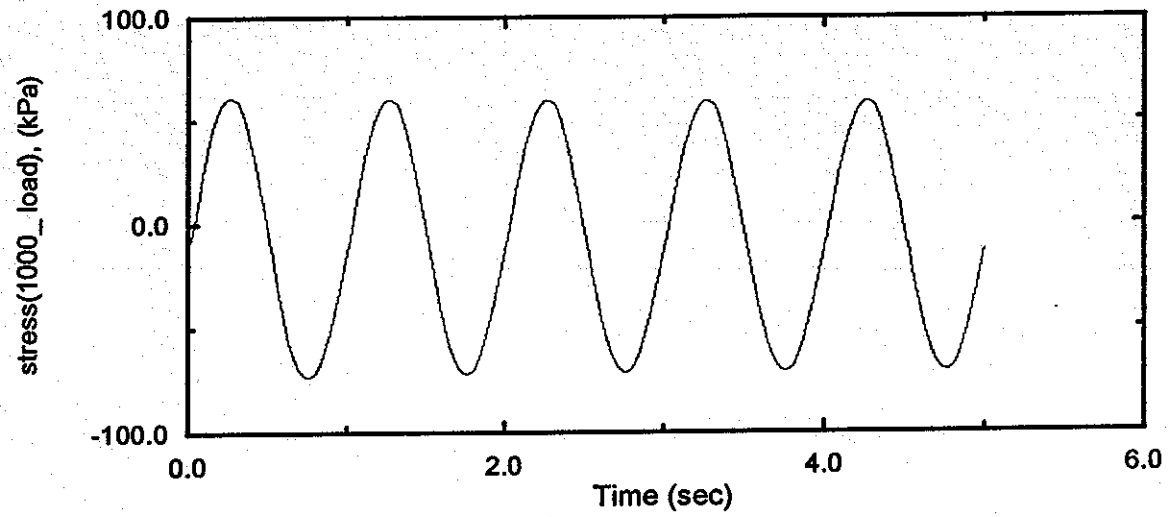

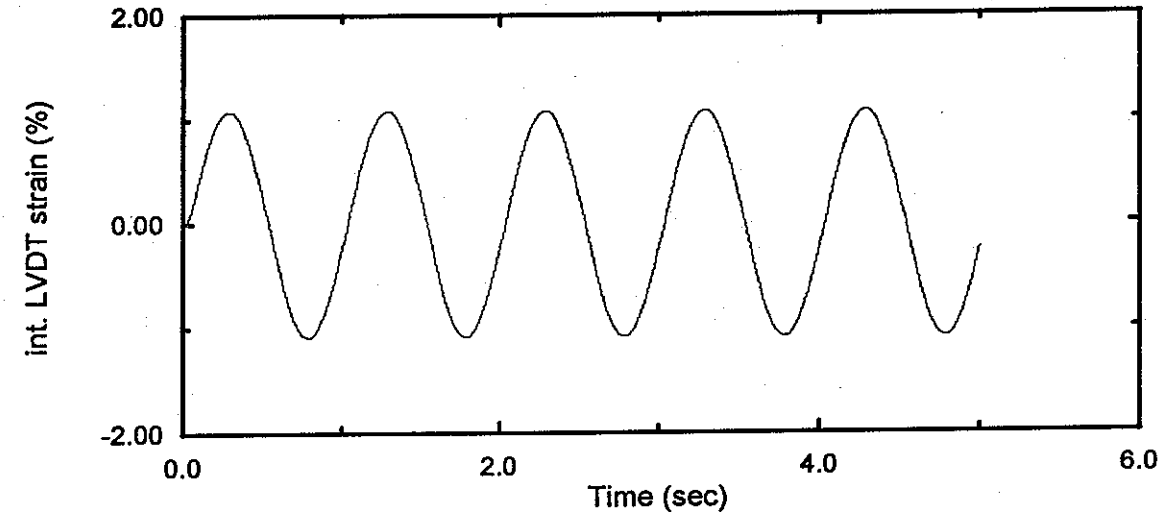

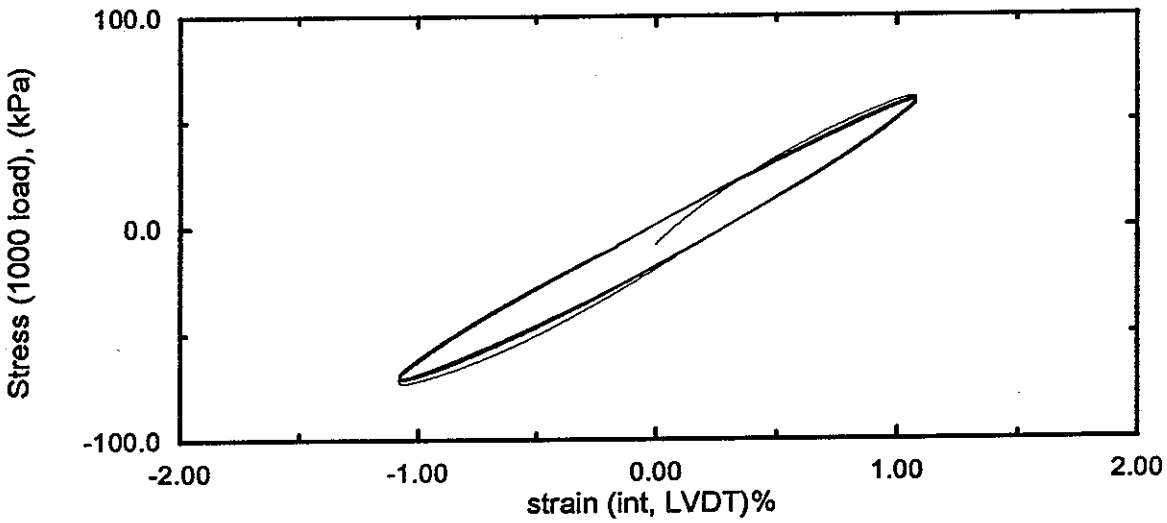

Test : DHPt1-j.ats

DHP-5D-P4

09/18/96

depth : 44.6'

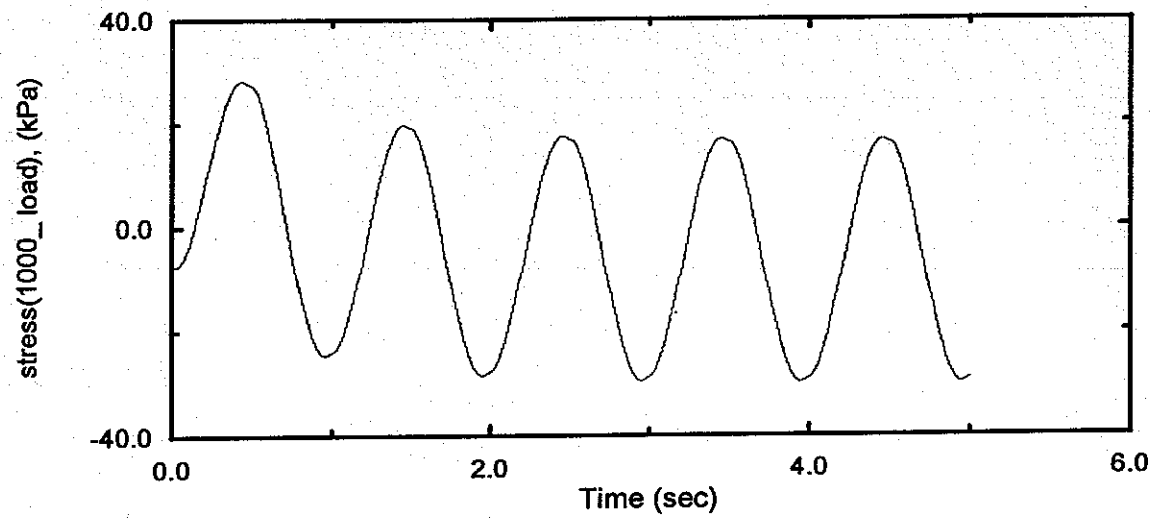

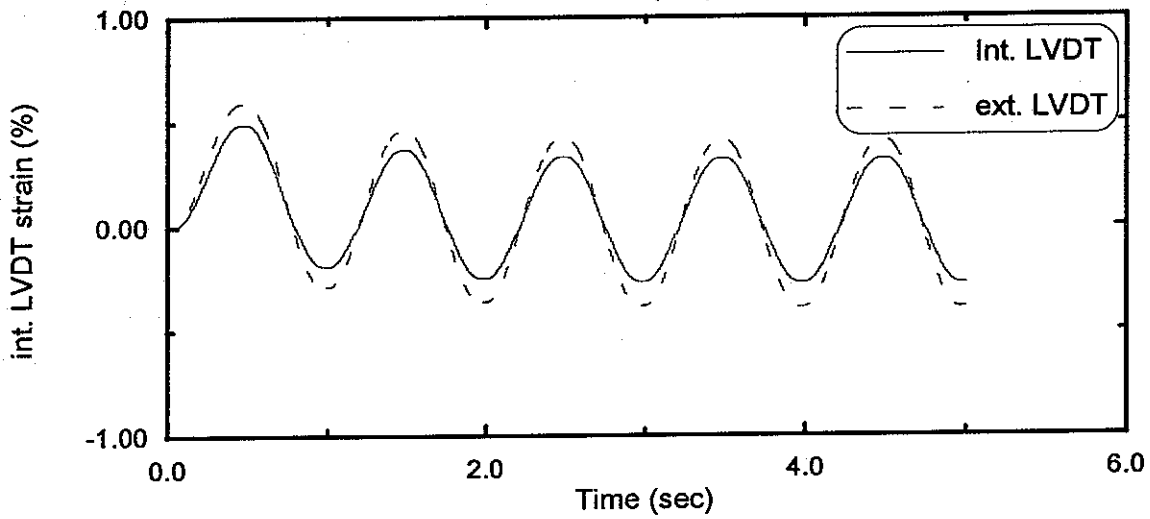

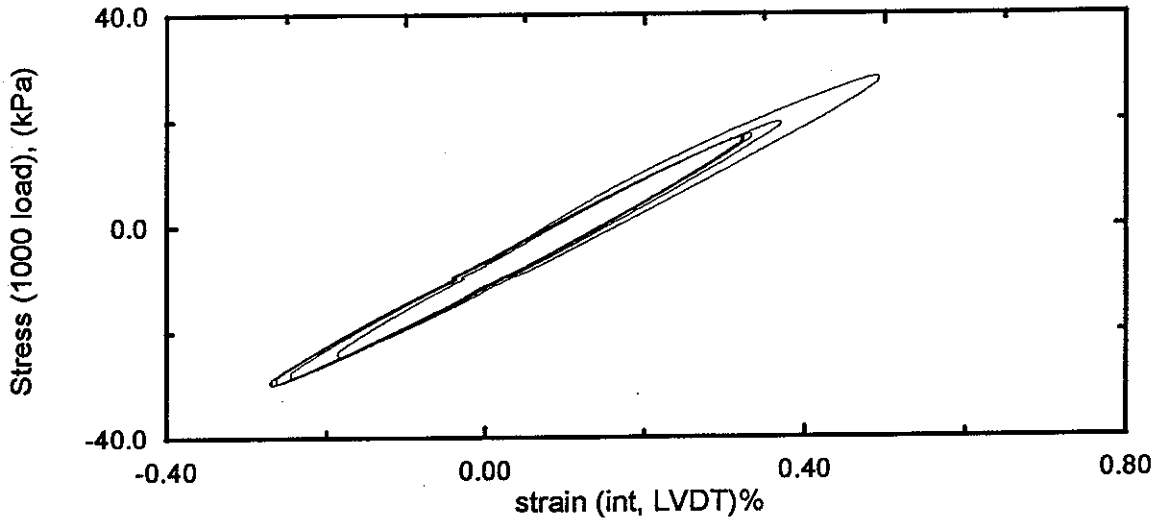

Test : DHPt1-k.ats

depth : 13.6 m(44.6')

DHP-5D-P4

09/18/96

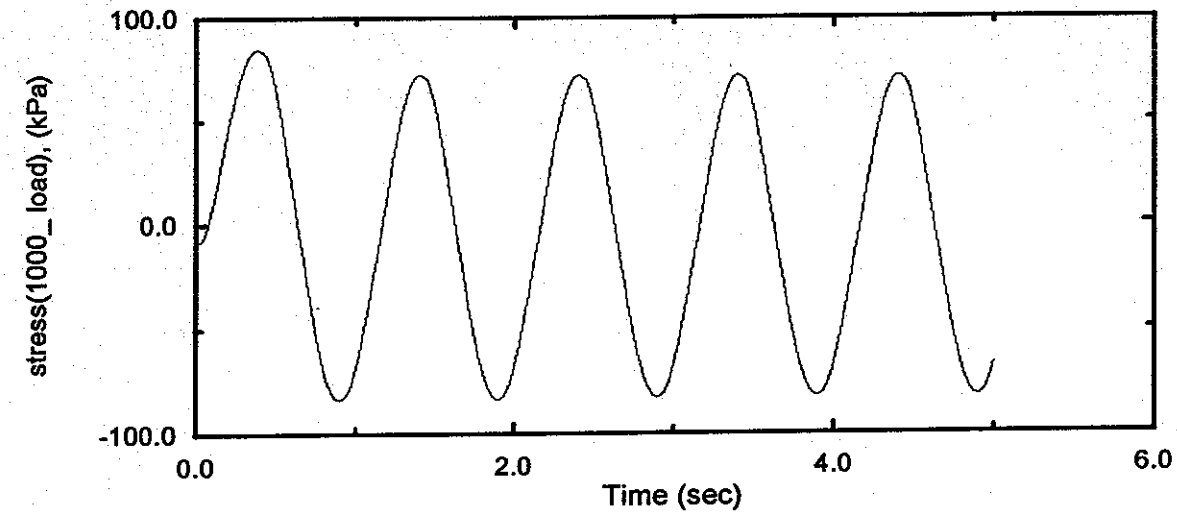

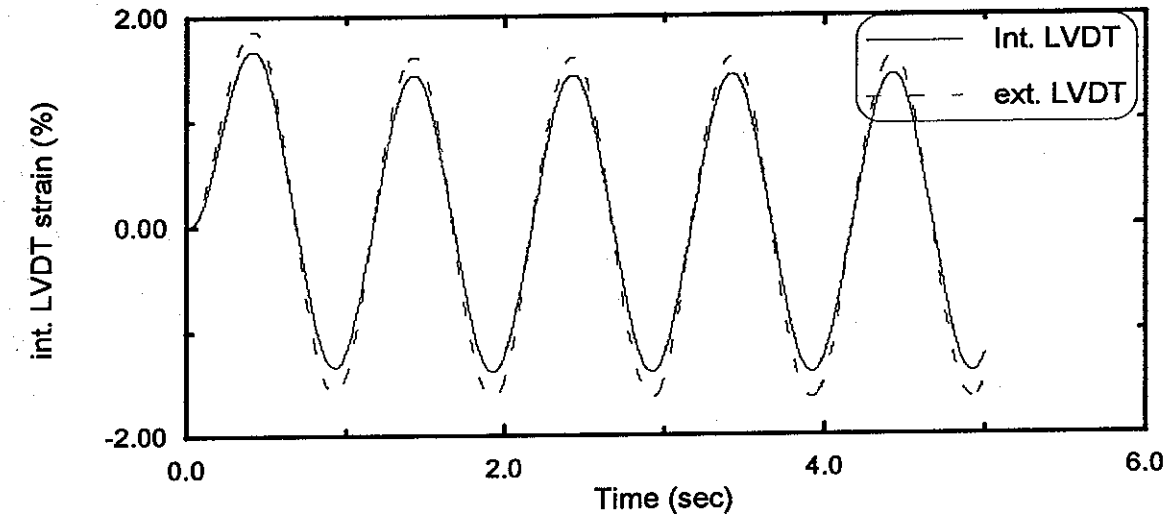

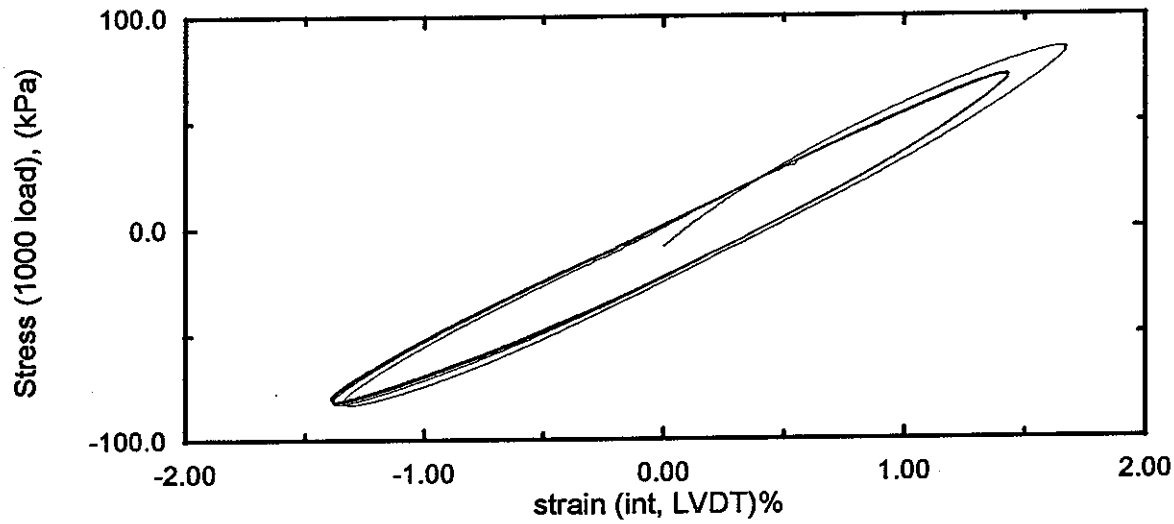

Test : DHPt1-I.ats

depth : 13.6 m(44.6')

DHP-5D-P4

09/18/96

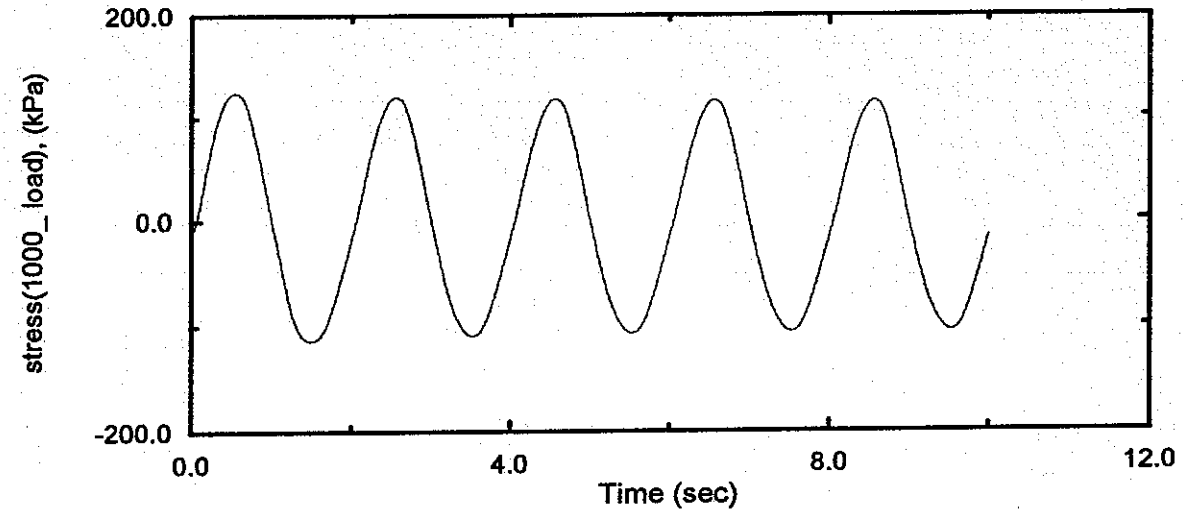

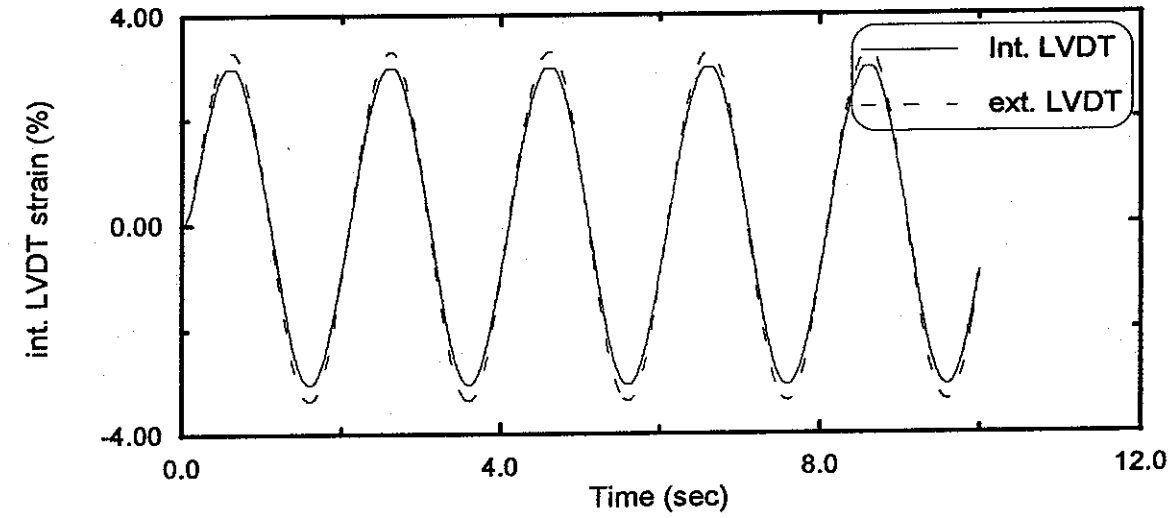

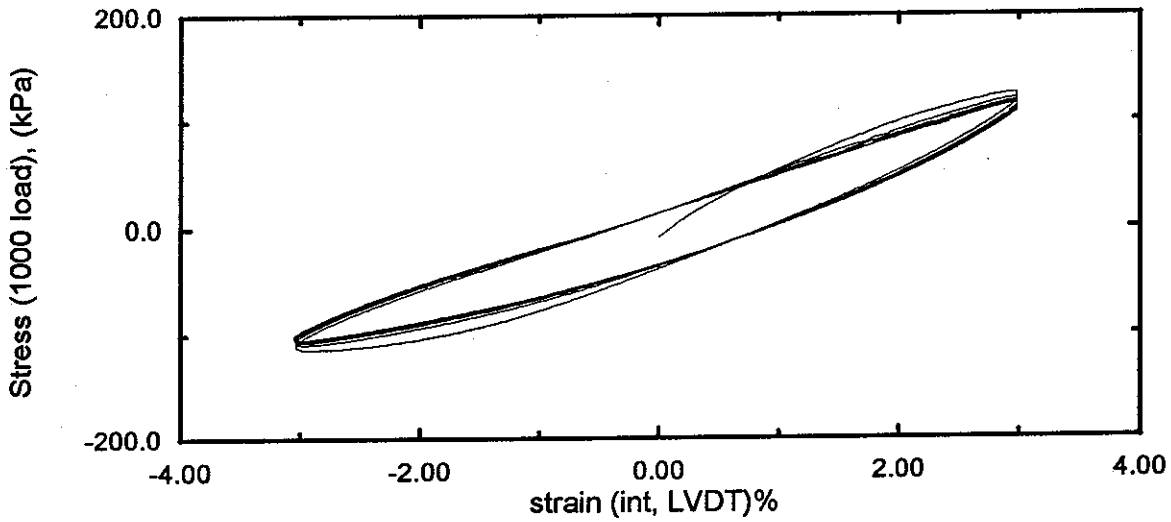

Test : DHPt1-m.ats

depth : 13.6 m(44.6')

DHP-5D-P4

09/18/96

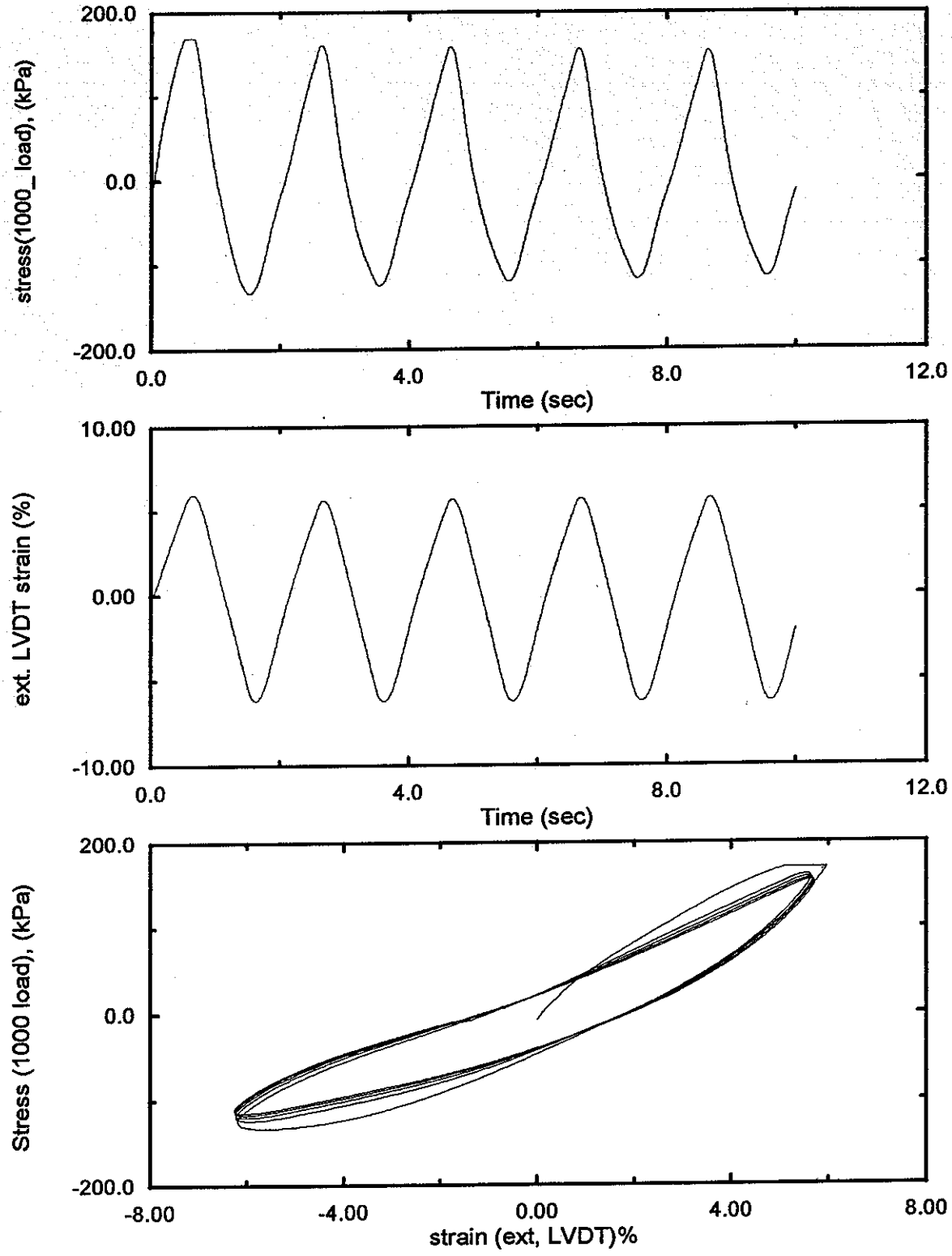

Test : DHPt1-n.ats

depth : 13.6 m(44.6')

DHP-5D-P4

09/18/96

APPENDIX C:

SUMMARY SHEETS FOR CYCLIC TRIAXIAL TESTS

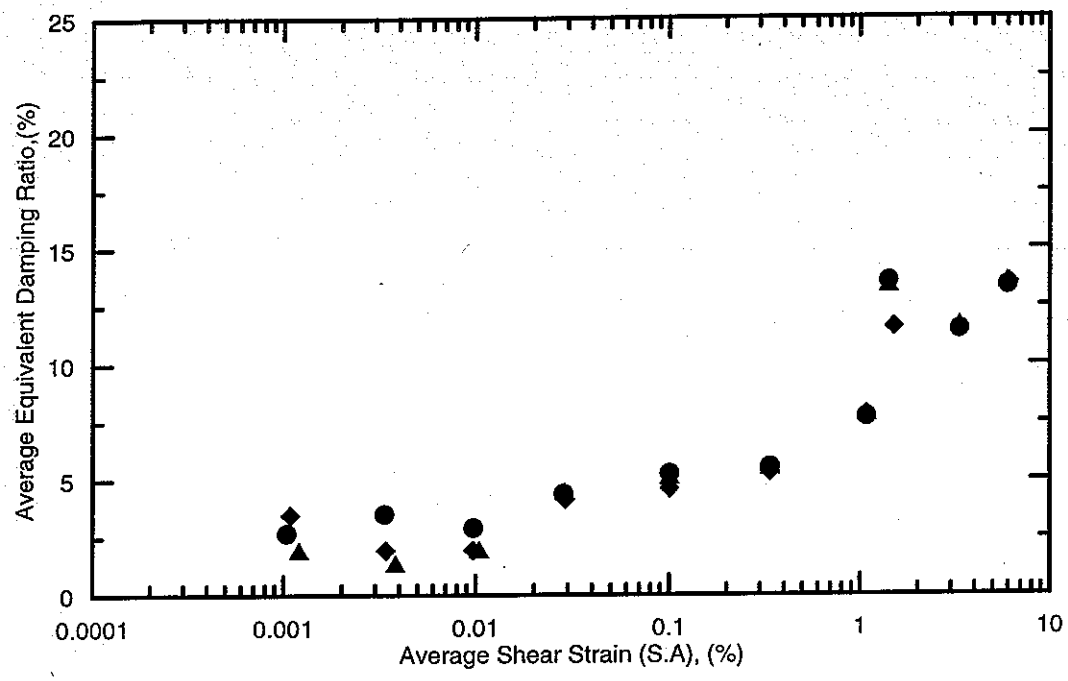

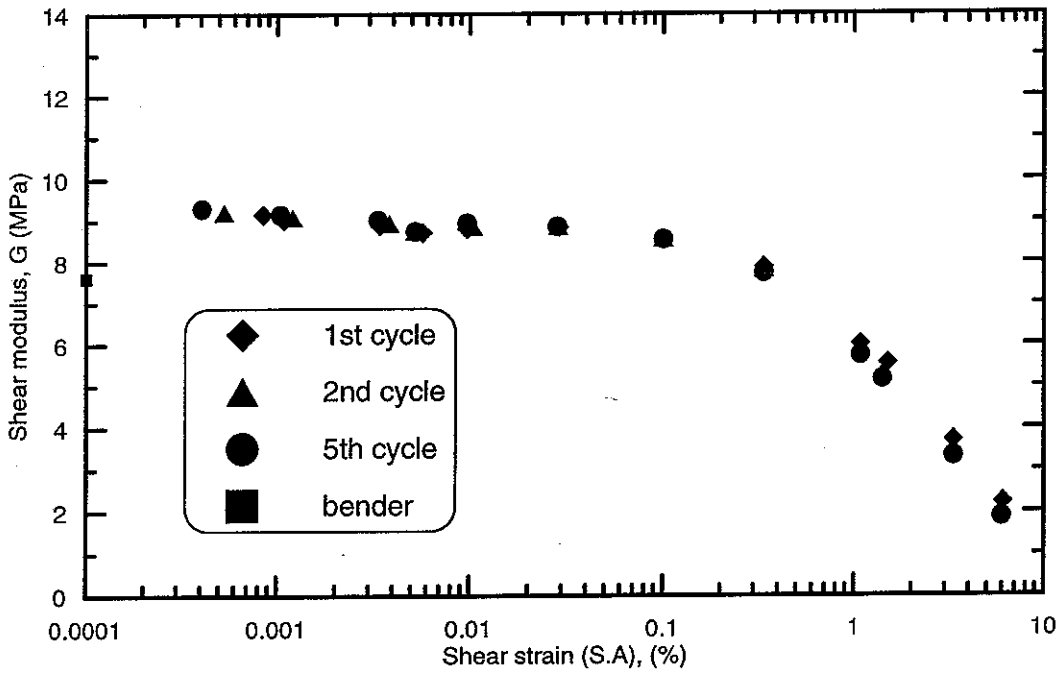

Project: Sherman Island	Depth : 13.6 m	Test Date :09/18/96	Tested by: R. Arulnathan
Sample description: peat soil, ash content =56 %		Consolidation Stress: 200 kPa	B-value =1.0
UNDRAINED CYCLIC TESTS AT DIFFERENT STRAIN LEVELS			Test No. DHPt1

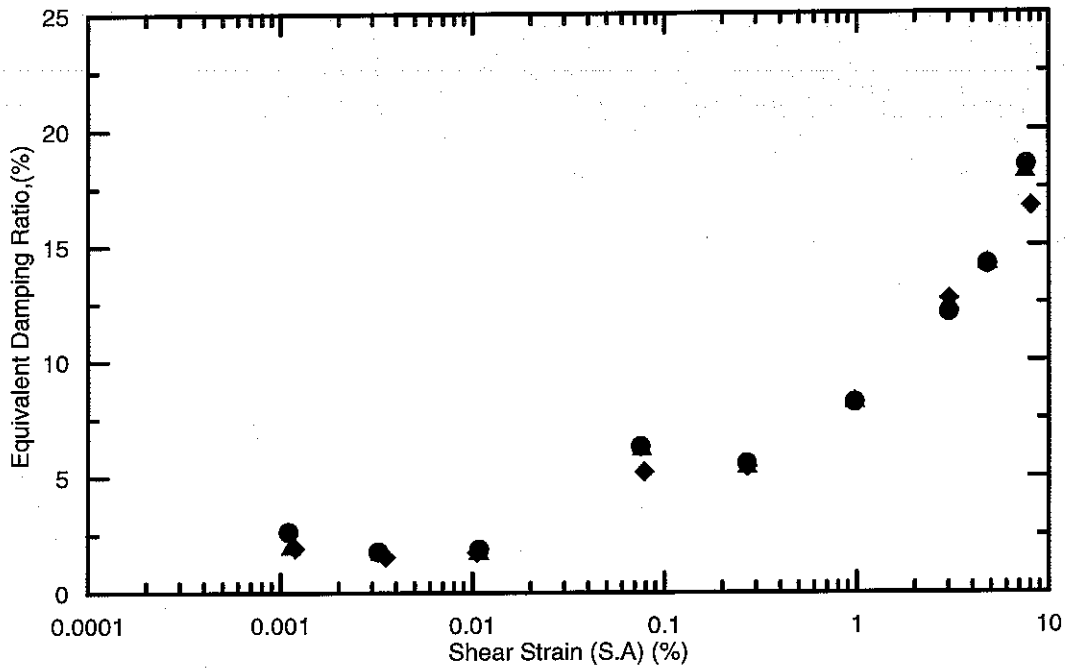

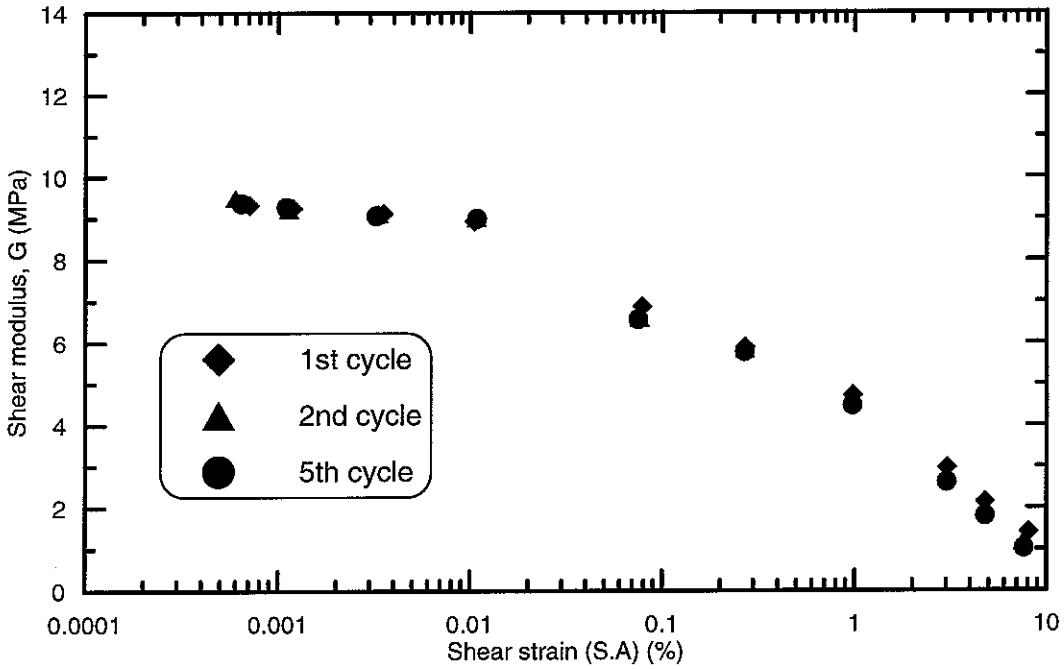

Project: Sherman Island	Depth : 13.5 m	Test Date :09/24/96	Tested by: R. Arulnathan
Sample description: peat soil, ash content =54 %		Consolidation Stress:132 kPa	B-value =1.0
UNDRAINED CYCLIC TESTS AT DIFFERENT STRAIN LEVELS			Test No. DHPt2

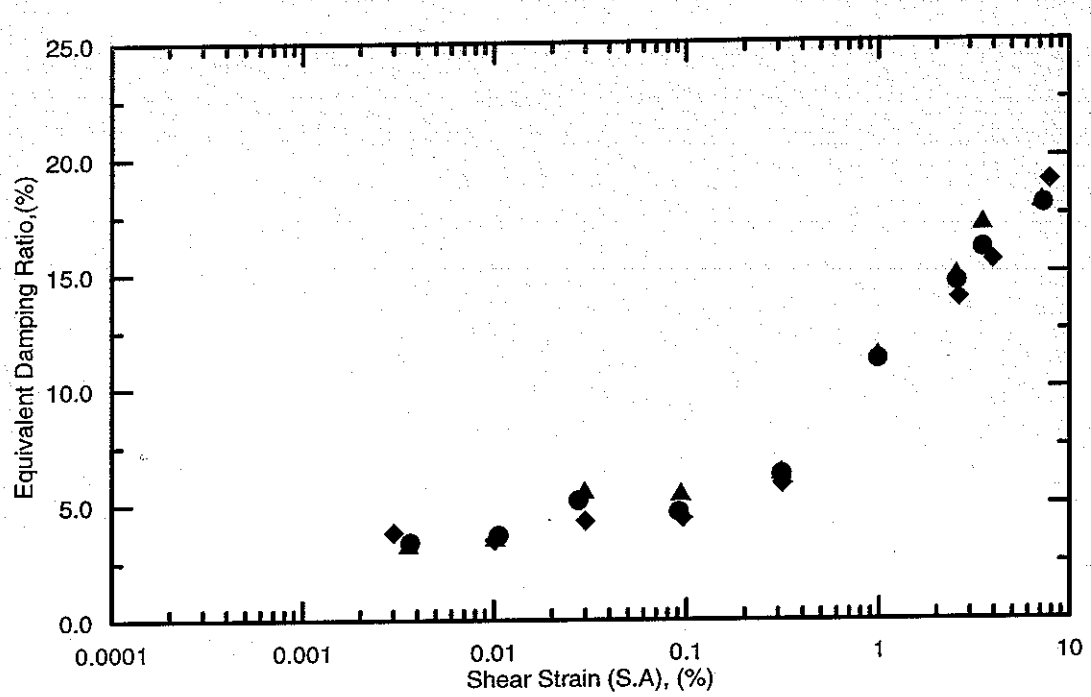

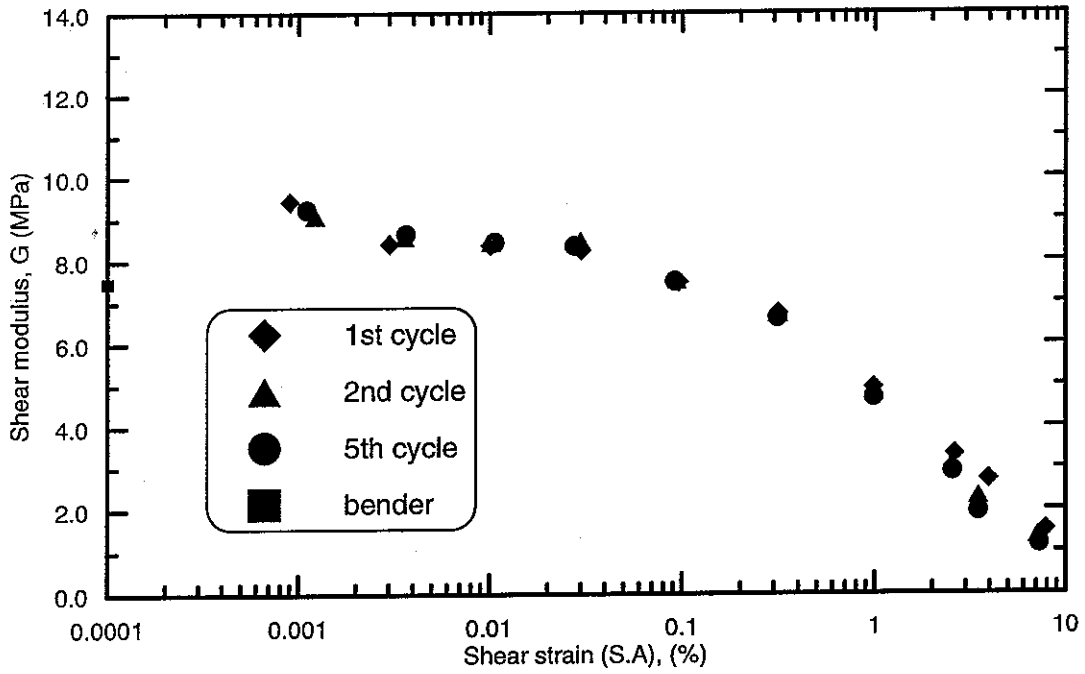

Project: Sherman Island	Depth : 13.35 m	Test Date :10/18/96	Tested by: R. Arulnathan
Sample description: peat soil, ash content =41 %		Consolidation Stress: 132 kPa	B-value =1.0
UNDRAINED CYCLIC TESTS AT DIFFERENT STRAIN LEVELS			Test No. DHPt3

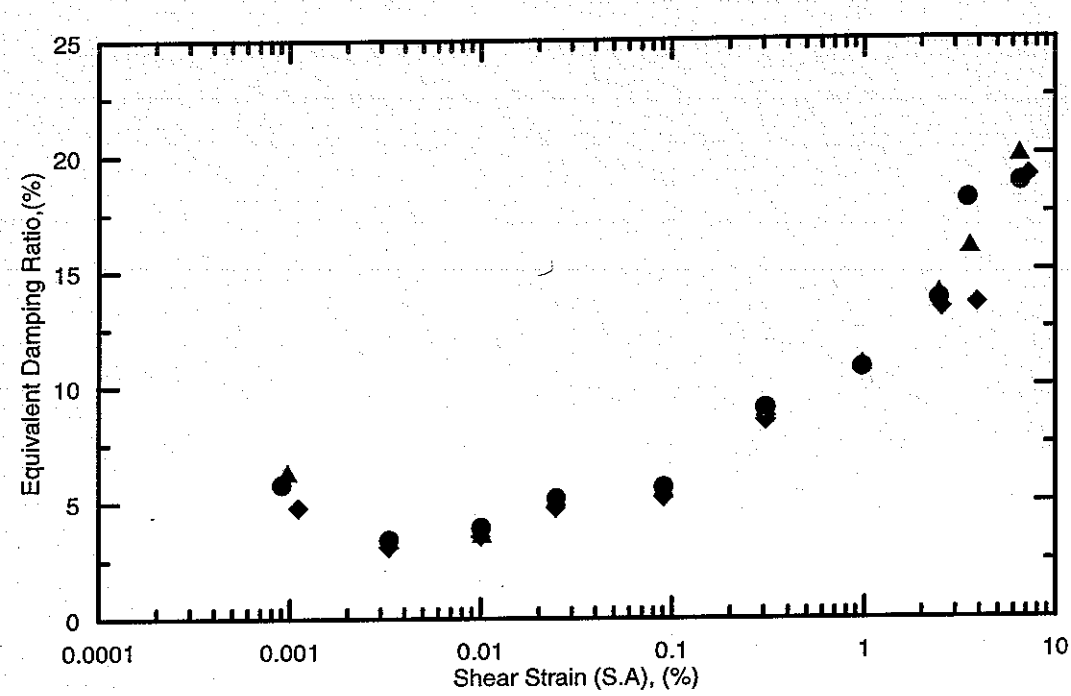

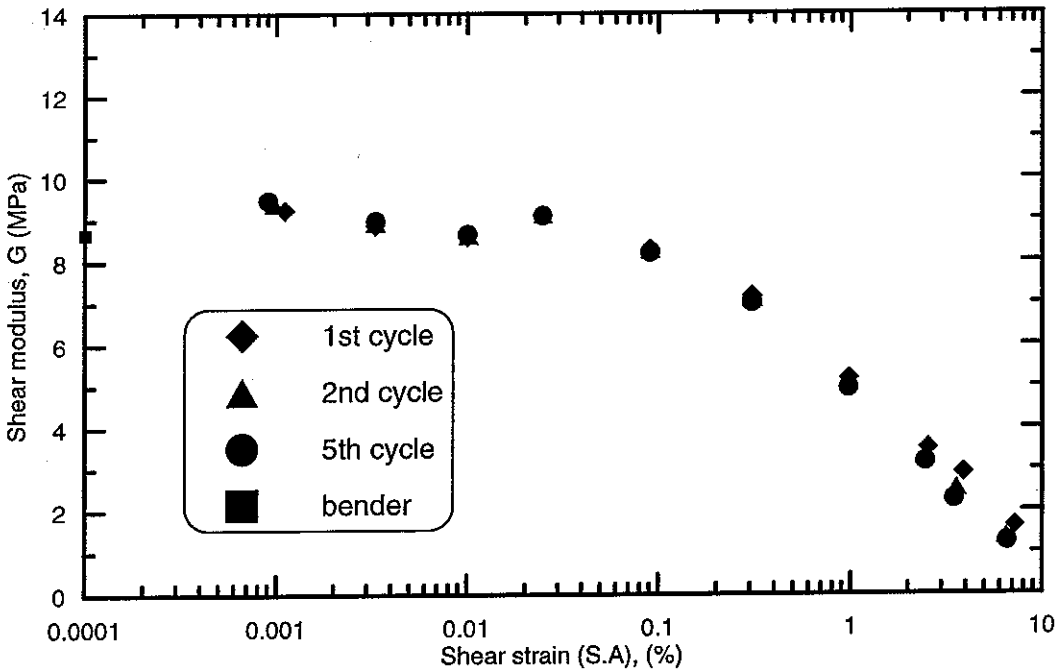

Project: Sherman Island	Depth : 13.17 m	Test Date :10/23/96	Tested by: R. Arulnathan
Sample description: peat soil, ash content =42 %		Consolidation Stress: 131 kPa	B-value =1.0
UNDRAINED CYCLIC TESTS AT DIFFERENT STRAIN LEVELS			Test No. DHPt4

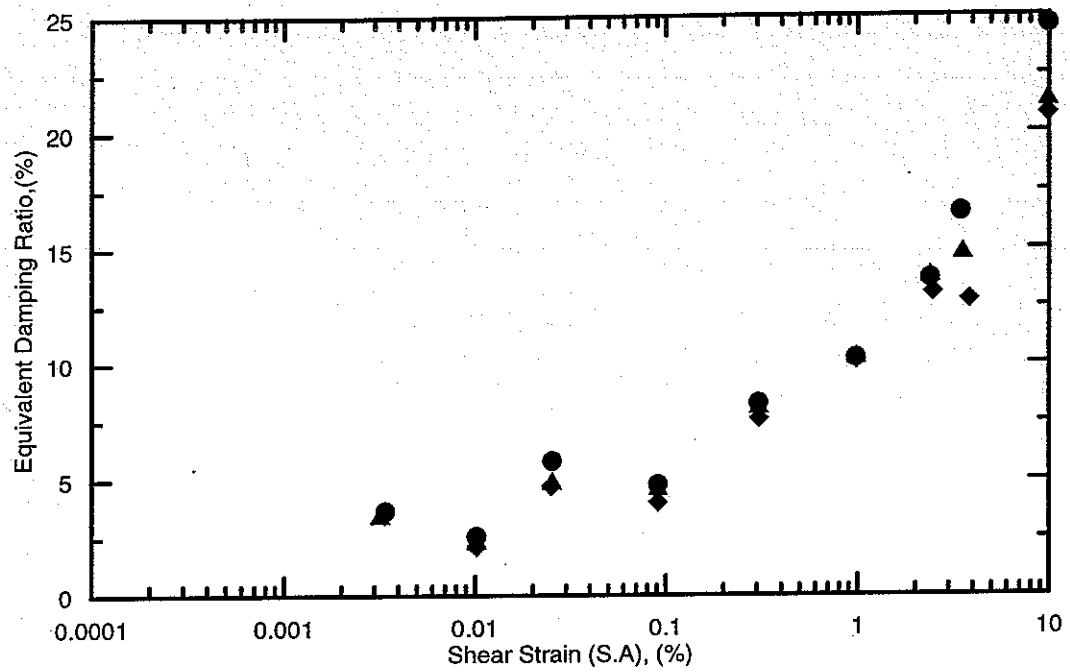

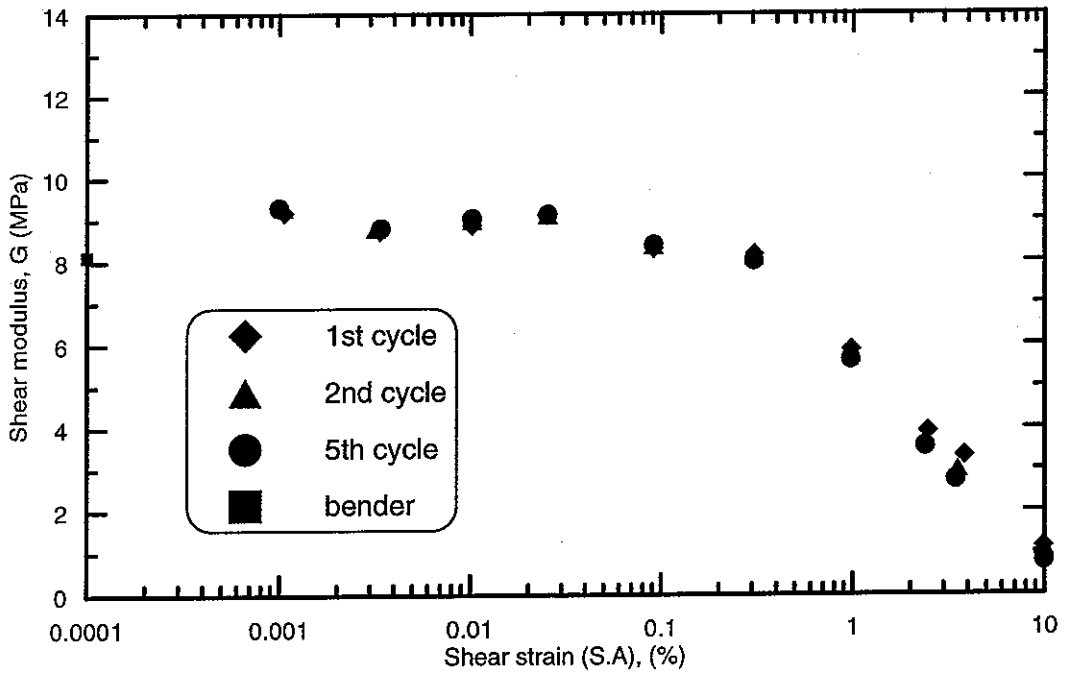

Project: Sherman Island	Depth : 13.7 m	Test Date :10/31/96	Tested by: R. Arulnathan
Sample description: peat soil, ash content =54 %		Consolidation Stress: 136 kPa	B-value =1.0
UNDRAINED CYCLIC TESTS AT DIFFERENT STRAIN LEVELS			Test No. DHPt5

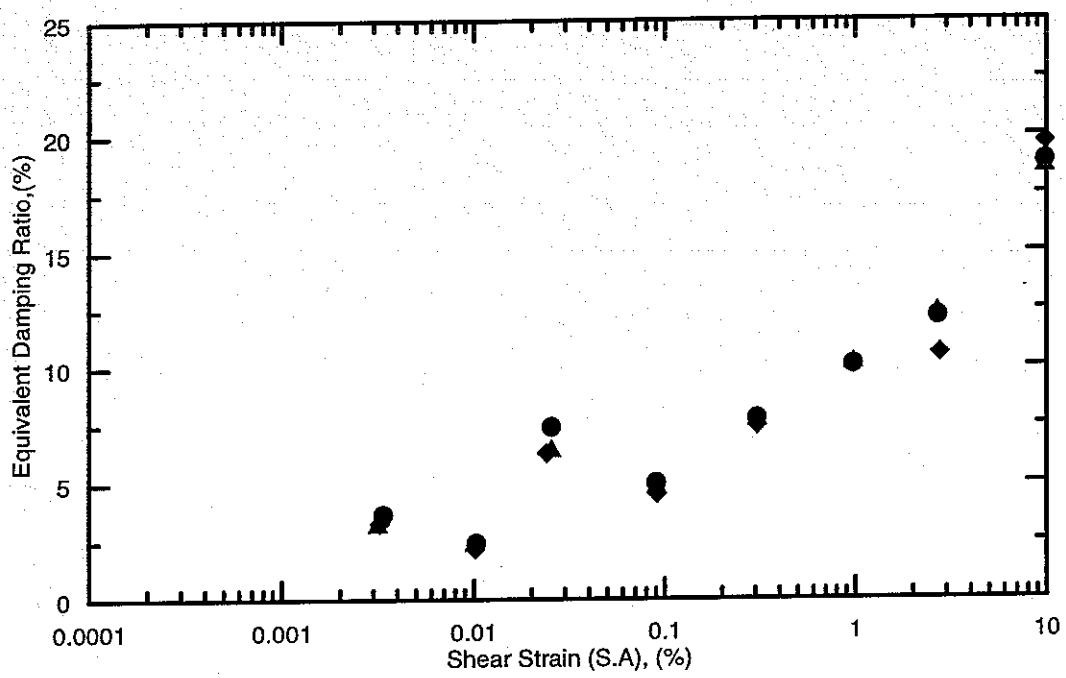

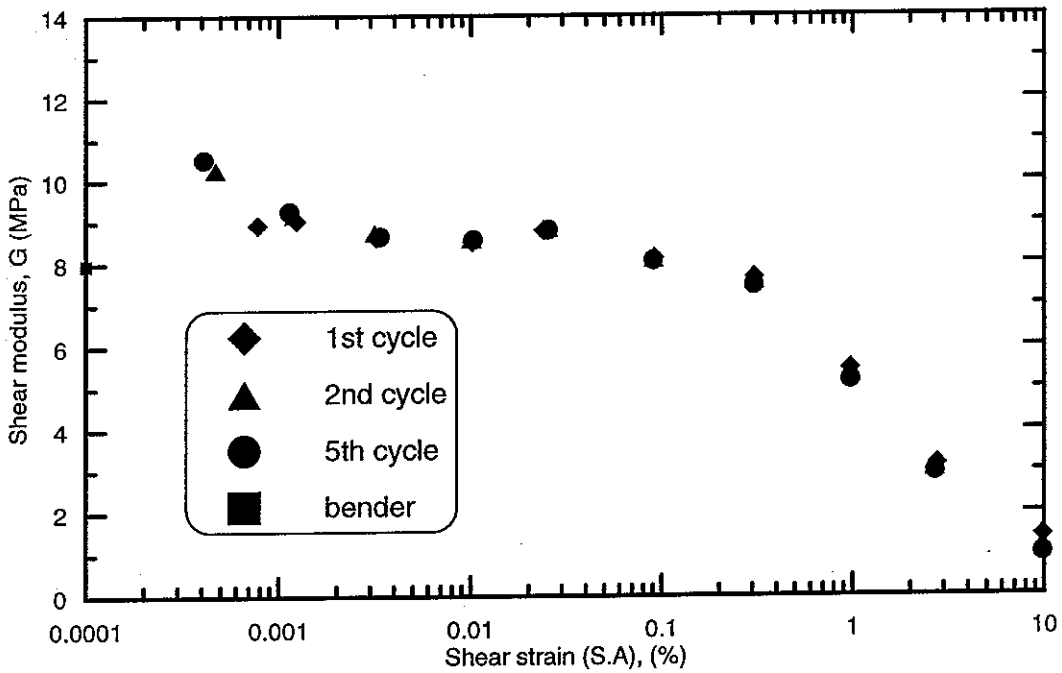

Project: Sherman Island	Depth : 13.5 m	Test Date :11/15/96	Tested by: R. Arulnathan
Sample description: peat soil, ash content =37 %		Consolidation Stress 132 kPa	B-value =1.0
UNDRAINED CYCLIC TESTS AT DIFFERENT STRAIN LEVELS			Test No. DHPt6

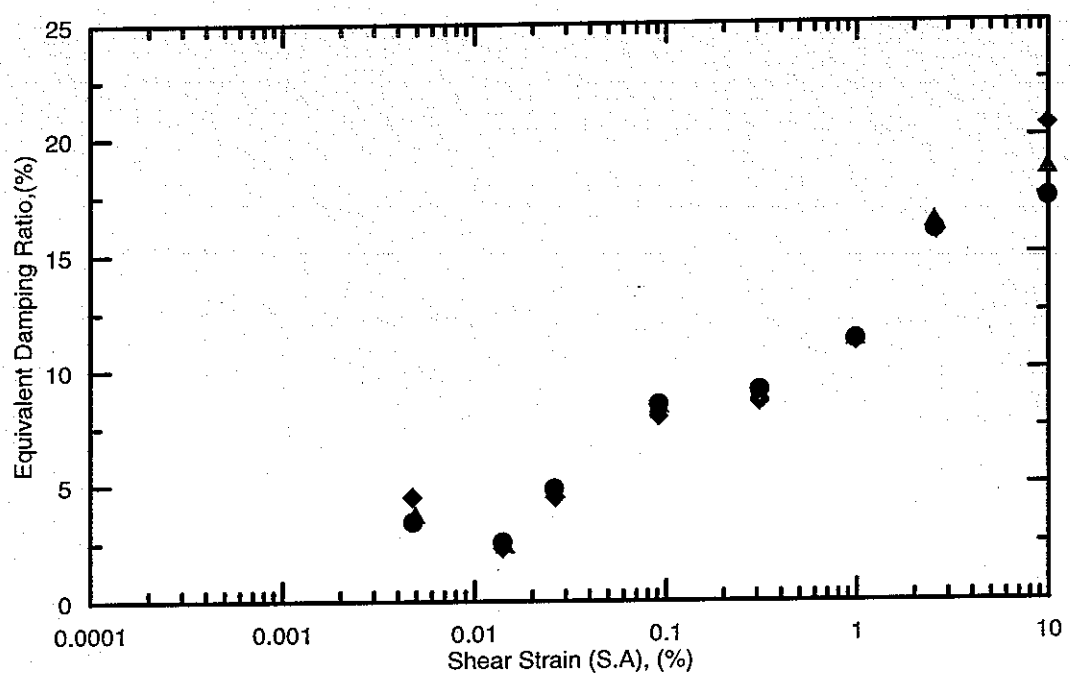

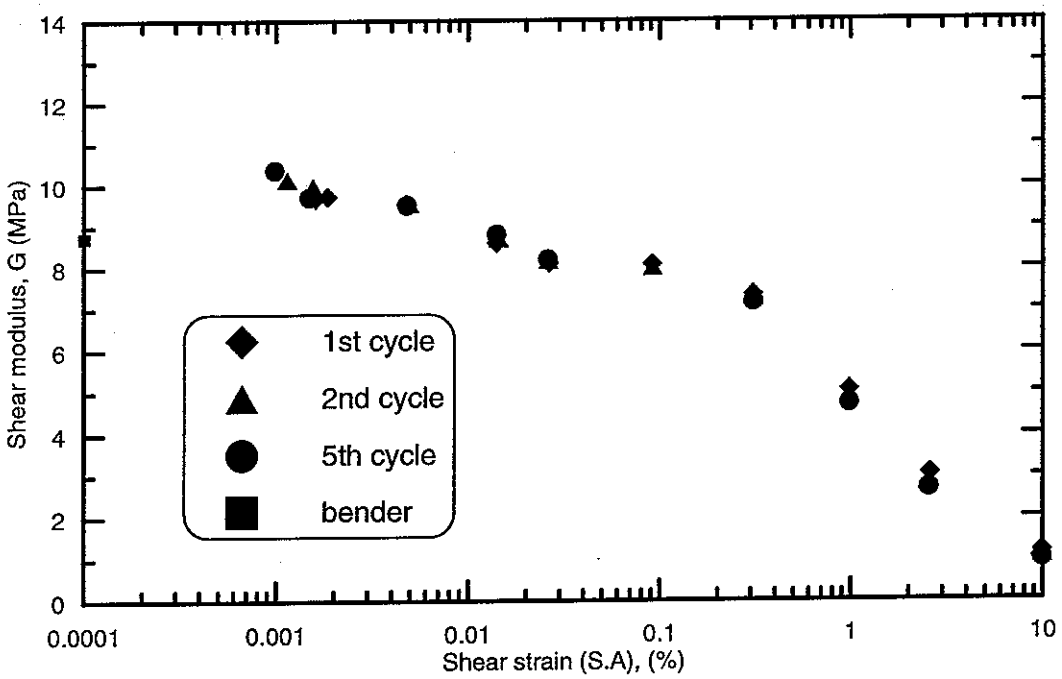

Project: Sherman Island	Depth : 13.3 m	Test Date :11/22/96	Tested by: R. Arulnathan
Sample description: peat soil, ash content =42 %		Consolidation Stress 200 kPa	B-value =1.0
UNDRAINED CYCLIC TESTS AT DIFFERENT STRAIN LEVELS			Test No. DHPt7

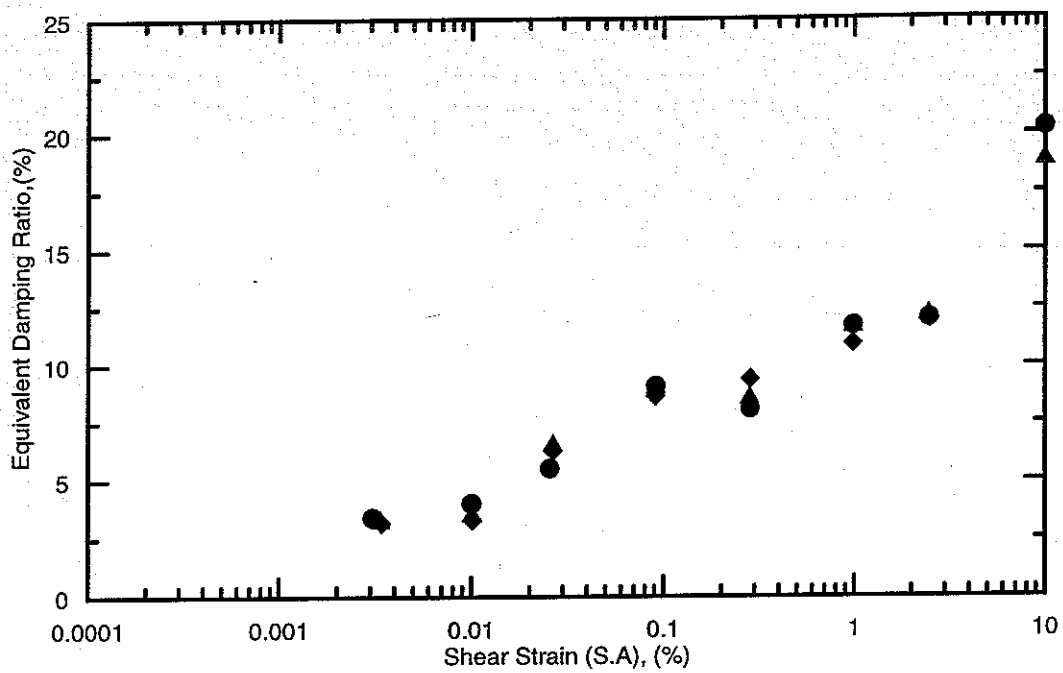

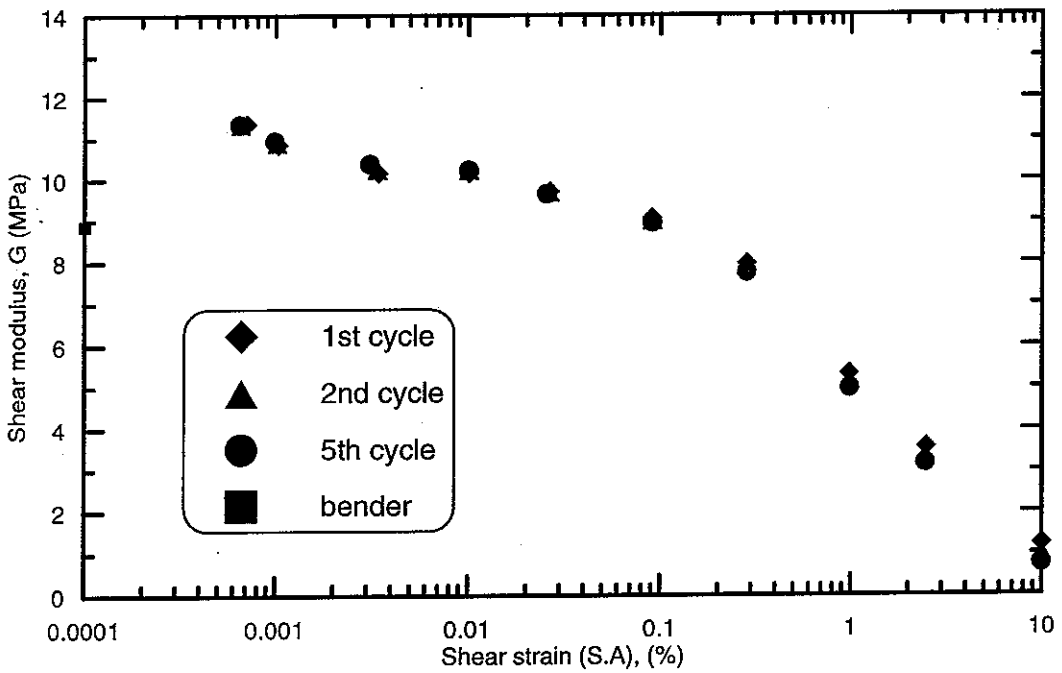

Project: Sherman Island	Depth : 13.5 m	Test Date :12/05/96	Tested by: R. Arulnathan
Sample description: peat soil, ash content =37 %		Consolidation Stress: 66 kPa	B-value =1.0
UNDRAINED CYCLIC TESTS AT DIFFERENT STRAIN LEVELS			Test No. DHPt9

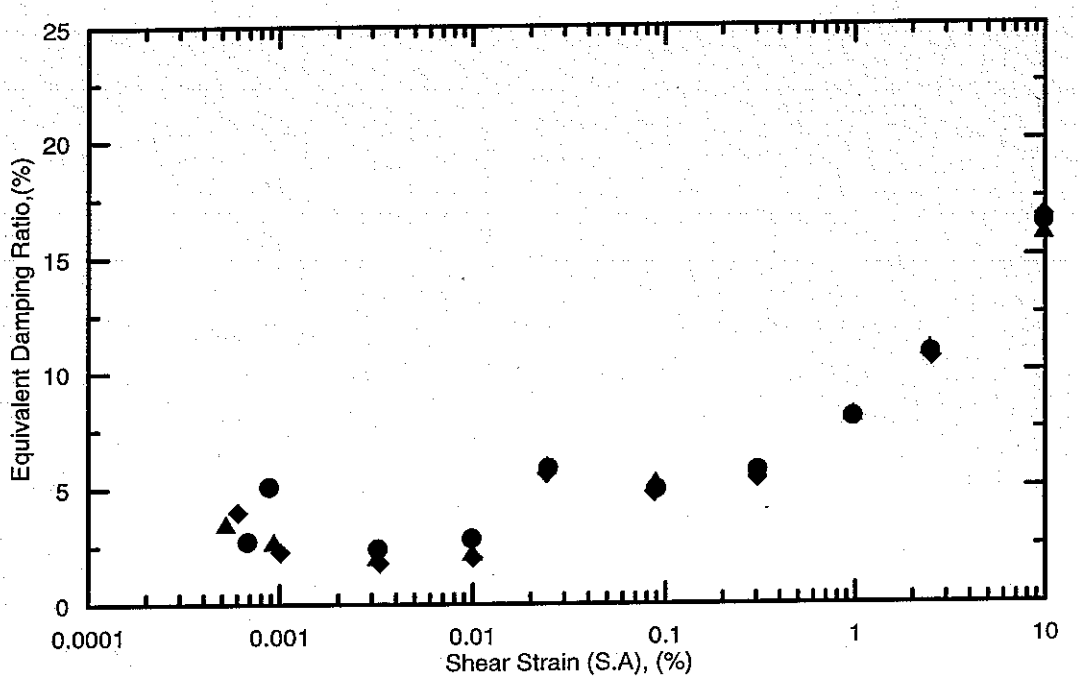

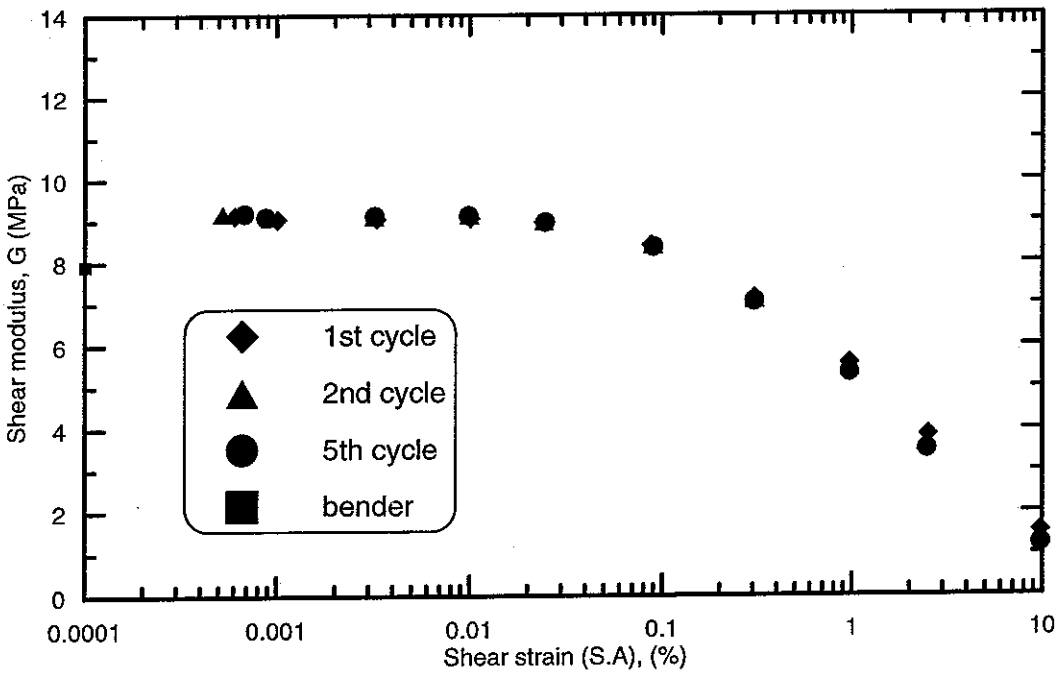

Project: Sherman Island	Depth : 13.3 m	Test Date :12/15/96	Tested by: R. Arulnathan
Sample description: peat soil, ash content =35 %		Consolidation Stress: 66 kPa	B-value =0.82
UNDRAINED CYCLIC TESTS AT DIFFERENT STRAIN LEVELS			Test No. DHPt10

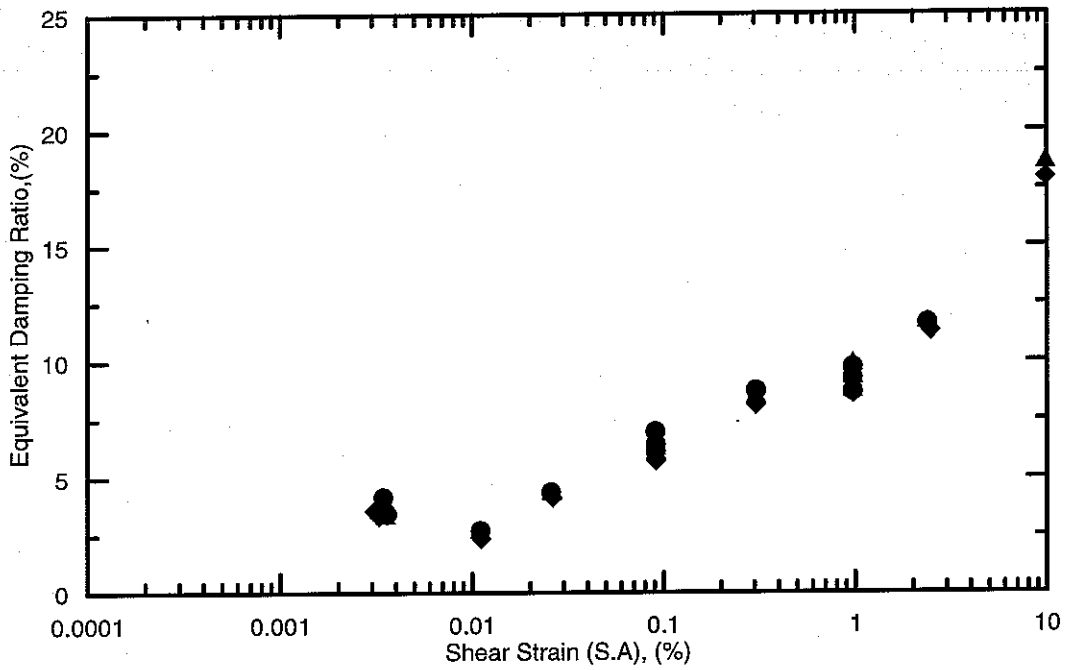

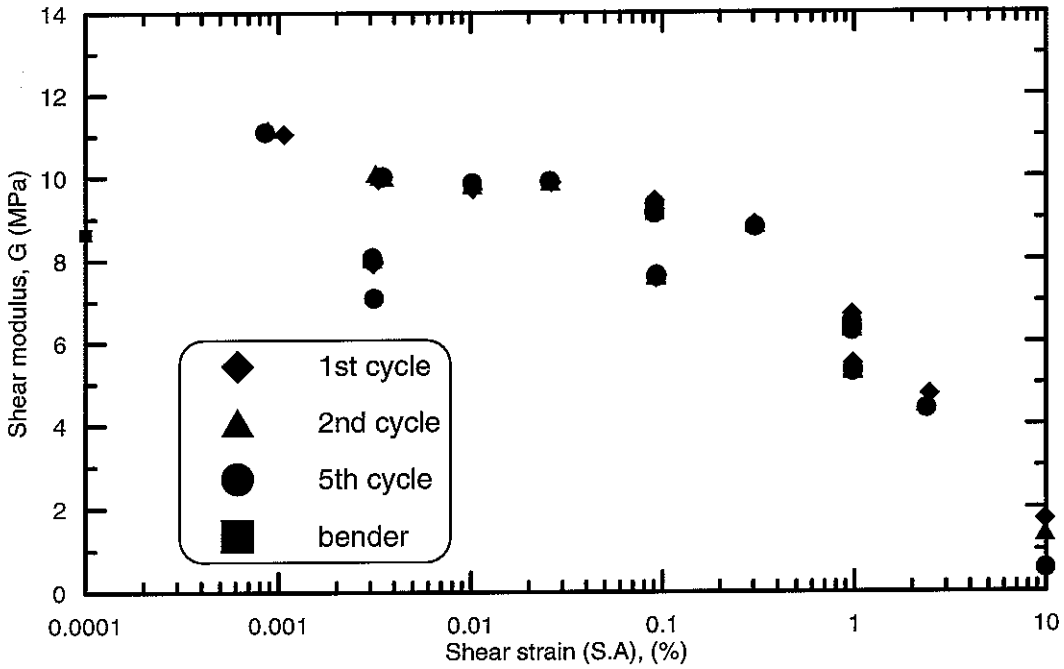

Project: Sherman Island	Depth : 12.8 m	Test Date :01/31/97	Tested by: R. Arulnathan
Sample description: peat soil, ash content =44 %		Consolidation Stress: 128 kPa	B-value =1.0
UNDRAINED CYCLIC TESTS AT DIFFERENT STRAIN LEVELS			Test No. DHPt12